Alma Mater Studiorum – Università di Bologna

in cotutela con Université de Bordeaux

DOTTORATO DI RICERCA IN

Chimica

Ciclo *XXIX*

Settore Concorsuale di afferenza: **03/B1**

Settore Scientifico disciplinare: **CHIM 03**

Development of luminescent semiconductor nanocrystals (Quantum Dots) for photoinduced applications

Presentata da: **Marcello La Rosa**

Coordinatore Dottorato   Relatore

Prof. Aldo Roda   **Prof. Alberto Credi**

                                                  Relatore

                                             Dr. Nathan D. McClenaghan

Esame finale anno 2017

To my parents

Contents

Chapter 3:

A novel method for modulating the solubility of Quantum Dots

Chapter 4:

Implementation of chiroptical properties of Quantum Dots

Chapter 5:

Quantum Dots with long-lived luminescence as result of the reversible electronic energy transfer

Chapter 6:

Thermal poling process for directing assembly of Quantum Dots on solid surface

List of Publications   **159**

Overview

Nanoscience is such a fast growing and emerging research frontier that it is considered the motor of the modern industrial revolution. It essentially focuses on the study and the manipulation of structure and function of materials on the nanometer scale. Under these conditions, light and matter behave in significantly different ways from those we are familiar with on the everyday macroscale.

Nanoscience has, actually, already impacted our lives with innovations ranging from stain-resistant fabrics, inspired by the nanoscale features found on lotus plants, to computer hard drives, which store information on magnetic strips that are just 20 nanometers thick. Scientists and engineers from several disciplines including physics, chemistry, biology and materials science use nanoscience principles for advanced applications in energy, medicine, information storage, computing and elsewhere.

The top down method has been initially the most important one to project and build such objects. However, since the miniaturization process has a size limit well-defined by physics, the interest has been shifted on the bottom up approach, which exploits atomic or molecular scaffolds to build nanodevices.

This PhD thesis has been focused on the development of colloidal semiconductor nanocrystals, also called Quantum Dots (QDs), which are considered highly promising nanostructured materials. The research project has been carried out through a joint supervision agreement between the University of Bologna and the University of Bordeaux (France), within the Vinci Programme 2013 supported by the Université Franco-Italienne.

The manuscript consists of six chapters. *Chapter 1* is a brief introduction to nanotechnology, illustrating the difference between top-down and bottom up approaches for building nanomaterials. Then basic concepts concerning the theory and the surface manipulation of quantum dots are discussed.

Chapter 2 illustrates the synthetic strategies used to prepare QDs of different types and sizes; the surface ligands involved in the experiments described in the fifth chapter, but also the experimental techniques adopted to characterize and investigate the systems reported in this thesis.

Chapter 3 introduces a new strategy for functionalizing the surface and modulating the solubility of quantum dots in a wide range of solvents of different polarity. Such a method offers several advantages compared to those ones already reported in literature.

Chapter 4 shows the functionalization of quantum dots with an enantiomerically pure ligands in order to introduce new chiroptical properties as well as the investigation of the size-dependence of such an induced effect.

Chapter 5 concerns a central aim of this PhD programme: the development of nanohybrids showing the so called reversible electronic energy transfer. Such a process can be referred to as a bi-directional energy transfer between quantum dots and suitable chromophoric units attached on their surface, whose the most important consequence is the elongation of the lifetime of nanocrystals at least of one order of magnitude.

This process has been only observed in supramolecular systems consisting of, for example, a ruthenium (II) polypyridine complex and a pyrenyl moiety connected through a molecular bridge, but never with QDs-based systems.

Chapter 6 describes a novel method to deposit QDs decorated with charged ligands on a glass surface locally polarized through a thermal pooling process. Such a method takes advantage of the electrostatic interaction between the charged surface ligands and the particular charge displacement of the glassy substrate.

This aspect of the project has been carried out with the collaboration of Dr. Marc Dussauze of the University of Bordeaux during my research period spent in France.

Chapter 1
Introduction

1.1 Nanotechnology and Nanomaterials

The word "nanotechnology" was used for the first time by Norio Taniguchi of the University of Tokyo in 1974.[1] It is interesting to point out that the first molecular-device was developed precisely in 1974[2] and few years later (i.e., 1981) were also invented the Atomic Force Microscope (AFM) and the Scanning Tunneling Microscope (STM), through which the investigation at nano-scale has actually begun.

Today nanotechnology ranges from the production to the application of physical, chemical and biological systems or devices, moving from individual atoms or molecules to submicron architectures, as well as providing the integration of the resulting nanostructures into larger systems.

One nanometer (i.e., 1 nm = 10^{-9} m) is approximately the distance from one end to the other of a line of five neighboring atoms in an ordinary solid.

A nanometer scale is illustrated in Figure. 1.1: if the size of a soccer ball ($\sim$ 30 cm = 3×10^{-1} m) is reduced 100.000 times we reach the width of a red globule in the blood ($\sim$ 3 μm = 3×10^{-6} m), then if we reduce the size of the red globule 3.000 times, we reach the width of a carbon nanotube ($\sim$ 1 nm = 1×10^{-9} m).
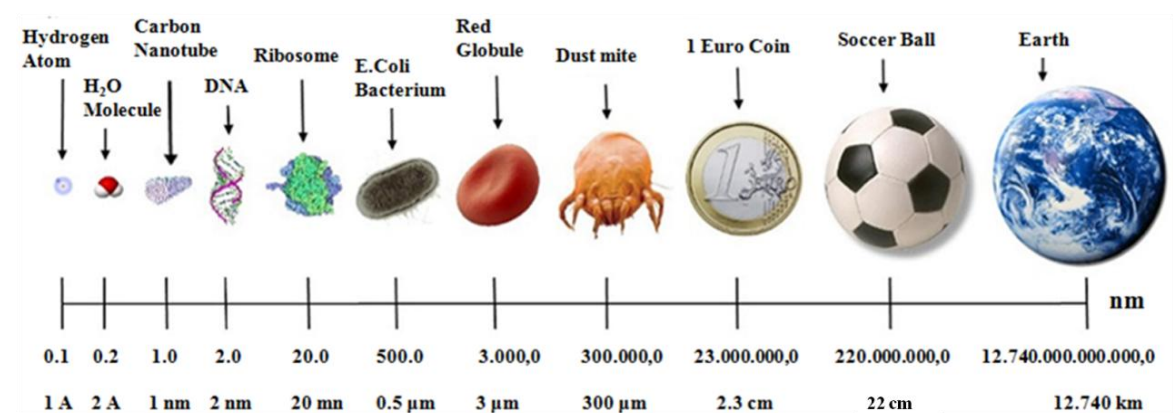

Figure 1.1 Matter dimension: from macro to nano.

Since the early 21st century, nanotechnology has been having a profound impact on our economy and society, comparable to that of semiconductor technology, information technology or cellular and molecular biology; so that its products are commercially available for the mass consumer.

Science and technology research in this field promise breakthroughs in areas such as materials and manufacturing, nanoelectronics, medicine and healthcare, energy, biotechnology, information technology and national security. It is widely felt nanotechnology is the result of the current Industrial Revolution.

Nanomatter is the bridge between atoms and the solid matter. Strictly speaking, the nanoworld has existed for a long time and it is up to chemists to study the structures and properties of molecules. They have learnt (together with physicists) to manipulate them and build more and more complex structures. Progress in observation tools (e.g., electron microscopes, scanning-tunneling microscopes and atomic force microscopes) as well as in analysis tools (e.g., X-ray, neutron and mass spectrometry) has been a relevant factor. The production of nanomaterials is constantly improving, as is the case for the process of catalysis[3] and surfaces used in the nanoworld. A substantial number of new materials with nanoelements such as ceramics, glass, polymers and fibers are making their way onto the market and are present in all shapes and forms in everyday life, from washing machines to architectures.

In 1959, the physicist Richard Feynman,[4,5] Nobel Prize winner for Physics in 1965 and historically considered as the father of Nanotechnology, explained an innovative as well as attractive concept by saying "*there is plenty of room at the bottom*" during a conference of the American Physical Society.

More specifically, Feynman's lecture concerned the possibility to write enormous quantities of information in a reduced space: "*Why cannot we write the entire 24 volumes of the Encyclopedia Britannica on the head of a pin* (i.e., in 1/25000 inch square)*?*" He also pointed out that matter on the small scale behaves in a different way respect to that in the macroscale: "*So, as we go down and fiddle around with the atoms down there, we are working with different laws, and we can expect to do different things. We can manufacture in different ways. We can use, not just circuits, but some system involving the quantized energy levels, or the interactions of quantized spins, etc. [...]At the atomic level, we have*

new kinds of forces and new kinds of possibilities, new kinds of effects. The problems of manufacture and reproduction of materials will be quite different."

Today it is known that two main approaches can be followed to "*manufacture*" nano-objects, as shown in Figure 1.2:
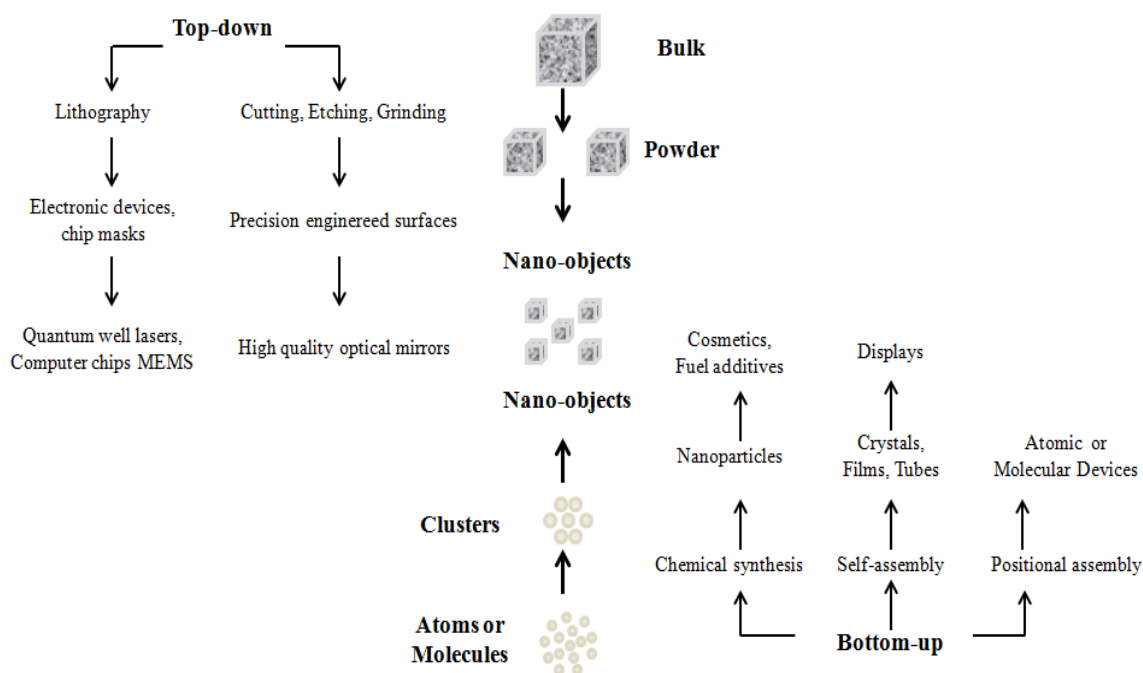
Figure 1.2 Comparison between top-down and bottom-up approaches.

The top–down approach is focused on the physical size-reduction of the starting material up to the nanometer-scale; in this case the "function"[6] of the new material is the same of the bulk material or induced during the miniaturization process. This is a typical engineering approach, which tends to produce very defined structures, stable, regular and, moreover, can help to achieve solid-state nanostructures by exploiting the high-energy radiation sources (e.g., X-rays, ions or electrons beams).

Conventional nano- and micro technology are a top-down technology; microstructures are fabricated by manipulating a large piece of material, typically a silicon crystal, using processes such as lithography,[7,8,9] etching,[10,11] and metallization.[12]

The top-down approach to microelectronics seems, however, to obey to an exponential time dependence. In 1965, when the most advanced integrated circuit contained only 64 transistors, Gordon E. Moore, the director of Fairchild Semiconductor Division, was the first to note such an exponential behaviour in his famous paper:[13]

"*When unit cost is falling as the number of components per circuit rises, by 1975 economics may dictate squeezing as many as 65,000 components on a single silicon chip*". Moore predicted a doubling of the number of transistors per circuit every year, such a prediction has become known as Moore's law (see Figure. 1.3).
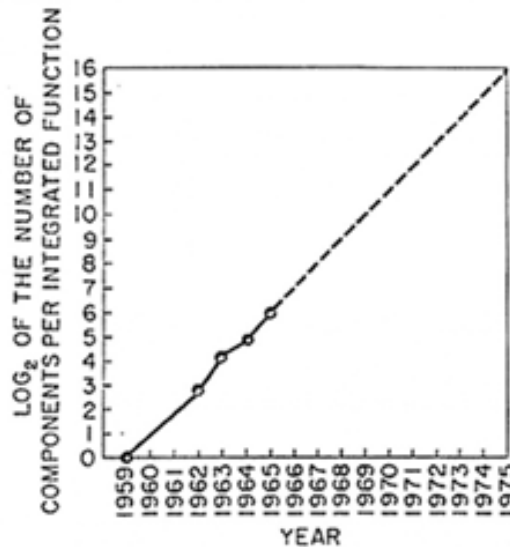
Figure 1.3 The doubling of the number of components per microchip each year predicted by Moore. Adapted from reference [13]. Copyright Electronics 1965.

Naturally, there will be physical limitations to the exponential behaviour expressed by the Moore's law and, obviously, also the economic barriers and limits will play a major or even better the decisive role in ending Moore's law. Also the price for fabricating microprocessor units rises exponentially for each generation of microchips; then, such a factor could very well slow down the rate of progress.

Bottom-up nanotechnologies exploit molecules[6] or atomic aggregates, able to self-organize or self-assemble, as starting material so they shift from a disordered situation to a more ordered and complex structure, owing to their particular geometric and electronic features. In this particular case chemists, as matter manipulators, are very suitable to help the development of nanoscience and nanotechnology. More in detail, molecules are much more useful and convenient than atoms[14] as building blocks to construct nanodevices,[15] owing to their stability and "fully predictable" properties, which can be manipulated through different inputs, but also to the fact that it is easier to work with molecules.

On the other hand atoms are quite reactive and we cannot managed easily this reactivity; nevertheless they can be manipulated through scanning microscopy techniques at low temperature and ultra-high vacuum[16] (e.g., AFM and STM). In this case the function of the nanomaterial is the simple combination of the functionality of nanoscale components.

The most useful advantage of such an approach is that an excessively expensive instrumental equipment is not required; however, the most important disadvantage arises from results strongly dependent on the experimental parameters adopted (e.g., type of the reactants, the times and the reaction conditions); then, a high level operator training is required.

Higher expectations are associated to the "bottom-up" approach which will allow us to build nanostructures by replicating, in controlled conditions, processes already occurring in nature; however, this approach is still in a stage of development both in aspects related to basic research and applications, while "top-down" protocols are more established.

1.2 Colloidal Semiconductor Nanocrystals Quantum Dots

The enormous potential of science and technology on nanoscale to impact our lives has been recognized. One emerging area of nanoscience connecting chemistry, physics, biology and material science is the field of colloidal semiconductor nanocrystals, also called Quantum Dots (QDs). They can be considered as inorganic–organic hybrid nanomaterials,[17] since they consist of an inorganic semiconductor core, such as cadmium selenide (CdSe), cadmium sulfide (CdS), cadmium telluride (CdTe), lead sulfide (PbS) or thin sulfide (ZnS) coated by a molecular layer of organic ligand providing them a colloidal stability or, in other words, which avoids their aggregation-flocculation.

The hybrid nature of these nanostructures provides also great flexibility in programming their physical and chemical properties; thus making possible the modulation of these properties simply by manipulating composition, size and shape of nanocrystals.

It is known that the properties of materials at the nanoscale can be very different from those at a larger scale, this particular behaviour is due to the quantum confinement effect, whose word *confinement* means a restriction of the motion of randomly moving electron in specific discrete energy levels and the word *quantum* reflects the atomic behaviour of particles.

The QDs can be consecutively described, from an electronic energy point of view, as in a middle configuration between corresponding bulk materials and general molecules, as shown in Figure 1.4:
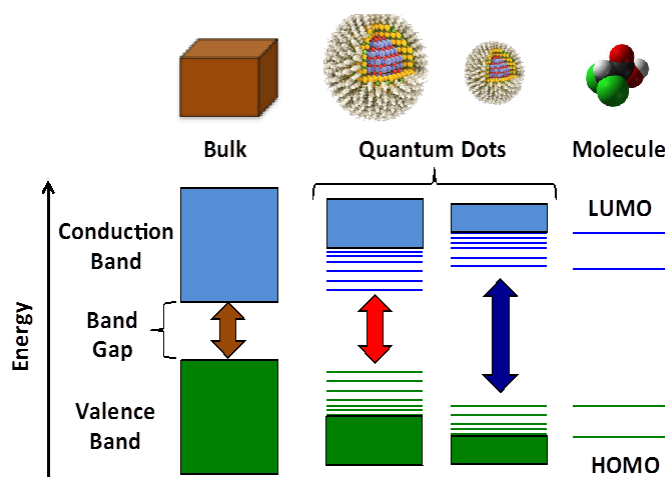
Figure 1.4 Comparison between bulk materials, QDs and general molecules in terms of electronic energy.

The electronic energy of a molecule can be described in terms of molecular orbitals,[18] which are simply a linear combination of the orbitals of atoms consisting that molecule; then, the highest occupied molecular orbital is called HOMO, while the lowest unoccupied molecular orbital is called LUMO. Essentially intrinsic properties such as paramagnetism or diamagnetism arises from the electronic redistribution through molecular orbitals

Then if we extend this linear combination over a huge number of atomic orbitals, as in the case of a bulk material, we are shifting from molecular orbital theory to band theory,[18] so from the discretization to a continuum of energetic levels. In this case, the highest filled band is called Valence Band and the lowest unfilled band is called Conduction Band; the energy difference between the two bands is defined as the band gap energy (E_g) and, depending on such a gap, we can distinguish between conductor, insulator or semiconductor materials.

The valence and conduction bands of a conductor material, such as a metal, are so close to be considered overlapped, so the electrons can move without restrictions; while for an insulator the energy band gap is so high that migration of electrons is forbidden. Finally, in the case of a semiconductor material the electrons can have enough energy to be promoted in the conduction band simply by increasing the temperature (i.e., thermal-conductivity); nevertheless, the amount of charge carriers will be smaller than that of a conductor material; or, alternatively, can be photo-excited from the valence band to the

conduction band (i.e., photo-conductivity), thus generating a couple hole-electron located in the valence band and in the conduction band respectively and called exciton. The electron and hole cannot move independently because of the Coulombic interaction, but they thermally relax to the band edge where finally they recombine with the emission of a photon of the same energy of the intrinsic band gap.[19] This process is referred to as band edge luminescence and is schematically represented in Figure 1.5:
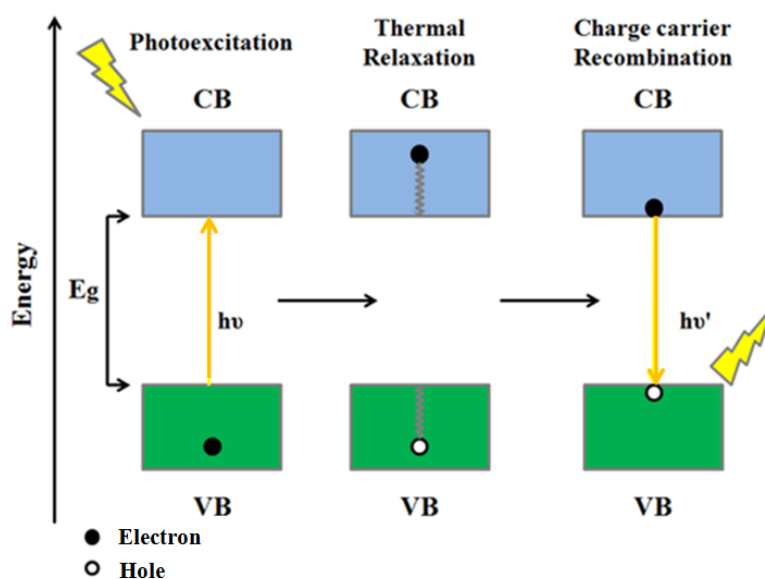
Figure 1.5 Schematic representation of the photoluminescence process in bulk material.

The colloidal semiconductor nanocrystals are between these two extreme situations due to the confinement effect, which occurs when their size is of the same order of magnitude of the Bohr radius (i.e., the electron-hole distance in the photogenerated exciton, a_0). For example, the Bohr radius for CdS and CdSe in bulk regime are, respectively, about 3 and 5 nm.[17] If their size approaches these values then the exciton size would exceed the crystal dimension; consecutively, the charge carriers must assume higher kinetic energies to be kept into the lattice, thus resulting in a new regime, where the density of electronic states and the energy separation follow now the quantum-mechanical model of a particle in a box.[18]

For such a reason colloidal semiconductor nanocrystals show strongly size-dependent optical properties; moreover, as the energy band gap increases by decreasing their size,[20] the smaller the size the higher the emission energy (see Figure 1.6).
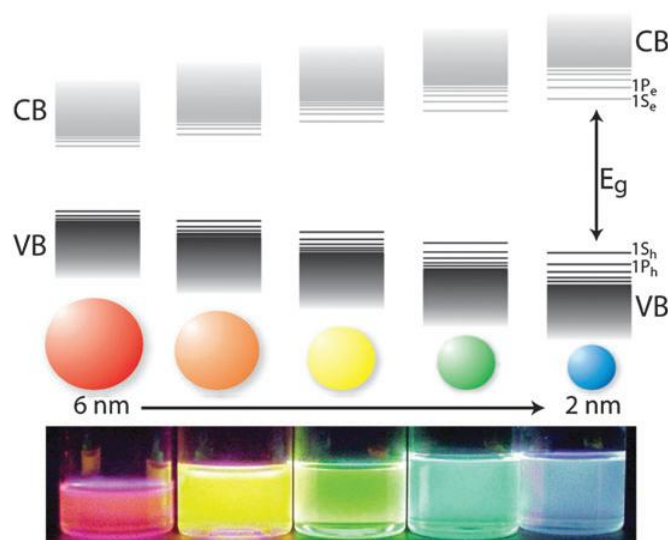
Figure 1.6 Schematic representation of size-dependent luminescence of QDs. Adapted from reference [17]. Copyright Philips Research Laboratories (Netherlands).

It is important to note that a_0 is inversely correlated to E_g, so the higher the value of the band gap the smaller the size at which the quantum confinement effect starts taking place. For example, the insulator materials have very small a_0 so they are affected by quantum confinement only for sizes ranging in the cluster regime (i.e., 20 atoms).[21]

Finally, depending on the entity of such a spatial confinement, it is possible to distinguish between quantum dots (QDs), quantum wires and quantum wells. To be more precise, nanomaterials whose exciton is confined in all three dimensions are referred to as QDs (i.e., zero dimensional object or 0D); if the exciton is confined only in one direction then nanomaterials are defined as quantum wires (1D); finally, if the confinement occurs in two dimensions we can talk about quantum wells (2D). So called Quantum rods (QRs) are nanocrystals moving from a 0D to a 1D confinement regime.[17]

1.2.1 The role of surface ligands

It is necessary to point out that, at the nanoscale, the surface also plays an important role. It is known that for any substance the surface-to-volume ratio is inversely correlated with its dimension, so surface can affect different properties such as solubility[22] and generate completely new effects such as plasmon resonance[23] and size-dependent catalytic activity.[24]

In this sense molecules binding to the surface, commonly called surface ligands or surfactants, are an essential component in developing and preparing nanocrystals both in terms of synthesis, because they control nucleation and growth stages,[25] and in terms of stability, since they screen nanocrystals from the surrounding environment and prevent their aggregation/flocculation by providing steric or electrostatic colloidal stability.[26]

Amphiphilic molecules are ideal surfactants[17] because their polar head is attached to the nanocrystal surface through donor atoms (e.g.,. N, O, S, P), while the apolar tail interacts with the surrounding medium.

It is possible to choose between a huge number of molecules for coordinating the metal components of QDs (e.g., cadmium, Cd or zinc, Zn): alkylamines (R_3-N, R_2-NH, R-NH_2) such as hexadecylamine (HDA) or octadecylamine (ODA); fatty acids (R–COOH) such as oleic acid (OA) or stearic acid; alkylphosphine oxides (R_3PO) such as tri-octylphosphine oxide (TOPO); phosphonic acids (R–POOH) such as n-octadecylphosphonic acid (ODPA) or n-tetradecylphosphonic acid (TDPA) and alkylthiols (R–SH) such hexanethiol (HT).

On the other hand the ligands to coordinate non-metal components of the QDs (e.g., selenium, Se, or telluride, Te) are only alkylphosphines (R_3P) such as n-trioctylphosphine (TOP) or tributylphosphine (TBP).

Surfactants with two polar heads connected by a hydrocarbon chain such as dithiols, HS–R–SH; mercapto n-alkyl acids, HS–R–COOH; hydroxyalkylphosphines or peptides have been also developed to cross-link nanocrystals in more complex architectures[27,28] or to render them water soluble.[29]

The model already adopted for describing the interaction occurring in coordination complexes and involving the ligands and the metal center[26] has been recently proposed[30,31,32] to rationalize also the interaction between surfactants and QD surface.

According to this model, it is possible to distinguish ligands of L-type (two-electron donors such as neutral Lewis bases), X-type (one-electron donors) and Z-type (two-electron acceptors such as Lewis acids). L-type ligands (e.g., amines, phosphines and phospine oxides) donate their lone pair to a surface metal atom, thus establishing a dative bond; X-type ligands are monovalent anions (e.g., carboxylates, phosphonates and thiolates) and interact with electron poor sites at the QD surface; finally, Z-type ligands play the role of Lewis acids and interact with electron rich sites (e.g., chalcogenide anions in metal chalcogenide nanocrystals).

Another important factor to consider is the lability of such an interaction; which allows the exchange of the 'native' ligands with others bearing organic or inorganic ions,[33,34] clusters,[35] and polymers[36] to improve or to add specific functions in more complex nanohybrids. Such a strategy will be discussed in the last paragraph of this chapter.

Last but not least, ligands can affect the optical, electrical and magnetic properties of nanocrystals. As highlighted above, the QDs exhibit valence and conduction bands split into discrete quantum-confined states;[37] however, since surface atoms are not saturated (i.e., not involved in any interaction), there are extra electronic energy levels rising from these dangling bonds, localized between the band edges and acting as a trap state, thus negatively affecting the photophysical properties of QDs. The interaction with surfactants introduces both new bonding and anti-bonding molecular orbitals, as represented in Figure 1.7:
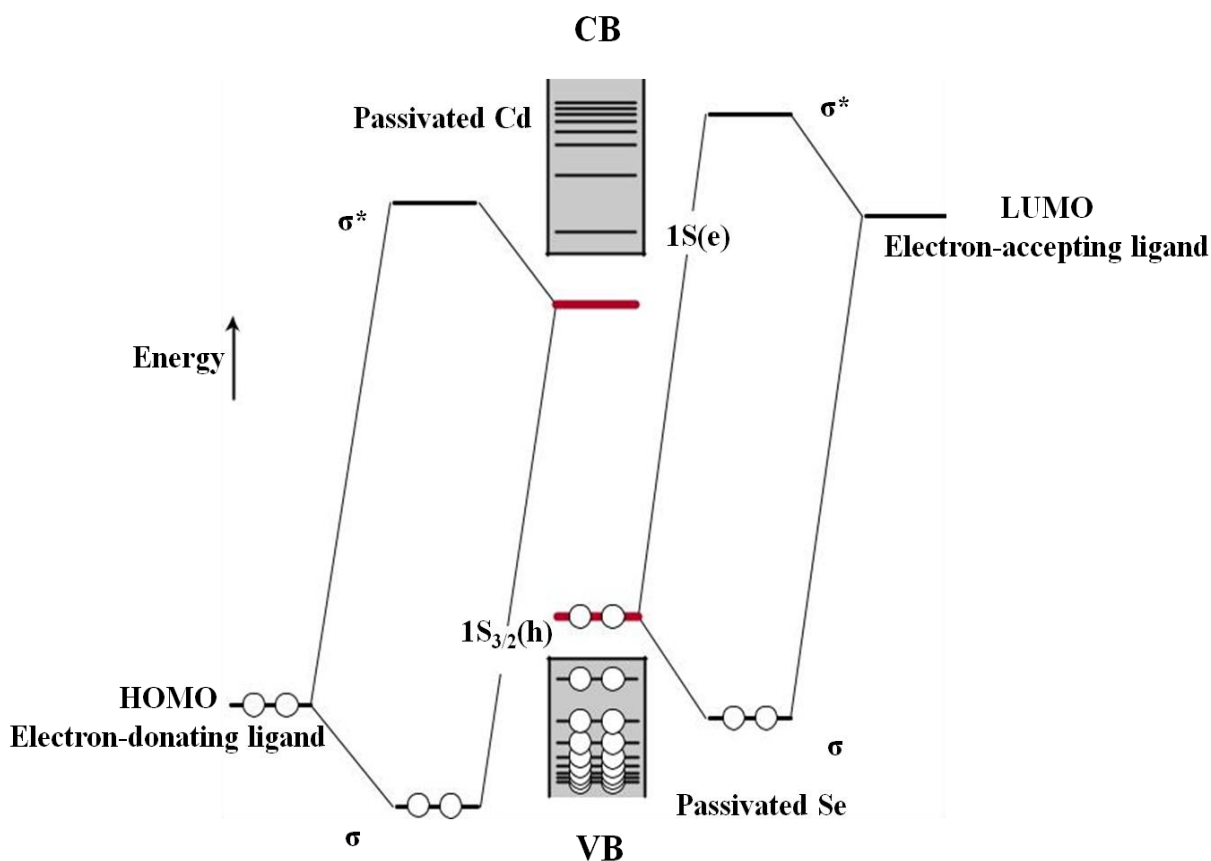
Figure 1.7 Schematic representation of electronic energy states of CdSe nanocrystals. Adapted from reference [30]. Copyright Nature Publishing Group 2016.

The stronger this interaction the more shifted are these new levels with respect to the band edges, thereby preventing non-radiative relaxation via these states. The entity of this interaction, of course, depends on the nature of the involved ligands.

In the case of CdSe QDs, for example, it has been observed that Lewis acids give rise to their quenching, while Lewis bases provide an enhancement[38] of their emission quantum yield. More in detail, concerning the previous case, linear monodentate ligands such as primary alkylamines provide a more efficient surface passivation than sterically-hindered ligands such as n-trioctylphosphine oxide, owing to a higher, so better, surface coating.

Surface states can be also shifted away from the band edges through a rearrangement of surface atoms, thus allowing a partial overlap between the dangling orbitals of neighboring cations and anions; which, ultimately, results in a new

redistribution of the electron density.[39] Such a process is defined surface self-passivation (or self-healing) and can be provided by surface relaxation and/or reconstruction.

Surface relaxation and reconstruction have been extensively investigated for technologically useful materials such as GaAs, ZnS and CdTe.[39] The first process involves a shortening of the bonds between the surface atoms and their neighbors immediately underneath, while the second is a more complex reorganization of the surface involving changes of both bond lengths and coordination geometry.

It has been recently observed that the surface relaxation is strongly dependent on the coordination number of the atom in the reticular habits[40] but also on the size of QDs, as in the case of CdSe QDs.[41]

Generally, linear molecules such as primary alkylamines can promote surface relaxation and reconstruction better than bulky molecules such as TOPO; which are unable to form ordered self-assembled monolayer at the surface[42,43] and therefore impose disorder and, eventually, also additional energy barriers for both such processes.

It is important to note that also post-synthetic ligand exchange treatments can dramatically affect the emission quantum yield, depending on the nature of the new surfactant and the entity of the exchange. For example, the emission quantum yield of CdSe QDs increases by one order of magnitude after the exchange of the native TOPO with primary alkylamines[44,45,46] while secondary alkylamines provide a relatively smaller enhancement (3 times more), which is even worse in the case of tertiary alkylamines (only 50%).[44]

Ligands able to decrease the emission quantum yield of the QDs have also been reported in the literature. Well-known examples of such ligands are methylviologen and alkylthiols, respectively efficient electron and hole acceptors from CdSe QDs.[47,48]

The ability of a molecule to catch photoexcited electrons or holes from QDs, so to avoid the charge recombination process, depends on its reduction or oxidation potential with respect to the size-dependent potential of conduction band or valence band of the QDs.[48] This kind of quenching is so efficient that it is detectable already at low acceptor concentrations[45,47,49] and can be exploited for probing the carrier localization regime.[50]

Finally, the impurities[41,45] of solvents used for synthesis and/or an excessive purification steps[41,43] can also negatively affect the emission quantum yield of QDs.

1.2.2 Preparation of Semiconductor Nanocrystals Quantum Dots

After pioneering work in the early 1980s,[51-54] the research in the field of semiconductor nanocrystals took advantage of a new synthetic protocol developed by Murray and co-workers[55] in 1993. This method has been the first affording the possibility of synthesizing monodisperse nanocrystals of II-VI type, such as CdSe, with a diameter ranging from 2 to 12 nm.

A sample is commonly referred to as monodisperse if the deviation from the main size is equal to 5-10%, which corresponds to a value of FWHM (i.e., the full width at the half maximum) of about 26-28 nm in the emission spectra.[19]

The synthetic method developed by Murray is also called the hot injection method and can be described as a three-steps process:[17]

Activation of metal and chalcogenide precursors: it concerns the decomposition of precursor and formation of monomers, which will assemble in nanocrystallites of increasing size. Such a step is, however, still not so clear, since exhaustive studies have been performed only for few cases.

Nucleation: in this process monomers assemble into crystal nuclei. The driving force of such a step is the difference between monomers in the crystal and in solution, in terms of free energy. The total free energy variation, ΔG_{TOT}, for the formation of a spherical nucleus of radius r with n monomers M (e.g., atoms, molecules or an ionic pair) in solution is provided by Equation 1.1:[17]

$$\Delta G_{TOT} = (4/3)\pi r^3 \Delta G_V + \Delta G_S = (4/3)\pi r^3 \rho \Delta\mu + 4\pi r^2 \gamma \qquad \text{(Eq.1.1)}$$

where ΔG_V is the volume excess free energy and ΔG_S is the surface excess free energy. ΔG_V will be negative because new chemical bonds have been formed in the crystal nucleus and the energy spent to break bonds between the monomers and the solvent and/or the surfactants is widely compensated. ΔG_S will be positive due to the fact that monomers at the surface have unsaturated bonds.

The factor ρ is referred to the density of the crystalline phase and $\Delta\mu$ is the chemical potential difference between nucleus and monomers in solution and can be approximated to:

$$\Delta\mu \approx -k\ T \ln S \qquad\qquad (Eq.1.2)$$

S is the amount of oversaturation and can be referred to as the ratio S_T over S_0, where S_T is the monomer concentration in the growth solution and S_0 the concentration at the equilibrium with a macroscopic crystal at temperature T, so its solubility. The factor γ represents the interfacial tension between the developing crystal and the supersaturated solution.

ΔG_V and ΔG_S have opposite signs and different size dependences, so ΔG_{TOT} will reach a maximum for nuclei with a critical radius r_C and then decrease with increasing radius (see Figure 1.8). This results in an energy barrier for nucleation, ΔG_C, thus establishing that the nuclei smaller than r_C will redissolve, while those larger than r_C can growth.

The critical radius is given by Equation 1.3:[17]

$$r_C = -2\gamma/(\rho\ k\ T \ln S) \qquad\qquad (Eq.1.3)$$

Equation 1.3 shows that the higher is the temperature and/or the supersaturation the smaller is r_C, in agreement with experimental results.[56]

Finally by comparing Equation 1.3 with the Arrhenius equation for the rate of any reaction; the number of critical nuclei per unit time in a unit volume of solution, J, can be calculated by Equation 1.4:[17]

$$J = J_0 \exp(-\Delta G_C/kT) \approx J_0 \exp[-16\ \pi\ \gamma^3/3\ k^3\ T^3\ (\ln S)^2] \qquad (Eq.1.4)$$

Where the pre-exponential factor J_0 depends both on the number of monomer units per critical nucleus and the diffusion coefficient of the monomers. Equation 1.4 explains the utility of the hot-injection method, since supersaturation at high temperature results in small r_C and high nucleation rates.

15

Growth: such a process can be split into two steps. The first is the transfer of monomers to the nuclei through the reaction mixture; so it essentially depends on the diffusion coefficient, D; the second one concerns the growth on the surface of nuclei. Total growth rate can be expressed with Equation 1.5:[19]

$$\frac{dr}{dt} = \frac{2\,\gamma DP}{\rho_m^2\,k_B T} \; \frac{1}{r}\left(\frac{1}{r_c} - \frac{1}{r}\right)$$
(Eq.1.5)

Where ρ_m is the density of monomers in the crystals, P is the vapor pressure of a flat surface and arises from Gibbs-Thompson Equation.

The general dependence of the growth rate on the radius of crystals is illustrated in Figure 1.8:
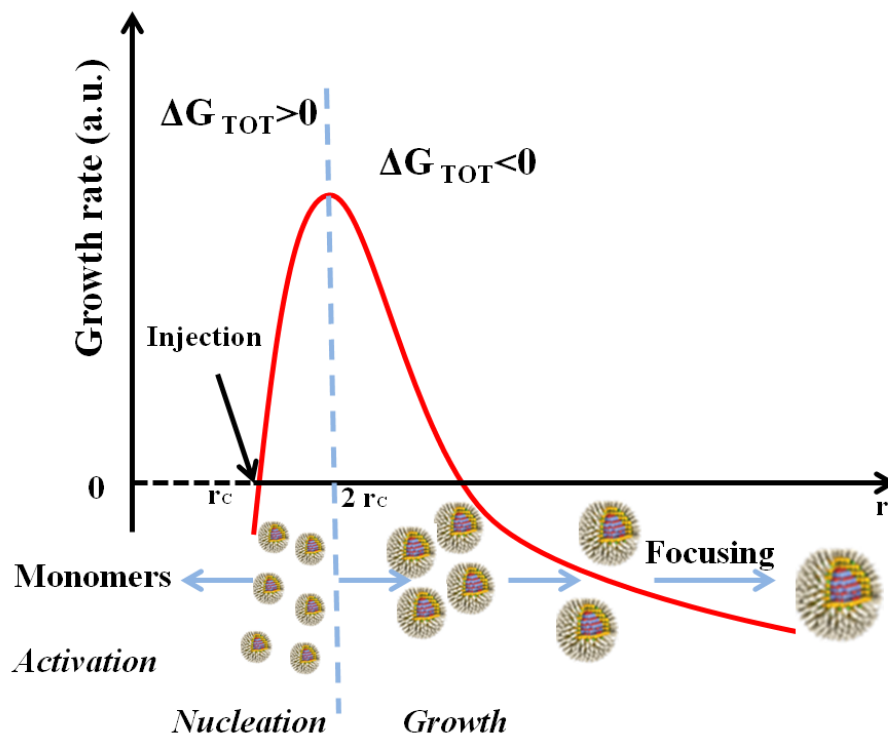

Figure 1.8 Schematic representation of the regimes of the hot injection method.

As predicted from the previous description of the nucleation stage, for nuclei smaller than r_c the growth rate is negative, so disaggregating of the crystallite is favored to the supply of fresh monomers; moreover, it is interesting to point out the maximum of the curve at a value of 2 r_c. If all crystals are bigger than this value then the smaller ones grow faster than the larger ones and the size distribution become narrower over time. This condition is called the size-focusing regime.

During the synthesis the stock of monomers decreases so the critical size increases and as soon as the parameter 2 r_c has reached a value at the lower end of the size distribution, the system goes to the broadening regime. Finally, when the smallest nanocrystals are smaller than r_c the Ostwald ripening occurs with the smallest nanocrystals disaggregating to free monomers which will incorporate then to the large nanocrystals, with a consecutive significant broadening of the size distribution.

It is simple to understand that the efficiency of the size-focusing is affected by the nucleation stage which, ideally, should finish before the diffusion controlled growth step could take place. If nucleation had not finished before growth has started then those nanocrystals nucleated first would have grown already too much, thus resulting in broad size distribution which cannot be improved by size focusing.

The hot injection method involves the pyrolisis of dimethyl cadmium ($CdMe_2$) and trioctylphosphine selenide (TOPSe) at 300°C in trioctylphosphine oxide (TOPO), as a high boiling point solvent. These precursors are usually prepared in an air-free dry-box by mixing the desired amount of $CdMe_2$ and selenium powder in trioctylphosphine, TOP.

The use of organometallic reagents as precursors was inspired by the procedure developed by Brus and co-workers[57] in 1988, through which CdSe nanoclusters were synthesized in reverse micelles by using bis(trimethylsilyl) selenium ($Se(TMS)_2$) and cadmium perchlorate ($Cd(ClO_4)_2$) as starting materials.

Since $CdMe_2$ is pyrophoric, toxic and requires an inert atmosphere,[58] researchers tried to find out novel strategies involving other cadmium sources. Peng and co-workers published in early 2000s many procedures on the synthesis of QDs[59,60] exploiting cadmium oxide (CdO) in combination with several fatty acids, amines or phosphonic acids for preparing high quality CdSe (see Figure 1.9).

With these works 1-octadecene (ODE) has been introduced as non-coordinating and less expensive solvent, thus replacing alkyl phosphines.
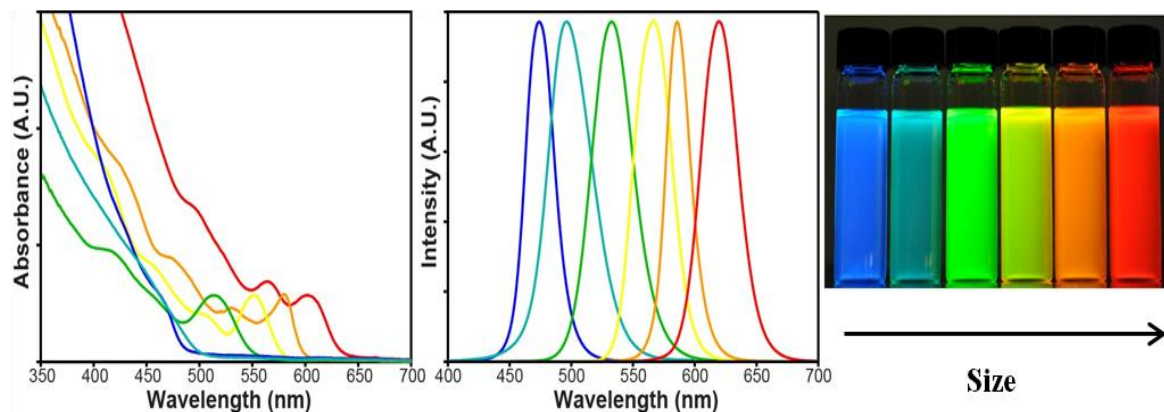

Figure 1.9 Schematic representation of the absorption and luminesce spectra of CdSe QDs of different size.

The QDs illustrated in this dissertation have been prepared by following Peng's protocol with minor modifications and a very recent one developed by Maitra and co-workers[61] which replaces CdO with cadmium deoxycholate as cadmium source.

Alternatively QDs can be fabricated by the high-resolution electron beam lithography and etching.[62,63] However, lithographic methods often produce contamination, defect formation, size non-uniformity, poor quality and are time-consuming and expensive processes; therefore, new more sophisticated techniques for QDs fabrication[64] are required.

One of these techniques is the Molecular Beam Epitaxy (MBE),[65] developed by Arthur and Cho[66] in 1975. Such a method provides a thin-film deposition of single nanocrystals and it is exploited in the manufacture of semiconductor devices, including transistors for cellular phones and Wi-Fi devices. In this case the QDs growth on a surface starting from special precursors in vapour phase; however, the size-control is more difficult.[67]

1.2.3 Core-Shell Quantum Dots

The surface of so-prepared QDs is covered by a monolayer of organic ligands, which can affect their photophysical properties as already discussed. For example, the synthesis in a TOPO/TOP surfactant mixture affords CdSe QDs with relatively low emission quantum yields (less than10%), while the HDA/TOPO/TOP mixture can provide CdSe QDs with relatively very high quantum yields (about 85%).[68]

Nevertheless, the surface cannot be considered as defect-free,[69] simply because of its intrinsic crystalline nature. In addition to dangling orbitals, such surface defects can act as charge-carrier trap states, thus negatively affecting the photophysical properties of the QDs.

However, the QDs can be passivated by another semiconductor material, in order to increase the chemical stability and the photophysical properties, thus providing core-shell systems, whose final properties will depend both on core and shell materials. More precisely, depending on the relative band level positions, three types of Core-Shell QDs can be distinguished,[17] as shown in figure 1.10:
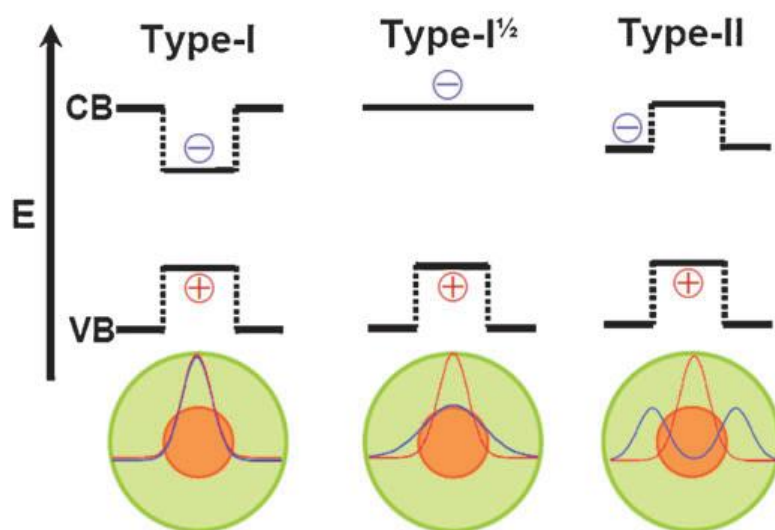

Figure 1.10 Schematic representation of the three limiting charge carrier localization regimes in core-shell quantum dots. Adapted from reference [17]. Courtesy of M. Vis and A.G.M. Brinkman (Utrecht University, Netherlands).

Type I: the band gap of the core is smaller than that of the shell, so the exciton will be physically confined in the core and screened from the surrounding environment, thus giving rise to a new system exhibiting the same optical properties of the core (e.g., absorption and emission spectra) and, at the same time, photophysical properties (e.g., luminescence quantum yields and lifetimes) improved by such a surface passivation.

It is important to note that the energy offsets within the core and the shell are finite, so the exciton can actually move through the shell. Such a process is referred to as exciton leakage and gives rise to the red shift of both absorption and emission spectra. The amount of such a shift is inversely correlated to the entity of the reduction in exciton confinement. So, the smaller the energy offsets the more significant such a red-shift.

The CdSe-ZnS Core-Shell QDs represent the prototype of such systems, but other similar ones such as CdS-ZnS[70] or InP/ZnS[71] have been developed and investigated.

Type I$^{1/2}$: in this system one charge-carrier is confined in the core or in the shell, while the other is delocalized over the entire nanostructure. Example of such a system are CdSe-CdS[72,73] and ZnSe/CdSe[74,75] QDs.

Type II: the staggered energy level alignment gives rise to the spatial separation of the electron and the hole over the whole nanostructure, thus leading to a spatially indirect exciton. These systems show longer radiative lifetimes,[49,74,76] increased exciton polarisability[74] and emission at lower energies respect to the band-gap of both materials.[49,74] Examples of such Core-Shell nanocrystals are CdSe-ZnTe QDs,[77,78] ZnSe-CdS[79] and ZnTe-ZnSe QDs.[80]

Many experiments described in this thesis have been performed with CdSe-ZnS Core-Shell QDs, so a brief discussion about their synthetic protocols is now introduced.

The overcoating of CdSe QDs was reported for the first time by Guyot-Sionnest and co-workers in 1996.[81] This protocol involved highly-reactive organometallic reagents such as diethyl zinc (ZnEt$_2$) and hexamethyldisilathiane (S(TMS)$_2$), which are injected, in only one step, in the reaction mixture containing bare CdSe core QDs. It is possible to obtain CdSe-ZnS QDs with relatively high luminescence quantum yield and photostability by using this method as well as its derivatives.[82]

Peng and co-workers developed in 2003 the so called Single Ion Layer Absorption and Reaction (SILAR) method as an alternative overcoating protocol which involved less reactive and air-stable precursors such as zinc stearate and elemental sulfur (S).[83]

Such a method allows us to deposit a precise number of shell monolayers as well as the preparation of multi-shell QDs, whose core is covered by a shell of different semiconductor materials.[84] In this case the precursors are alternatively injected to the reaction mixture containing bare CdSe core QDs until obtaining a shell of a desired thickness.

Finally, protocols showing the preparation of CdSe-ZnS Core-Shell QDs by using different ZnS precursor, such as zinc diethyldithiocarbamate ($Zn(S_2CNEt_2)_2$),[85] have been recently developed.

1.2.4. Experimental techniques for characterizing Quantum Dots

Spectroscopic, scattering, imaging and computational techniques are required to fully characterize and/or investigate QDs. These techniques provide complementary information about interactions occurring on their surface; composition, structure and intrinsic properties such as thickness, density and dielectric constant of bound ligands.[30]

Absorption spectroscopies: UV-vis spectroscopy allows us to identify the first excitonic peak which is directly correlated with the E_g of nanocrystals, so with their size.

FT-IR allows the investigation of surface ligands such as fatty acids, which exhibit a typical absorption around 3000 cm^{-1} and 1500 cm^{-1}. Moreover, the infrared resonances provide information about the conformation of the capping layer.

Nuclear Magnetic Resonance spectroscopy (NMR): the bound ligands show a typical broadening due to dipolar coupling but cannot be resolved from the signal of the free ligands. Dynamic NMR experiments, such as DOSY, are suitable for resolving such signals.

Small-angle X-ray scattering (SAXS) and *dynamic light scattering (DLS)* focuses on the analysis of the thickness of the capping layer and its contribution to the total hydrodynamic radius.

Transmission electron (TEM) and *scanning probe (STM, AFM) microscopy* allow the morphological investigation of QDs.

Density functional theory (DFT) and *molecular dynamics (MD)* are used to model ligand-surface interactions.

1.2.5 Functional Quantum Dots by post-synthetic surface modification

The QDs are emerging nanostructured materials with unique photophysical properties, that are not observed in their corresponding bulk materials[27,86] such as broad absorption bands with high absorption cross section and high luminescence quantum yield, longer luminescence lifetimes in comparison with classical fluorophores,[87] high photostability[88] and emission wavelengths which can be tuned with their dimension.[22]

Moreover, QDs can be differently decorated through post-synthetic treatments, essentially for making hydrophilic and biocompatible nanohybrids or to attach functional molecules in order to perform specific functions, such as sensing,[89] or processes, such as catalysis.[90,91]

How to obtain water-soluble QDs will be discussed in the third chapter of the thesis.

Bare QDs are not attractive as luminescent sensors because their photophysical properties are hardly affected by the presence of analytes in the surrounding medium (with the exception of some metal ions that can exchange with those on the nanocrystal surface). Then, QDs have to be decorated with ligands bearing a molecular functionality to introduce new recognition functionality; thus providing, for example, a QD based luminescent-chemosensor.[92]

In such a system one (or more) input signal(s), coded for by a change in the analyte(s) concentration, produces a change in a luminescence output.[93,94] A luminescent chemosensor generally consists of a luminophore (L), emitting light upon photoexcitation, a quencher (Q), which can avoid the emission of L by some mechanisms and a control component which can affect the behaviour of Q, as consequence of the external stimulation. A general luminescent chemosensor is represented in Figure 1.11:
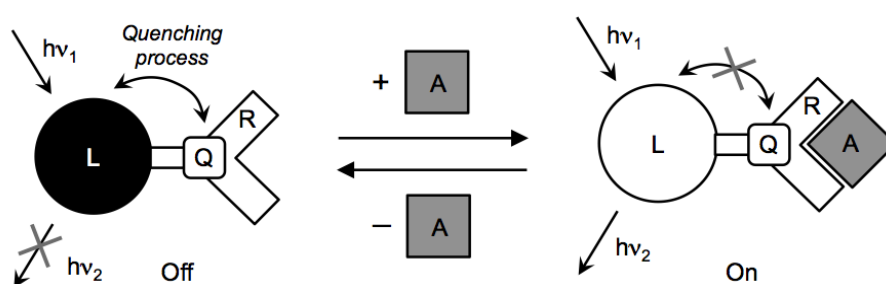

Figure 1.11 Scheme of the analyte-modulated 'turn on' photoluminescence response in a luminophore-quencher-receptor multicomponent chemosensor. Adpated from reference [92]. Copyright Springer 2016.

The ability of the quencher to alter the emission of the luminophore is essentially affected by the binding of the analyte to the receptor. In many cases the quencher and the control component are the same entity.

Both the photoinduced electron and electronic energy transfer processes are useful to provide the modulation of luminescence intensity in supramolecular systems.[93,95] In this chapter some examples of QD-chemosensor based on photoinduced electron transfer (PET) are described, while those based on the electronic energy transfer will be illustrated in Chapter 5.

If a QD is connected to a molecular electron acceptor A, whose LUMO orbital is lower in terms of energy than that of the conduction band edge, then a photoinduced electron transfer from the photoexcited QD to A can occur, accompanied by the quenching of its luminescence (see Figure 1.12 a). Conversely, if a QD is connected with an electron donor D, whose HOMO orbital is higher than that of the valence band edge, an electron transfer from D to the photoexcited QD can occur (see Figure 1.12 b).
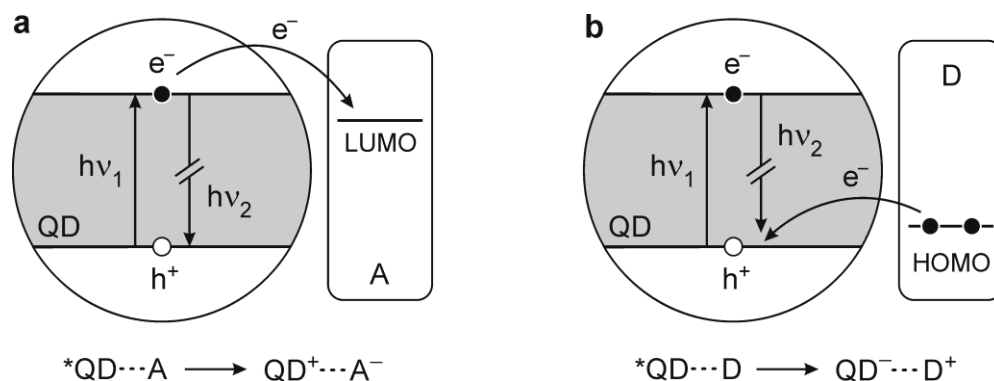
Figure 1.12 Schematization of the PET occurring (a) from the photoexcited QD to an electron acceptor A, and (b) from an electron donor D to a photoexcited QD. Adapted reference [92]. Copyright Elsevier 2014.

The kinetics of the PET processes will depend on redox potentials, distance, electronic coupling of the components; so, if one or more of such parameters can be affected by external stimulation then a switching behaviour can be achieved.

Mews and coworkers[96] have investigated CdTe and CdSe QDs functionalized with surfactants consisting of a 1,10-phenanthroline moiety directly bound to an azacrown ether. In such a system QDs are quenched because of the PET occurring from the phenanthroline to the photoexcited QDs. By taking advantage of a host-guest interaction between the azacrown ether moiety and Ba^{2+} ions it is possible to modulate the PET efficiency in a way that depends both on the dimension and the composition of the nanocrystals. More in detail, for CdSe QDs with a diameter of 2.5 and 3 nm, and for CdTe QDs 2.5 nm in diameter, the emission intensity decreases by adding Ba^{2+} ions. Larger CdTe QDs show the reverse behaviour, since in this case the host-guest interaction lowers the HOMO level of the ligands below the valence band edge of QDs, thus avoiding the PET to the photoexcited QD, as shown in figure 1.13:
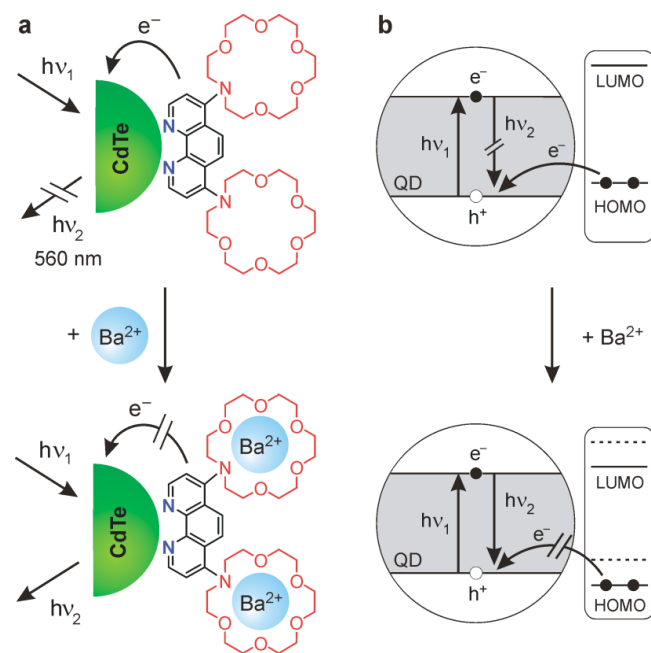
Figure 1.13 Schematic representation (a) and simplified energy-level diagram (b) of the luminescent sensing of Ba^{2+} ions with CdTe QDs functionalized with 1,10-phenanthroline-azacrown ether ligands. Adapted from reference [92]. Copyright Springer 2016.

PET can also occur from QDs to the ligands, as in the case of QDs-urea nanohybrids.[97] The luminescence is quenched by the thiol moieties of functional ligands, which can play as hole-acceptors. If the ureidic moiety complexes CO_3^{2-} anions, then an enhancement of the luminescence intensity of QDs occurs. In this case the binding of the analyte gives rise to the shift of the reduction potential of the ligands to more negative value as well as to their rigidification, thus avoiding the photoinduced electron transfer process.

These nanohybrids exhibit remarkable selectivity for CO_3^{2-} with respect to several anions (e.g., halides, NO_3^-, HPO_4^{2-}, $H_2PO_4^-$, HCO_3^-, HSO_4^-).

A chloride ion sensor was also developed by decorating CdSe-ZnS Core-Shell QDs with lucigenin,[98] an acridinium dication able to detect Cl⁻ anions. In absence of chloride anions, both QDs and lucigenin are quenched because of PET occurring from the nanocrystals to the ligand (see Figure 1.14); while in presence of Cl⁻ ions, a further decrease of lucigenin emission and an enhancement of QDs luminescence were observed. Such a chemosensor has been also seen to have a negligible response with respect to several anions (e.g., SO_4^{2-}, NO_3^-, PO_4^{3-}, CH_3COO^-, $HClO_4^-$, HCO_3^-) and tested both in simulated physiological experiments and fluorescence lifetime imaging applications, exhibiting a promising applicability.[99]
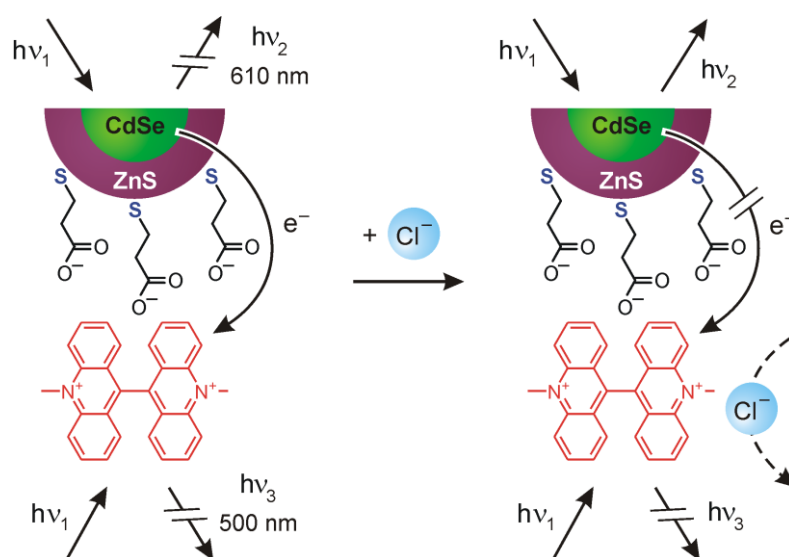

Figure 1.14. Schematic representation of Cl⁻ sensing occurring in CdSe-ZnS QDs and lucigenin based chemosensor. Adapted from reference [92]. Copyright Springer 2016.

Nanohybrids not showing any interaction with the QDs and the functional ligands have also been developed. In this case the QD provides a luminescent signal useful as an internal reference for ratiometric sensing. An example of such a system is the ratiometric oxygen sensor[100] schematized in Figure 1.15:
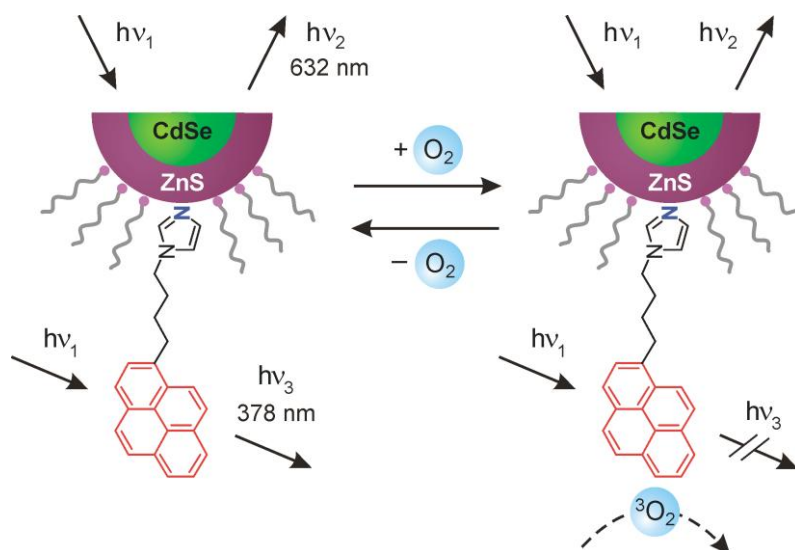
Figure 1.15 Schematic representation of the oxygen sensor consisting of CdSe-ZnS QDs decorated with an imidazole-based surfactant bearing a pyrenyl unit. Adapted from reference [92]. Copyright Springer 2016.

This system has been obtained by decorating CdSe-ZnS Core-Shell QDs with an imidazole based surfactant bearing a pyrenyl moiety. The luminescence spectrum of such a species exhibits two bands with different dependence on the oxygen (see Figure 1.16); in particular the pyrene type emission is dynamically quenched by oxygen (following the Stern-Volmer relation), while the QD emission is unaffected by the presence of oxygen. Therefore, the QD emission can be used as an internal standard for normalizing the response signal of the pyrenyl moiety, thus forming the basis for a ratiometric sensor.
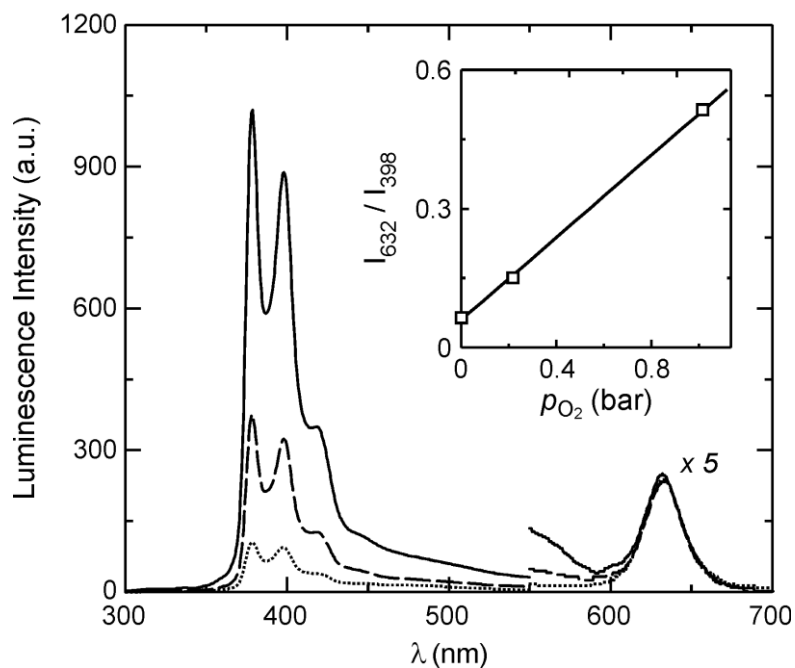
Figure 1.16 Luminescence spectra of the QD-pyrene nanohybrids in chlorform as a function of the O_2 pressure: 0 (———), 0.213 (– – –) and 1.013 (······) bar. The spectra have been recorded by exciting at 275 nm. The inset shows the linear correlation between the ratiometric photoluminescence response (calculated as the QD-to-pyrene emission intensity ratio) and the O_2 partial pressure. Adapted from reference [100]. Copyright RSC Publishing 2011.

References

(1) Taniguchi, N. *On the Basic Concept of Nano-Technology* **1974** Proc. Intl. Conf. Prod. Eng. Tokyo, Part II, Japan Society of Precision Engineering.

(2) Aviram, A.; Ratner, M.A. *Chem. Phys. Lett.* **1974**, *29*, 277-283.

(3) Serp, P.; Philippot, K. *Nanomaterials in Catalysis* **2013** Wiley-VCH Verlag GmbH & Co. KGaA.

(4) Feynman, R.P. *Eng. Sci.* **1960**, *23*, 22-36.

(5) Feynman, R.P. There's a plenty of room at the bottom http://www.its.caltech.edu/~feynman/plenty.html

(6) Balzani, V. *Small* **2005**, *1*, 278-283.

(7) Service, R.F. *Science* **2001**, *293*, 785-786.

(8) Totzeck, M.; Ulrich, W.; Göhnermeier, A.; Kaiser, W. *Nat. Photonics* **2007**, *1*, 629-631.

(9) Perry, J.W. *Science* **2009**, *324*, 892-893.

(10) Schmidt, O.G.; Eberl, K. *Nature* **2001**, *410,* 168.

(11) Hana, H.; Huangb, Z.; Lee, W. *Nanotoday* **2014**, *9*, 271-304.

(12) Ruoshan, W.; Pedone, D.; Zurner A.; Doblinger M.; Rant, U. *Small* **2010**, *6*, 1406-1414.

(13) Moore, G.E. *Electronics* **1965**, *38*, 82-85.

(14) Balzani, V.; Credi, A.; Venturi, M. *Molecular Devices and Machine-Concepts and Perspectives for the Nanoworld*; 2nd ed.; Wiley-VCH Verlag: Weinheim, 2008.

(15) Balzani, V.; Credi, A.; Venturi, M. *Chem. Eur. J.* **2002**, *8*, 5524-5532.

(16) Hla, S.-W.; Meyer, G.; Rieder, K.-H. *Chem. Phys. Chem.* **2001**, *2*, 361-366.

(17) de Mello Donegà, C. *Chem. Soc. Rev.*, **2011**, *40*, 1512-1546.

(18) Atkins, P.W. *Chimica Fisica* **1997** Zanichelli: Bologna.

(19) Rogach, A.L. (Ed.) *Semiconductor Nanocrystal Quantum Dots*; Springer-Verlag: Wien, 2008.

(20) Efros, A.L.; Rosen, M. *Annu. Rev. Mater. Sci.* **2000**, *30*, 475-521.

(21) Zych, E.; Meijerink, A.; de Mello Donega, C. *J. Phys.: Condens.Matter* **2003**, *15*, 5145-5155.

(22) Murray, C.B.; Kagan, C.R.; Bawendi, M.G. *Annu. Rev. Mater. Sci.* **2000**, *30,* 545-610.

(23) Ozbay, E. *Science*. **2006**, *311*, 189-193.

(24) Bell, A.. *Science* **2003**, *299*, 1688-1691.

(25) Yin, Y.; Alivisatos, A.P. *Nature* **2005**, *437*, 664-670.

(26) Green, M.L.H *J. Organomet. Chem.* **1995**, *500,* 127-148.

(27) Talapin, D.V.; Lee, J.; Kovalenko, M.V.; Shevchenko, E.V. *Chem. Rev.* **2010**, *110*, 389-458.

(28)   Koole, R.; Luigjes, B.; Tachiya, M.; Pool, R.; Vlugt, T.J.H.; de Mello Donegà, C.; Meijerink, A.; Vanmaekelbergh, D. *J. Phys.Chem. C*, **2007**, *111*, 11208-11215.

(29)   Medintz, I.L.; Mattoussi, H.; Clapp, A.R. *Int. J. Nanomedicine* **2008**, *3*, 151-167.

(30)   Bole, M.A.; Ling, D.; Hyeon, T.; Talapin, D.V. *Nature Mater.* **2016**, *15*, 141-153.

(31)   Anderson, N.C; Hendricks, M.P.; Choi, J.J, Owen, J.S *J. Am. Chem. Soc.* **2013**, *135*, 18536-18548.

(32)   Owen, J. *Science* **2015**, *347*: 615-616.

(33)   Kovalenko, M.V.; Scheele, M.; Talapin, D.V. *Science.* **2009**, *324*, 1417-1420.

(34)   Nag, A.; Kovalenko, M.V.; Lee, J.S.; Liu, W.; Spokoyny, B.; Talapin, D.V. *J. Am. Chem. Soc.* **2011**, *133*, 10612-10620.

(35)   Llordes, A.; Garcia, G.; Gazquez, J.; Milliron, D.J. *Nature.* **2013**, *500*, 323-326.

(36)   Pellegrino, T.; Manna, L.; Kudera, S.; Liedl, T.; Koktysh, D.; Rogach, A.L.; Keller, S.; Rädler, J.; Natile, G.; Parak, W.J *Nano Lett.* **2004**, *4*, 703-707.

(37)   Brus, L. *J.Phys. Chem.* **1986**, *90*, 2555-2560.

(38)   Seker, F.; Meeker, K.; Kuech, T.F.; Ellis, A.B. *Chem. Rev.* **2000**, *100*, 2505-2536.

(39)   Kahn, A. *Surf. Sci.* **1994**, *299-300*, 469-486.

(40)   Huang, W.J.; Sun, R.; Tao, J.; Menard, L.D.; Nuzzo, R.G.; Zuo, J.M. *Nat. Mater.* **2008**, *7*, 308-313.

(41)   Lovingood, D.D.; Achey, R.; Paravastu, A.K.; Strouse, G.F. *J. Am. Chem. Soc.* **2010**, *132*, 3344-3354.

(42)   Schwartz, D.K. *Annu. Rev. Phys. Chem.* **2001**, *52*, 107-137.

(43)   Jackson, A.M.; Hu, Y.; Silva, P.J.; Stellacci, F. *J. Am. Chem. Soc.* **2006**, *128*, 11135-11149.

(44)   Bullen, C.; Mulvaney, P. *Langmuir,* **2006**, *22*, 3007-3013.

(45)   Munro, A.M.; Plante, I.J.; Ng, M.S.; Ginger, D.S. *J. Phys. Chem. C* **2007**, *111*, 6220-6227.

(46)   Kalyuzhny, G.; Murray, R.W. *J. Phys. Chem. B* **2005**, *109*,7012-7021.

(47)   Matylitsky, V.V.; Dworak, L.; Breus, V.V.; Basche, T.;´ Wachtveitl, J. *J. Am. Chem. Soc.* **2009**, *131*, 2424-2425.

(48)   Wuister, S.F.; de Mello Donega, C.; Meijerink, A. *J. Phys. Chem. B* **2004**, *108*, 17393-17397.

(49)   Koole, R.; Schapotschnikow, P. de Mello Donega, C.; Vlugt, T.J.H.; Meijerink, A. *ACS Nano* **2008**, *2*, 1703-1714.

(50)   de Mello Donegà, C. *Phys. Rev. B* **2010**, *81*, 165303-20.

(51)   Efros, A.L. *Soviet Physics Semiconductors* **1982**, *16*, 772-775.

(52)   Henglein, A. *Phys. Chem. Chem. Phys* **1982**, *86,* 301-305.

(53)   Rossetti, R.; Brus, L. *J. Phys. Chem* **1982**, *86*, 4470-4472.

(54)   Rossetti, R.; Nakahara, S.; Brus, L. *J. Chem. Phys* **1983**, *79,* 1086-1088.

(55) Murray, C.B.; Norris, D.J.; Bawendi, M.G. *J. Am. Chem. Soc.* **1993**, *115*, 8706-8715.

(56) Bullen, C.; Mulvaney, P. *Nano Lett.* **2004**, *4*, 2303-2307.

(57) Steigerwald, M.L.; Alivisatos, A.P.; Gibson, J.M.; Harris, T.D.; Kortan, R.; Muller, A.J.; Thayer, A.M.; Duncan, T.M.; Douglass, D.C.; Brus, L.E. *J. Am. Chem. Soc.* **1988**, *110*, 3046-3050.

(58) Material safety data sheet_Dimethyl Cadmium http://www.strem.com/catalog/v/48-5040/10/cadmium_506-82-1.

(59) Qu, L.; Peng, Z.A.; Peng, X. *Nano Lett.* **2001**, *1*, 333-337.

(60) Yu, W.W.; Peng, X. *Angew. Chem. Int. Ed.* **2002**, *41*, 2368-371.

(61) Chakrabarty, A.; Chatterjee, S.; Maitra, U. *J. Mater. Chem. C* **2013**, *1,* 2136-2144.

(62) Ng, J *Microelectron. J*. **2006**, *37*, 1446-1450.

(63) Djenizian, T.; Balaur, E.; Schmuki, P. *Nanotechnology* **2006**, *17*, 2004-2007.

(64) Dai, C.A.; Wu, Y.L.; Lee, Y.H.; Chang, C.J.; Su, W.F. *J. Cryst. Growth* **2006**, *288*, 128-136.

(65) Xin, S.H.; Wang, P.D.; Yin, A.; Kim, C.; Dobrowolska, M.; Merz, J.L.; Furdyna, J.K.. *Appl. Phys. Lett.* **1996**, *69*, 3884-3886.

(66) Cho, A.Y.; Arthur, J.R. *Solid State Chem*. **1975**, *10*, 157-192.

(67) Shirasaki, Y.; Supran, G.J.; Bawendi, M.G.; Bulović, V. *Nat. Photonics* **2013**, *7*, 13-23.

(68) de Mello Donegà, C.; Hickey, S.G.; Wuister, S.F.; Vanmaekelbergh, D.; Meijerink, A. *J. Phys. Chem. B* **2003**, *107*, 489-496.

(69) Kuno, M.; Lee, J.K.; Dabbousi, B.O.; Mikulec, F.V.; Bawendi, M.G. *J. Chem. Phys.* **1997**, *106*, 9869-9882.

(70) Fanga, D.F.; Zhangb, Z.M.; Wangb, Z.P.; Dinga, Z.J. *Physics Procedia* **2012**, *32*, 920-925.

(71) Brunetti, V.; Chibli, H.; Fiammengo, R.; Galeone, A.; Malvindi, M.A.; Vecchio, G.; Cingolani, R.; Nadeaub, J.L.; Pompa, P.P. *Nanoscale* **2013**, *5*, 307-317.

(72) Pandey, A.; Guyot-Sionnest, P. *J. Chem. Phys.* **2007**, *127*, 111104-4.

(73) Li, J.J.; Wang, Y.A.; Guo, W.; Keay, J.C.; Mishima, T.D.; Johnson, M.B; Peng, X. *J. Am. Chem. Soc.* **2003**, *125*, 12567-12575.

(74) Ivanov, S.A.; Piryatinski, A.; Nanda, J.; Tretiak, S.; Zavadil, K.R.; Wallace, W.O.; Werder, D.; Klimov, V.I. *J. Am. Chem. Soc*. **2007**, *129*, 11708-11719.

(75) Blues, J.; Carayon, S.; Reiss, P. *Phys. E.* **2004**, *21*, 331-334.

(76) Oron, D.; Kazes, M.; Banin, U. *Phys. Rev. B* **2007**, *75*, 035330-7.

(77) Kim, S.; Fisher, B.; Eisler, H.; Bawendi, M.G. *J. Am. Chem. Soc*. **2003**, *125*, 11466-11467.

(78) Xie, R.; Kolb, U.; Basche, T. *Small* **2006**, *2*, 1454-1457.

(79) Hewa-Kasakarage, N.N.; Kirsanova, M.; Nemchinov, A.; Schmall, N.; El-Khoury, P.Z.; Tarnovsky, A.N., Zamkov, M. *J. Am. Chem. Soc.* **2009**, *131*, 1328-1334.

(80) Bang, J.; Park, J.; Lee, J.H.; Won, N.; Nam, J.; Lim, J.; Chang, B.Y.; Lee, H.J.; Chon, B. Shin, J.; Park, J.B; Choi, J.H.; Cho, K.;. Park, S.M.; Joo, T.; Kim, S. *Chem. Mater.* **2010**, *22*, 233-240.

(81) Hines, M.; Guyot-Sionnest, P. *J. Phys. Chem.* **1996**, *100*, 468-471.

(82) Dabbousi, B.O.; Mikulec, F.V; Heine, J.R.; Mattoussi, H.; Ober, R.; Jensen, K.F.; Bawendi, M.G. *J. Phys. Chem. B* **1997**, *101*, 9463-9475.

(83) Li, J.J.; Wang, Y.A.; Guo, W.; Keay, J.C.; Mishima, T.D.; Johnson, M.B.; Peng, X. *J. Am. Chem. Soc.* **2003**, *125*, 12567-12575.

(84) Xie, R.; Kolb, U.; Li, J.; Basche, T.; Mews, A. *J. Am. Chem. Soc.* **2005**, *127*, 7480-7488.

(85) Dethlefsen, J.R.; Døssing, A. *Nano Lett.* **2011**, *11*, 1964-1969.

(86) Alivisatos, A.P. *J. Phys. Chem.* **1996**, *3654*, 13226-13239.

(87) Lounis, B.; Bechtel, H.A.; Gerion, D.; Alivisatos, A.P.; Moerner, W.E. *Chem. Phys. Lett.* **2000**, *329*, 399-404.

(88) Jaiswal, J.K.; Mattoussi, H.; Mauro, J.M.; Simon, S.M. *Nat. Biotechnol.* **2003**, *21*, 47-51.

(89) de Silva, A.P.; Gunaratne, H.Q.N.; Gunnlaugsson, T.; Huxley, N.A.J.M; McCoy, C.P.; Rademacher, J.T.; Rice, T.E. *Chem. Rev.* **1997**, *97*, 1515-1566.

(90) Chaudhary, G.R.; Bansal, P.; Mehta S.K. *Chem. Eng. J.* **2014**, *243*, 217-224.

(91) Jensen, S.C.; Homan, S.B.; Weiss, E.A. *J. Am. Chem. Soc*. **2016**, *138*, 1591-1600.

(92) Silvi, S.; Baroncini, M.; La Rosa, M.; Credi, A. *Topics in Current Chemistry (Z)* **2016**, *374*, 65.

(93) Yildiz, I.; Deniz, E.; McCaughan, B.; Cruickshank, S.F.; Callan, J.F.; Raymo, F.M. *Langmuir* **2010**, *26*, 11503-11511.

(94) Baly, B.; Ling, J.; de Silva, A.P. *Chem. Soc. Rev*. **2015**, *4,* 4203-4211.

(95) Erathodiyil, N.; Ying, J.Y. *Acc. Chem. Res.* **2011**, *44*, 925-935.

(96) Völker, J.; Zhou, X.; Ma, X.; Flessau, S.; Lin, H.; Schmittel, M.; Mews, A. *Angew. Chem. Int. Ed.* **2010***, 49,* 6865-6868.

(97) Han, C.; Cui, Z.; Zou, Z.; Tian, S.D.; Li, H. *Photochem. Photobiol. Sci.* **2010**, *9*, 1269-1273.

(98) Ruedas-Rama, M.J.; Orte, A.; Hall, E.A.H.; Alvarez-Pez, J.M.; Talavera, E.M. *Analyst* **2012**, *137*, 1500-1508.

(99) Avellini, T.; Lincheneau, C.; Vera, F.; Silvi, S.; Credi, A. *Coord. Chem. Rev*. **2014**, *151***,** 263-264.

(100) Amelia, M.; Lavie-Cambot, A.; McClenaghan, N.D.; Credi, A. *Chem. Commun.* **2011**, *47*, 325-327.

Chapter 2
Materials, experimental procedures and techniques

2.1 Chemical Reagents

Cadmium oxide (CdO, 99.99%), cadmium nitrate tetrahydrate ($Cd(NO_3)_2$, 98%), selenium powder (Se, 99.5%, 100 mesh), sulfur elemental (S, 99.98%, powder), n-trioctylphosphine oxide (TOPO, 90%), n-trioctylphosphine (TOP, 97%), tributylphosphine (TBP, mixture of isomers, 97%), 1-octadecene (ODE), n-hexadecylamine (HDA, 98%), stearic acid (reagent grade, 95%), oleic acid (OLA, ≥99%), deoxycholic acid (≥99%, HPLC), sodium deoxycholate (≥97%), n-octadecylamine (ODA, 97%), diethyl zinc ($ZnEt_2$, 1 M solution in n-heptane), hexamethyldisilathiane ($S(TMS)_2$, synthesis grade), lipoic acid (LA, (±)-α-lipoic acid, ≥98%), R-(+)- α-lipoic acid (≥98.0% (HPLC)), tetrabutylammonium borohydride ($TBABH_4$, 98%), sodium borohydride ($NaBH_4$, ReagentPlus®, 99%) Amberlite IRA 400 (chloride form), N-hydroxysuccinimide (NHS, 98%) polyethylene glycol 400 (PEG_{400}, average Mn 400), dicyclohexylcarbodiimide (DCC, 99%); 4-(dimethylamino)pyridine (DMAP, puriss. ≥99%) lithium diisopropylamide (LDA, 2.0 M soution in tetrahydrofuran), phthalimide potassium salt (98%), hydrazine hydrate (reagent grade, N_2H_4 50-60 %), magnesium sulfate ($MgSO_4$, reagent grade, ≥99.5%) have been purchased from Sigma Aldrich and used without further purification. Zinc oxide (ZnO, 99.99% (metals basis)), sulfur powder (S, 99.5%, -325 mesh) were purchased from Alfa Aesar. Ruthenium (II) bis(bipyridyl) dichloride was purchased from Strem.

Solid samples have been weighted on a Mattles AT261 balance (sensitivity 0.01 mg, experimental error estimated less than 10%).

Synthetic grade hexane, cyclohexane, toluene (Tol), chloroform ($CHCl_3$), diethyl ether (Et_2O), methanol (MeOH), ethanol (EtOH), acetone ($CO(CH_3)_2$), ethyl acetate (EtOAc), tetrahydrofuran (THF), acetonitrile (CH_3CN) and dimethylformamide (DMF) have been purchased from Sigma-Aldrich.

Deuterated solvents Chloroform (Chloroform-d, "100%", 99.96 atom % D) and Acetonitrile (Acetonitrile-d, "100%", 99.96 atom % D) were purchased from Sigma Aldrich and used for the NMR characterization.

Chloroform, methanol, hexane, acetonitrile, provided by UvaSol have been used for spectroscopy measurements.

Millipore Amicon Ultra-15 mL centrifugal filters (30 KDa cut off) were purchased from Sigma-Aldrich.

2.2 Synthesis of Semiconductor Nanocrystal Quantum Dots

CdSe and CdS Core and CdSe-ZnS Core-Shell(s) Quantum Dots (QDs) used in the experiments described in this manuscript have been synthesized following literature methods.

2.2.1 Synthesis of CdSe Quantum Dots

Hydrophobic CdSe Core QDs have been prepared following the protocols developed by Peng and coworkers[1] or Maitra and co-workers[2] with slight modifications.

Peng's protocol: CdO (25.62 mg, 0.2 mmol), stearic acid (227.58 mg, 0.8 mmol) and 2 g of ODE were mixed in a 25 mL three-neck flask and heated to about 200°C until a colorless clear solution had been obtained.

After this solution had been cooled to room temperature, 1.5 g of ODA or 1.34 g of HDA (5.56 mmol) and 0.5 g (1.29 mmol) of TOPO were added into the flask. The resulting mixture was first degassed under vacuum at about 120°C for 1 hour, then re-equilibrated with argon and reheated to about 300°C. In a nitrogen filled dry box (MBraun Lab-Star, MB10), 160 mg of selenium in powder (2 mmol) were mixed with 2 mL of TOP in a 8 mL glass vial equipped with rubber septum. The TOP-Se precursor solution was quickly injected to the cadmium precursor solution.

After the injection, the growth temperature was set to a value 20°C-30°C lower than the injection temperature, and the mixture turned very rapidly from colorless to light yellow, orange and dark red colors. During the synthesis, aliquots were taken to check the size of growing nanocrystals.

When the desired size had been reached, the reaction was stopped by cooling down the mixture to room temperature, then an extraction procedure[2] was used to purify the nanocrystals from side products and unreacted precursors. The nanocrystals remained in the hydrophobic hexanes/ODE layer, while the unreacted precursors and the free-ligand excess were extracted with methanol. Alternatively, QDs were dissolved in a small amount of $CHCl_3$ and suspended by adding MeOH in order to remove excess free ligands, and finally centrifuged at 5000 rpm for 10 minutes at 25°C. The supernatant was removed and the QDs redissolved in $CHCl_3$. Such a cycle of solution/suspension/centrifugation was repeated at least three times.

Finally QDs were redissolved and stocked in hexane or chloroform solutions for further investigation and/or manipulations. The concentration of QDs was determined by the Lambert-Beer's law with the reported extinction coefficients of CdSe nanocrystals.[3]

Maitra's protocol: A solution of $Cd(NO_3)_2$ in MeOH (30 mL, 50 mM) was added to a methanolic solution of sodium deoxycholate (180 mL, 25 mM) and stirred. A fine precipitate of cadmium deoxycholate started appearing within a minute and the solution became viscous. After 15 min the formation of a gel had been observed and the mixture has been stirred for another 45 min. The white precipitate was filtered off, washed with cold MeOH (2 x 5 mL) and dried overnight under vacuum.

Then cadmium deoxycholate (0.049 g, 0.05 mmol), deoxycholic acid (0.128 g, 0.32 mmol), HDA (1 g, 4.14 mmol) and TOPO (1 g, 2.6 mmol) were placed in a three neck round bottom flask, degassed under vacuum and heated up to 300°C under argon flow.

0.5 mL of TOPSe solution was prepared by dissolving selenium powder (0.039 g, 0.5 mmol) in TOP (0.5 mL, 1.1 mmol) and quickly injected to the cadmium precursor solution. After the injection, the growth temperature was kept at 290°C.

During the synthesis, aliquots were taken to check the size of growing nanocrystals. When the desired size had been reached, the reaction was stopped by cooling the mixture to room temperature.

Finally QDs were purified by precipitation using acetone/MeOH (5:1, v/v). The precipitate was isolated by decantation and centrifugation, and redissolved in $CHCl_3$ for further studies.

2.2.2 Synthesis of CdSe-ZnS Core-Shell Quantum Dots

CdSe-ZnS Core-Shell Quantum Dots can be synthesized by following two different methods depending essentially on their size. The first one is the Single Ion Layer Adsorption and Reaction (SILAR), developed by Peng and co workers[4] and the second one is the one-time precursors injection developed by Guyot-Sionnest and coworkers.[5]

The SILAR method consists essentially of alternate injections of zinc (Zn) and sulfur (S) precursors in a solution containing bare CdSe nanocrystals. The amount of Zn and S precursors required for each ZnS shell is determined by the number of surface atoms of a given core QD sample, by taking into account the relative small (i.e., 10%) lattice mismatch between CdSe and ZnS bulk crystals in the wurtzite structure.

The average thickness of one ZnS shell is 0.31 nm. So the first ZnS shell should increase the diameter of a CdSe nanocrystal by 0.62 nm.

Shell precursors have been prepared in two different 20 mL scintillation vials equipped with rubber septa. The zinc precursor was prepared by dissolving 0.325 g (4 mmol) of ZnO, 0.904 g (3.2 mmol) of OLA and 7.09 g of ODE at 250°C. The sulfur precursor was prepared by dissolving 12.8 mg (0.4 mmol) of elemental sulfur in 7.88 g of ODE at 150°C. During the heating step, both solutions are degassed under vacuum and equilibrated with argon. Before the injection, the precursors were allowed to cool down to 80°C.

In a typical synthesis, bare CdSe core QDs (1.6×10^{-4} mmol, 3.4 nm in size) dissolved in a minimum amount of chloroform or hexane, were mixed with 2.4 g (8.9 mmol) of ODA and 8 g of ODE in a 100 ml three-neck round bottom flask. The mixture was carefully degassed under vacuum at 30°C to remove low-boiling point solvents.
Then, the solution was kept under reduced pressure for 1 h and 30 min. Additional heating at 120°C for 15 min was performed in order to remove any traces of solvents and water. Then, under argon flow, the temperature was increased at 230°C for the growth of the shell. In such conditions 2.74×10^{-2} mmol of Zn and S precursors are required for the first shell, 3.67×10^{-2} mmol for the second layer and 4.72×10^{-2} mmol for the third layer and so on.

After injection, the solution was kept under stirring at 230°C for 20 minutes before the injection of the second precursor, in this case the S precursor. These injection cycles were repeated to reach the desired shell thickness; then, the reaction was stopped by cooling the reaction mixture at room temperature.

Finally CdSe-ZnS Core-Shell QDs were purified as just described above for CdSe core samples.

The one-time precursors injection reaction was reported the first time by Guyott-Sionnest[5] in 1996 and further developed by Dabbousi and co-workers in 1997.[6] This method is based on the simultaneous single injection of the precursors required for a desired shell thickness. Highly reactive diethyl zinc ($ZnEt_2$) and hexamethyldisilathiane ($S(TMS)_2$) were used as zinc and sulfur precursors respectively.

This method allows to coat small CdSe QDs since the reaction temperature is relatively low. The amount of precursors were calculated in the same way as the SILAR method.

In a typical synthesis, 13 g (3.3 mmol) of TOPO and 1.3 g (4.82 mmol) of ODA were loaded in a 100 mL three-neck round bottom flask and degassed under reduced pressure at 120°C followed by equilibrating with argon. Temperature was decreased to 30°C and a hexane solution containing (1.6×10^{-4} mmol) of 3.4 nm CdSe core QDs was added to the mixture. The solvent was removed under vacuum and the reaction mixture was further heated at 115°C for 15 minutes in order to remove any traces of water.

Under argon flow the temperature was further increased to a proper value, depending on the size.[6] For example, in the case of 3.4 nm CdSe core the temperature was 150°C. A proper amount of Zn and S precursor (0.1 M in TOP) prepared in a nitrogen filled dry box, was injected dropwise over a period of 5-10 minutes. Then the temperature was dropped to 90°C for several hours in order to allow the coating of the shell on the CdSe core.

Finally, the solution was allowed to cool down, chloroform was added and, finally, QDs were purified by either the extraction procedure or the dissolution/suspension/centrifugation method.

The choice between the first and the second method depends on the dimension of the CdSe core. For small QDs (diameter < 3.4 nm) the one pot method is more suitable, simply because it requires the use of very reactive zinc and sulfur precursors such as $ZnEt_2$ and $S(TMS)_2$ but the reaction can be performed at relatively low temperature at which smaller CdSe nanocrystals are stable without undergoing to the Ostwald ripening process.

For relatively large QDs (diameter > 3.4 nm) both methods can be used; however, the SILAR is more convenient and safe owing to the use of less reactive precursors such as ZnO and elemental sulfur and, moreover, it allows a fine modulation of the zinc sulfide shell thickness. Nevertheless the reaction temperature in this case has to be higher for activating the precursors.

2.2.3 Synthesis of CdS Quantum Dots

Hydrophobic CdS core QDs were synthesized through a method reported by Peng and coworkers.[7]

Typically, a mixture of 0.0128 g (0.10 mmol) of CdO, 0.282 g (1 mmol) of OLA and 3.7 g of ODE was heated to 300°C. A solution of sulfur, made by dissolving 0.016 g (0.05 mmol) in 2 mL of ODE was swiftly injected into this hot solution, and the reaction mixture was allowed to cool to 250°C for the growth of CdS nanocrystals. Aliquots were taken during the growing; when the desired size was reached the reaction mixture was allowed to cool to room temperature. The same procedure described above for purificating CdSe nanocrystals were adopted also for CdS QDs. The particle concentration of the purified CdS solution in hexanes was measured using Beer's law with the reported extinction coefficients of CdSe nanocrystals.[3]

2.3 Synthesis of lipoic acid-based surface ligands

2.3.1 Synthesis of *2,5-dioxopyrrolidin-1-yl 5-(1,2-dithiolan-3-yl) pentanoate*
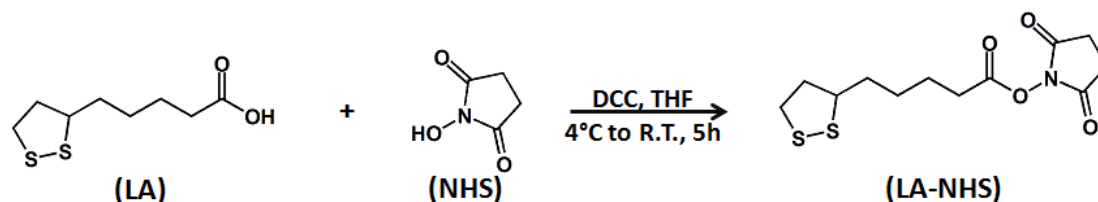
Scheme 2.1 Synthetic route for preparing the activated ester of lipoic acid (LA-NHS).

Synthetic procedure:

2,5-Dioxopyrrolidin-1-yl 5-(1,2-dithiolan-3-yl)pentanoate (LA-NHS) was prepared from lipoic acid (LA) by following a reported procedure.[8]

Briefly, a solution of DCC (6.00 g, 29.1 mmol) in 10 mL of THF was added dropwise to a solution of LA (5.00 g, 24.23 mmol) and NHS (3.35 g, 29.1 mmol) in 150 mL of THF at 4°C. The mixture was then warmed to room temperature and stirred for 5 h. The precipitate was removed by filtration under vacuum; then the solvent was evaporated under reduced pressure. The crude product was redissolved in 100 mL of EtOAc and filtered once again. Finally, the product was recrystallized from a solution of EtOAc/Hexane (1:1; v/v) as a pale-yellow solid (yield =80%).

The NMR spectrum recorded is in agreement to that already reported in literature:
^{1}H NMR (300 MHz, CDCl$_3$); δ (ppm): 3.58 (m, 1H), 3.13 (m, 2H), 2.84 (s, 4H), 2.63 (t, J = 7.1 Hz, 2H), 2.50 (m, 1H), 1.99-1.46 (m, 7H).

2.3.2 Synthesis of *5-(1,2-dithiolan-3-yl)-N-(pyren-1yl-methyl) pentanamide*
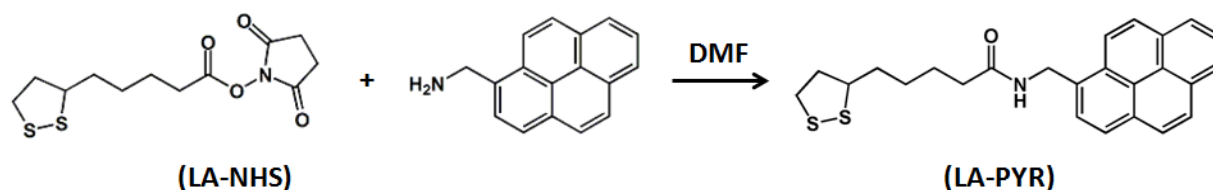
Scheme 2.2 Synthetic route for preparing LA-PYR.

Synthetic procedure:

5-(1,2-Dithiolan-3-yl)-N-(pyren-1-ylmethyl)pentanamide (LA-PYR).

1-Methylamine pyrene hydrochloride (1g, 3.73 mmol) was suspended in 50 mL of an aqueous solution of sodium bicarbonate in excess in order to deprotonate the amino group and extracted with Et$_2$O (3 x 20 mL).


The organic phases were combined and dried over MgSO$_4$ and the solvent was removed under reduced pressure. LA-NHS (500 mg, 1.6 mmol) and 1-methylamine pyrene (740 mg, 3.2 mmol) were dissolved in 10 mL of DMF and stirred at room temperature overnight. CHCl$_3$ (30 mL) was added and the mixture was washed with water (3 x 15 mL). The organic phase was then dried over MgSO$_4$, filtered and the filtrate concentrated under reduced pressure. The crude solid product was recrystallized from EtOH (yield=30%).

^{1}H NMR (300 MHz, CDCl$_3$): δ (ppm) 8.3-8 (m, 9H), 5.8 (b. s., 1H), 5.2 (d, J = 5.3 Hz, 2H), 3.58 (m, 1H), 3.13 (m, 2H), 2.63 (m, 1H), 2.2 (t, J = 7.4 Hz, 2H), 1.99-1.46 (m, 7H).

^{13}C NMR (300 MHz, CDCl$_3$): δ (ppm) 172.32, 131.21, 128.25, 127.56, 127.32, 126.13, 125.42, 124.76, 122.85, 77.49, 77.07, 76.65, 56.37, 41.95, 40.13, 38.40, 36.41, 34.55, 28.83, 25.44.

HRMS-ESI: Calcd. for C$_{25}$H$_{25}$NOS$_2$ [M+Na]$^+$ 442.13. Found 442.127.

2.3.3 Synthesis of napthalimide-based ester of lipoic acid
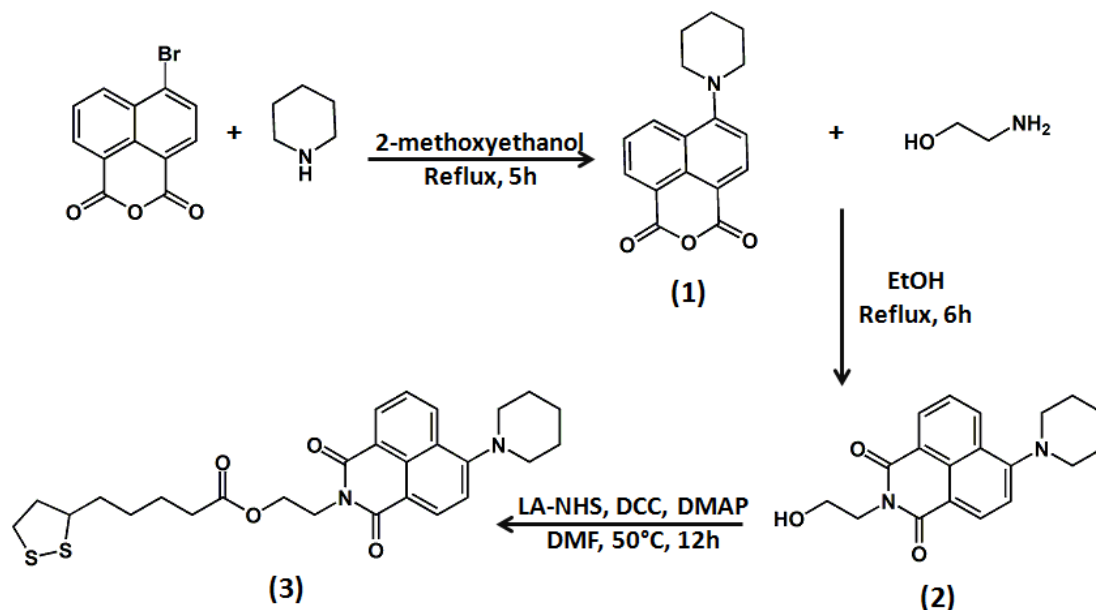
Scheme 2.3 Synthetic route for preparing LA-NAP.

Synthetic procedure:

4-Piperidine-1,8-napthalic anhydride (1) was synthesized by following a reported procedure.[9] Briefly, 4-bromo-1,8-naphthalic anhydride (2.77 g, 10.0 mmol) and piperidine (1.97 mL, 20 mmol) were dissolved in 25 mL of 2-methoxyethanol and stirred under reflux for 5 h. The reaction mixture was then cooled to room temperature to provide a yellow solid, which was purified by recrystallization from EtOH to give 2.41 g of **1** as orange needles (yield=86%).

The NMR spectrum recorded is in agreement to that already reported in literature:
^{1}H NMR (300 MHz, CDCl$_3$); δ (ppm): 8.54 (d, J = 7.0 Hz, 1H), 8.46 (d, J = 8.0 Hz, 1H), 8.41 (d, J = 8.0 Hz, 1H), 7.68 (t, J = 8.0 Hz, 1H), 7.17 (d, J = 8.0 Hz, 1H), 3.29 (s, 4H), 1.90 (s, 4H), 1.75 (s, 2H).

Compound (2) was synthesized by following a reported procedure.[9]

Compound **1** (1.90 g, 5 mmol) and ethanolamine (1.2 mL, 20 mmol) were dissolved in 15 mL of EtOH and stirred under reflux and a nitrogen atmosphere for 6 h. A yellow precipitate was observed after cooling, which was filtered off and washed with cold EtOH. The crude product was finally purified by chromatography using CH_2Cl_2/EtOAc (2:1; v:v) as eluent to provide 1.28 g of **2** as a yellow solid (yield=79%).

The NMR spectrum recorded is in agreement to that already reported in literature:
^{1}H NMR (300 MHz, $CDCl_3$); δ (ppm): 8.56 (d, J = 7.0 Hz, 1H), 8.48 (d, J = 8.0 Hz, 1H), 8.38 (d, J = 8.5 Hz, 1H), 7.68 (t, J = 8.0 Hz, 1H), 7.16 (d, J = 8.5 Hz, 1H), 4.43-4.44 (m, 2H), 3.96 (s, 2H), 3.23 (s, 4H), 2.69 (s, 1H), 1.88 (s, 4H), 1.72 (s, 2H).

Compound 3 (LA-NAP).

LA-NHS (500 mg, 1.6 mmol) and compound **2** (1 g, 3.2 mmol) were dissolved in 10 mL of DMF and catalytic amounts of DCC and DMAP. The resulting mixture was stirred at 50°C overnight. Then $CHCl_3$ (30 mL) was added and the mixture was washed with water (3 x 15 mL); the organic phase was then dried over $MgSO_4$, filtered and the solvent removed under reduced pressure. The crude product was finally purified by chromatography using EtOAc/Cyclohexane (1:4; v:v) as eluent to afford **3** as orange powder (yield=50%).

^{1}H NMR (300 MHz, $CDCl_3$) δ (ppm): 8.56 (d, J = 7.3 Hz, 1H), 8.48 (d, J = 8.1 Hz, 1H), 8.38 (d, J = 8.4 Hz, 1H), 7.68 (t, J = 8.4 Hz, 1H), 7.16 (d, J = 8.1 Hz, 1H), 4.62-4.44 (m, 4H), 3.56-3.43 (m, 1H), 3.3-3.0 (m, 6H), 2.5-2.0 (m, 3H), 1.91-1.2 (m, 13H).

^{13}C NMR (300 MHz, $CDCl_3$): δ (ppm) 132.85, 131.16, 130.84, 126.30, 125.38, 114.75, 77.48, 77.05, 76.63, 61.66, 56.26, 54.55, 40.11, 38.85, 38.45, 34.56, 33.90, 28.66, 26.23, 24.42, 24.34.

HRMS-ESI: Calcd. for $C_{27}H_{32}N_2O_4S_2$ [M+Na]$^+$ 535.17. Found 535.168.

2.3.4 Synthesis of lipoic acid-conjugated polypyridyl ruthenium (II) complex
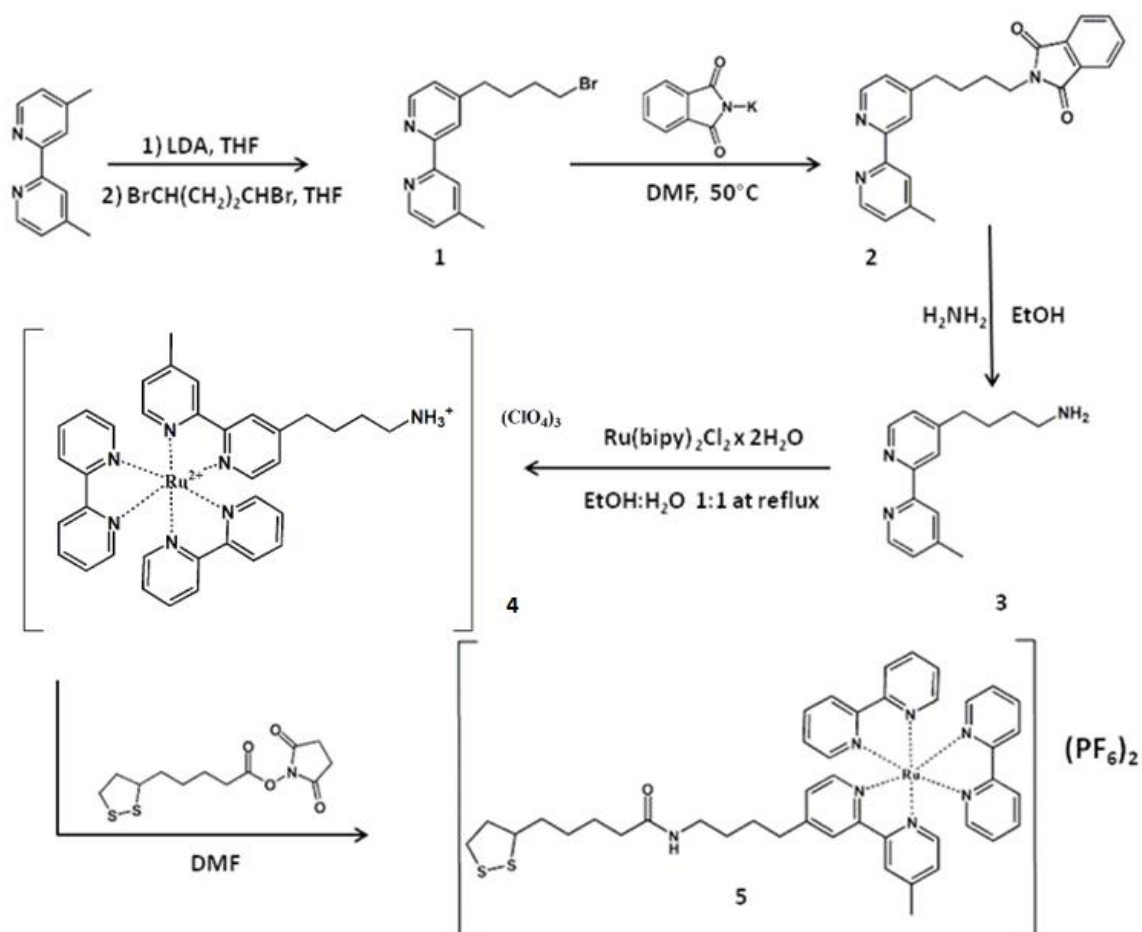
Scheme 2.4 Synthetic route for preparing LA-Ru.

Synthetic procedure:

4(4-Bromobutyl)-4'-methyl-2,2'-bipyridine (1) was prepared by following a reported procedure.[10] LDA (3.5 g, 0.033 mol) was placed in a 1000 mL round-bottom flask equipped with a dropping funnel in a drybox. The flask was cooled in an ice bath; then 50 mL of THF were added dropwise with stirring to afford an orange-brown solution. 4,4'-dimethyl-2,2'-bypyridine (5.0 g, 0.027 mol) was then added dropwise in 150 mL of THF resulting in a dark brown solution, which was stirred for 20 min.

1,3-Dibromopropane (5 mL, 0.049 mol) was dissolved in 50 mL of THF and added in one time to the dark brown solution, which became dark blue. The solution was stirred in an ice bath for one hour. During this time its colour became pale yellow.

The reaction was quenched by slowly adding 10 mL of water. The dropping funnel was removed, the flask was removed from the ice bath, and the reaction mixture was allowed to warm to room temperature. 100 mL of a concentrated phosphate buffer (pH = 7) were then added and the reaction mixture was extracted with Et_2O. The organic layer was dried over $MgSO_4$ and the solvent removed under reduced pressure.

The resulting yellow-brown oil was redissolved in $CHCl_3$, placed on a short silica column and eluted with Et_2O. The product elutes as a yellow band while the brown impurity remains on the column. Finally, the solvent was removed under reduced pressure affording **1** as a yellow oil, which upon standing becomes a waxy solid (yield=87%).

The NMR spectrum recorded is in agreement to that already reported in literature:
^{1}H NMR (300 MHz, $CDCl_3$); δ (ppm): 8.59-8.51 (m, 2H), 8.25-8.23 (m, 2H), 7.14-7.07 (m, 2H), 3.40 (t, J = 6.5 Hz, 2H), 2.70 (t, J = 7.5 Hz, 2H), 2.41 (s, 3H), 1.83-1.79 (m, 4H).

4-(4-Phthalimidobutyl)-4'-methyl-2,2'-bipyridine (2) was prepared by following a reported procedure.[11] Compound **1** (10.0 g, 32.8 mmol) was dissolved in 50 mL of DMF and added to a suspension of potassium phthalimide (6.07 g, 32.8 mmol) in 100 mL of DMF. The resulting mixture was stirred at 50-60°C for 2 h and then allowed to cool to room temperature. 300 mL of water were then added and the mixture was extracted with $CHCl_3$ (3 x 200 mL). The organic layers were combined, washed first with 150 mL of 0.2 M NaOH solution and then with 100 mL of water and finally dried over Na_2SO_4.

The solvent was removed under reduced pressure to provide a yellow oil, which was purified by chromatography using Toluene/EtOAc (1:l; v:v). The product was finally recrystallized from acetone containing a small amount of ethanol to afford **2** as a white crystalline solid (yield=92%).

The NMR spectrum recorded is in agreement to that already reported in literature:

^{1}H NMR (300 MHz, CDC1$_3$); δ (ppm): 8.58-8.53 (m, 2H), 8.24-8.22 (m, 2H), 7.16-7.10 (m, 2H), 3.76 (t, J = 6.6 Hz, 2H), 2.76 (t, J =7.3 Hz, 2H), 2.44 (s, 3H), 1.90-1.71 (m, 4H).

4-(4-Aminobuty1)-4'-methyl-2,2'-bipyridine (3) was prepared by following a reported procedure.[11] Compound **2** (1.00 g, 2.69 mmol) was suspended in 30 mL of EtOH and treated with 200 mL of hydrazine hydrate (206 mg, 4.12 mmol). The resulting mixture was refluxed for 6 h, allowed to cool to room temperature, poured into 100 mL of brine and treated with a solution of NaOH (50%; w/w) to pH=12. The organic phase was then extracted with CH$_2$Cl$_2$ (3 x 25 mL); then the extracts were combined, dried over Na$_2$SO$_4$ and evaporated under reduced pressure to afford **3** as yellow oil (yield=98%).

The NMR spectrum recorded is in agreement to that already reported in literature:

^{1}H NMR (300 MHz, CDCl$_3$); δ (ppm): 8.58-8.53 (m, 2H), 8.22-8.20 (m, 2H), 7.16-7.09 (m, 2H), 2.78-2.63 (m, 4H), 2.43 (s, 3H), 2.01 (s, NH$_2$), 1.87-52 (m, 4H).

Bis(2,2'-bipyridine)[4-(4'-methyl-2,2'-bipyridine)butylamine] ruthenium(II) tris-perchlorate (4) was prepared by following a reported procedure.[12] Compound **3** (583 mg, 2.42 mmol) and Ru(bpy)$_2$Cl$_2$ dihydrate (1.05 g, 2.01 mmol) were suspended in 100 mL of ethanol/water solution (1:1, v:v). The resulting dark brown mixture was refluxed for 8 h under argon flow. During this time the mixture became dark orange; then the solvent was removed under reduced pressure to about 15 mL of volume. The product was purified on a Sephadex SP C-25 column (2.5 x 20 cm). The nonionic impurities were removed by eluting with water, while the desired product was eluted as a dark orange-red band by adding a solution of NaCl, whose concentration was gradually increased from 0.25 to 0.4 M. The fractions containing the product were combined and evaporated up to obtaining 100 mL of volume. Finally, 1 mL of HCl 37% and 7 mL of NaClO$_4$ 5 M solution were added and the resulting solution turned cloudy and was kept at 4 °C overnight.

The precipitate was scratched and sonicated at 60°C to afford compound **4** as a fine powder. The product was finally collected on a sintered glass filter (porosity 4), washed with a few drops of ice water and dried under vacuum over P_2O_5 (yield=49%).

The NMR spectrum recorded is in agreement to that already reported in literature:

^{1}H NMR (300 MHz, CD$_3$CN); δ (ppm): 8.51-8.48 (m, 6H), 8.06-8.02 (m, 4H), 7.75-7.70 (m, 4H), 7.56 (d, J= 5.9 Hz, 1H), 7.52 (d, J= 5.9 Hz, 1H), 7.45-7.36 (m, 4H), 7.25-7.22 (m, 2H), 6.64 (b s, 3H, NH$_3^+$), 3.01 (t, J= 7.0 Hz, 2H), 2.82 (t, J=7.0 Hz, 2H), 2.54 (s, 3H), 1.81-1.72 (m, 4H).

Bis(2,2'-bipyridine)[4-(4'-methyl-2,2'-bipyridine)butylamido lipoic acid] ruthenium(II) bis hexafluorophospate (5) was prepared by following a reported procedure.[12] LA-NHS (500 mg, 1.6 mmol) and compound **4** (3 g, 3.2 mmol) were dissolved in 20 mL of CH$_3$CN and stirred at room temperature for 5 hours. The crude product was purified by chromatography using a mixture of CH$_3$CN/toluene (3:1, v/v) to afford compound **5** as a dark red powder (yield=30 %).

^{1}H NMR (300 MHz, CD$_3$CN): δ (ppm) 8.51-8.48 (m, 6H), 8.06-8.02 (m, 4H), 7.75-7.70 (m, 4H), 7.56 (d, J= 5.9 Hz, 1H), 7.52 (d, J= 5.9 Hz, 1H), 7.45-7.36 (m, 4H), 7.25-7.22 (m, 2H), 6.64 (b s, 1H), 3.2 (m, 3H), 3.01 (t, J= 7.0 Hz, 2H), 2.82 (t, J=7.0 Hz, 2H), 2.75 (m, 6H), 2.54 (s, 3H), 1.81-1.72 (m, 4H).

2.3.5 Synthesis of pegylated conjugate of lipoic acid
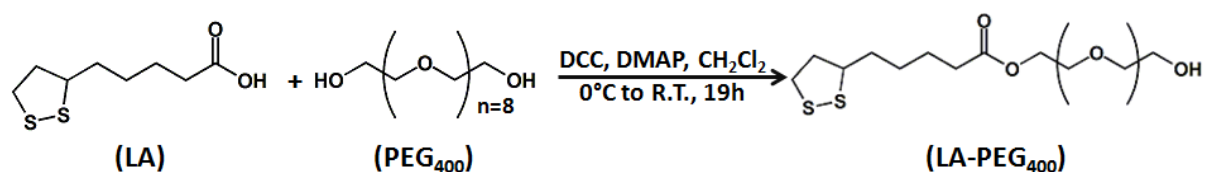
Scheme 2.5 Synthetic route for preparing PEG$_{400}$-tagged lipoic acid.

Synthetic procedure:

LA-PEG$_{400}$ was prepared by following the procedure developed by Mattoussi and co-workers.[13]

Briefly, LA (6.19 g, 30 mmol), PEG$_{400}$ (120 g, 300 mmol), DMAP (1.1 g, 9 mmol) were dissolved in 300 mL of CH$_2$Cl$_2$, previously degassed with a stream of nitrogen for 20 min. This mixture was cooled to 0°C in an ice bath, then a solution of DCC (6.8 g, 33 mmol) in 20 mL of CH$_2$Cl$_2$ was added dropwise and the resulting solution was stirred at 0°C for 1 h, then warmed to room temperature and stirred for 20 h. The precipitate formed was filtered over a plug of celite and the yellow filtrate washed with brine (3 x 75 mL). The organic layer was dried over MgSO$_4$ and the solvent removed under reduced pressure to afford a yellow oil. The crude product was finally purified by chromatography using a mixture of CHCl$_3$/MeOH/Acetone (90:5:5, v:v:v) as eluent to provide LA-PEG$_{400}$ as a yellow oil (yield=75%).

The NMR spectrum recorded is in agreement to that already reported in literature:
^{1}H-NMR (300 MHz, CDCl$_3$); δ(ppm): 4.09 (t, J = 4.8 Hz, 2H), 3.52 (m, ≈ 36H), 3.02 (m,2H), 2.52 (s, 1H), 2.33 (m, 1H), 2.22 (t, J = 7.4 Hz, 2H), 1.79 (m, 1H), 1.54 (m, 4H), 1.34 (m, 2H).

2.4 Electronic Absorption Spectra

The experiments described in this manuscript have been carried out at room temperature in air-equilibrated or deareated conditions in quartz cuvettes whose optical path length is 1cm. Absorption spectra in the 210-800 nm range have been recorded with a Varian Cary 300 spectrophotometer. The precision on the wavelength values was $\pm$ 1nm. Molar absorption coefficient values were determined using the Lambert-Beer law; the experimental error is estimated to be $\pm5\%$.

2.5 Circular Dichroism Spectra

The CD spectra shown in Chapter 4 have been recorded at room temperature in air equilibrated conditions in quartz cuvette whose optical path length is 10 cm. Circular Dichroism spectra in the 280-600 nm range have been recorded with a Jasco-810 spectropolarimeter.

The instrumental conditions adopted were: high sensitivity 5 mdeg; scan mode continuous; speed 100 nm/min; band width 4 nm; data pitch 0.5 nm; response 1 second. The number of accumulation has been set to 10 in order to record as well as possible CD signals.

2.6 Luminescence Spectra

Luminescence emission, both in fluorescence and phosphorescence mode, and excitation spectra in the 250-800 nm range have been recorded with a Perkin Elmer LS-55 spectrofluorometer. The precision on the wavelength values was $\pm$ 2nm.

All the spectra have been recorded at room temperature in quartz cuvettes whose optical path length is 1 cm and corrected form the response of the detector, inner filter and geometrical effects.[14]

2.6.1 Luminescence Quantum Yield measurements

Emission quantum yields have been determined at room temperature by comparing samples with a standard compound whose emission quantum yield is known, following the protocol for optically-matched dilute samples described by Demas and Crosby[15] which is resumed by Equation 2.1:

$$\Phi_X = \Phi_S \left(\frac{A_S}{A_X}\right)\left(\frac{n_X}{nS}\right)^2 \qquad \text{(Eq. 2.1)}$$

where Φ, A and n are referred as the luminescence quantum yield, the area subtended by the emission spectrum and the refractive index of the solvent in which samples are dispersed, respectively. Subscripts X and S correspond to the sample and standard, respectively.

The emission spectra must be recorded at the same experimental conditions such as the excitation wavelength and the length of the slits, in order to follow such a method. Moreover the sample and the standard must have the same absorbance value at the excitation wavelength, which should be less than 0.1 in order to minimize the inner filter effect. Different standards have been managed depending on the spectral region of interest.[16]

2.6.2 Luminescence Lifetime measurements

Lifetime measurements in the 500 ns range have been performed at room temperature with an Edinburgh Analytical Instruments time-correlated single photon counting (TCSPC) equipment. Figure 2.1 shows a schematic representation of such an instrument. A pulsed diode laser provided by Picoquant was used as the light source, while the detector was a photomultiplier tube (Hamamatsu R928P) cooled to -20°C and suitably amplified.
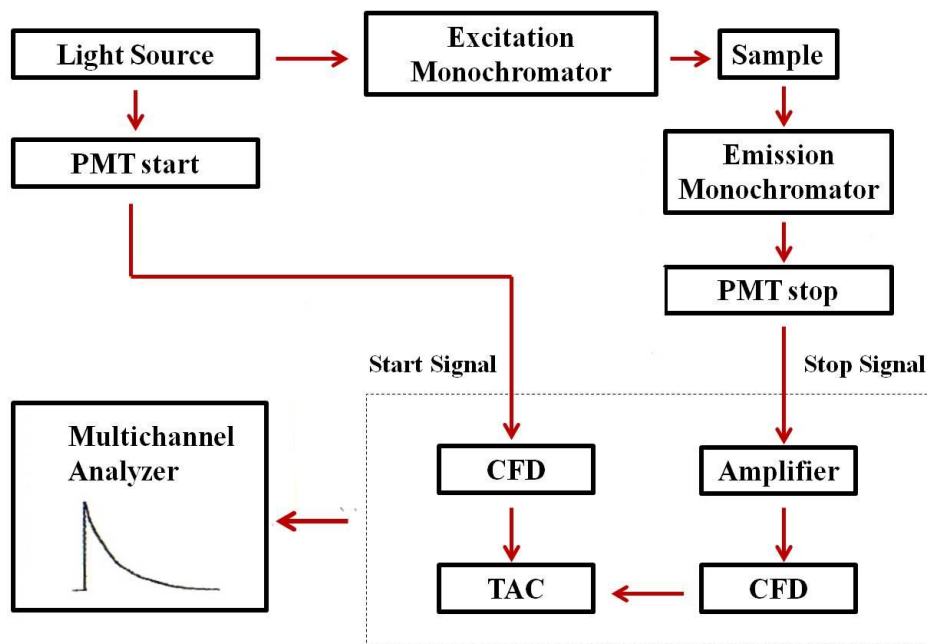
Figure 2.1 Schematization of TCSPC instrumentation.

This technique is based on the probability that a single photon emitted by a luminescent sample is detected by an appropriate detector. Such a probability is then statistically correlated to the variation of the excited state concentration during the time. Briefly, when the light source emits an excitation pulse the photomultiplier start (PMT start) sends a signal to the time-to-amplitude converter component (TAC), which will generate a voltage varying linearly with time period established by the operator. Such a voltage is stopped when the photomultiplier stop (PMT stop) will detects a single photon emitted by the sample. Finally the multichannel analyzer will receive a signal which is numerically accumulated in a channel temporally defined by the voltage value corresponding the stop moment. Successive excitation-emission cycles will be iteratively accumulated to collect a number of signals (i.e., counts) to correlate the emission intensity decrease with time.

This curve coincides with the decay curve of the excited state only if the ratio of the stop signal over the start one is less than 0.02, thus allowing each photon to have a finite probability to be detected.[17] Data elaboration have been performed with EAI F900 software version 6.35.

2.7 Transmission Electron Microscopy

A Philips CM 100 transmission electron microscope operating at 80 kV have been used for characterizing the morphology of quantum dots. Each image reported in this thesis have been obtained by using a Formvar® resin film supported on conventional copper microgrids, which was dried overnight under vacuum after deposition of a drop of quantum dots dissolved in a suitable solvent such as hexane.

2.8 Confocal Fluorescence Microscopy

The experiments described in Chapter 6 have been performed with the patterned surface facing the objective lens of a PicoQuant Microtime 200 time-resolved confocal fluorescence microscope, based on an Olympus IX71 inverted microscope, using two Single Photon Avalanche Diodes (SPADs) as detectors. The SymPhoTime software (Version 5.2.3.2, PicoQuant) controls the piezoscanner and the detecting units. Monochromatic excitation was provided by a PicoQuant LDH-D-C-375 laser diode providing either continuous or 40-300 ps (power dependent) pulses with a frequency of 5 MHz. The excitation light was reflected to the objective by a spectrally flat 80 R/20 T beam splitter and focused in a ~200nm spot at the sample plane.

Fluorescence emission was collected through the same objective and transmitted by the same beam splitter to the confocal unit (i.e, Tube-Lens, pinhole, and SPADs) after a 405 nm long-pass filter rejected the backscattered excitation light. The laser scanning was made by physically scanning the objective in the 3 dimensions by means of piezo stages.

The excitation source for wide field epifluorescence was a Thorlabs M365LP1 LED, which has a spectrum centered at 365 nm and has a FWHM of ~20 nm. As these sources often have a spectrally large continuum that can mask weak fluorescence signals, a clean-up band pass filter, centered at 365nm and with a 25nm bandwith, have been used. A lens-based epi-illumination setup provided even illumination of the sample via the objective itself. The exciting light was reflected by a 376 nm dichroic mirror towards the

objective. Fluorescence emission was transmitted by the dichroic mirror, and the backscattered excitation light was rejected by a long-pass filter cutting at 390 nm placed before the tube lens of the microscope. Images were recorded by a sCMOS camera (i.e., ORCA-Flash4.0 V3 Digital sCMOS camera C13440-20CU) from Hamamatsu.

For confocal hyperspectral imaging, the fluorescence was diverted after the pinhole into an Andor Shamrock spectrophotometer equipped by a Newton EMCCD camera able to record a spectrum within 6 ms, the integration time of each pixel. The objective used for hyperspectral images was a 100x oil immersion objective from Olympus (UPLSAPO) with a numerical aperture (N.A.) of 1.4, while the wide field images were obtained with a 20x air objective whose N.A.=0.40.

2.9 Nuclear Magnetic Resonance Spectroscopy

The ^{1}H and ^{13}C NMR spectra were recorded by using a 300 MHz Bruker-SpectroSpin spectrometer.

References

(1)   Peng, Z.; Peng, X. *J. Am. Chem. Soc*. **2001**, *123*, 183-184.

(2)   Chakrabarty, A.; Chatterjee, S.; Maitra, U. *J. Mat Chem. C* **2013**, *1*, 2136-2144.

(3)   Yu, W.W.; Qu, L.; Guo, W.; Peng, X. *Chem. Mater.* **2003**, *15*, 2854-2860.

(4)   Li, J.J.; Wang, Y.A.; Guo, W.; Keay, J.C.; Mishima, T.D.; Johnson, M.B.; Peng, X. *J. Am. Chem. Soc.* **2003**, *125*, 12567-12575.

(5)   Hines, M.A.; Guyot-Sionnest, P. *J. Phys. Chem*. **1996**, *100*, 468-471.

(6)   Dabbousi, B.O.; Mikulec, F.V; Heine, J.R.; Mattoussi, H.; Ober, R.; Jensen, K.F.; Bawendi, M.G. *J. Phys. Chem. B* **1997**, *101*, 9463-9475.

(7)   Yu, W.W.; Peng, X. *Angew. Chem. Int. Ed*. **2002**, *41*, 2368-2371.

(8)   Liu, W.; Howarth, M.; Greytak, A.B.; Zheng, Y.; Nocera, D.G. Ting, A.Y.; Bawendi M.G. *J. Am. Chem. Soc*. **2008**, *130*, 1274-1284.

(9)   Wang, D.; Zhang, X.; He, C.; Duan, C. *Org. Biomol. Chem*. **2010**, *8*, 2923-2925.

(10)   Yonemoto, E.H.; Saupe, G.B.; Schmeh1, R.H. ; Hubig, S.M.; Riley, R.L.; Iverson, B.L.; Mallouk, T.E. *J. Am. Chem. Soc*. **1994**, *116*, 4786-4795.

(11)   Della Ciana, L.; I. Hamachi, I.; Meyer, T.J. *J. Org. Chem*. **1989**,*54*, 1731-1735.

(12)   Zanarini, S.; Rampazzo, E.; Bich, D.; Canteri, R.; Della Ciana, L.; Marcaccio, M.; Marzocchi, E.; Montalti, M.; Panciatichi, C.; Pederzolli, C.; Paolucci, F.; Prodi, L.; Vanzetti, L. *J. Phys. Chem. C* **2008**, *112*, 2949-2957.

(13)   Uyeda, H.T.; Medintz, I.L.; Jaiswal, J.K.; Simon, S.M.; Mattoussi, H. *J. Am. Chem. Soc.* **2005**, *127*, 3870-3878.

(14)   Credi, A.; Prodi, L. *Spectrochimica Acta A* **1998**, *54*, 159-170.

(15)   Demas, J.N.; Crosby, G.A. *J. Phys. Chem*. **1971**, *75*, 991-1024.

(16)   Montalti, M.; Credi, A.; Prodi, L.; Gandolfi, M.T. *Handbook of Photochemistry-Third Edition*; CRC Press: Boca Raton, FL (USA), 2006.

(17)   Moggi, L., Juris, A.; Gandolfi, M.T. *Il manuale del fotochimico,* Bononia University Press, 2006.

Chapter 3:
A novel method for modulating the solubility of Quantum Dots

3.1 Introduction

As discussed in Chapter 1; QDs, due to their unique size-dependent electronic and optical properties, are emerging nanomaterials for potential applications in several fields from sensing[1-5] to medical diagnostics and therapy[6,7,8] as well as components of photodetectors,[9] light-emitting devices[10,11] and solar cells.[12,13]

However; several applications, especially those in nanomedicine, require nanocrystals compatible with and soluble in aqueous media or, at least, in polar solvents. Then, it is an attracting challenge to develop suitable strategies to make high quality hydrophilic quantum dots, able to be dissolved in water as well as involved in bioconjugate reactions or processes.

Despite several protocols reported for synthesizing QDs in aqueous media, for example by using phosphates[14] or thiols [15-18] as stabilizing ligands, the most adopted synthetic approaches are still based on reactions in organic solvents.[19] Such methods, as discussed in Chapter 1, allow the fabrication of QDs with accurate control of size, shape and properties but, on the other hand, with a surface coated by a layer of hydrophobic ligands.[20-25] These QDs are, therefore, only soluble in apolar organic solvents (e.g., toluene, hexane or chloroform) so that an extra post-synthetic step is required to achieve biocompatibility or, more generally, solubility in polar media.

One possibility in this sense is the encapsulation of the QDs with extra amphiphilic ligands by taking advantage of both hydrophobic intercalation between the alkyl chains and the free hydrophilic head providing aqueous solubility. Surfactants such as phospholipids,[26,27,28] α-cyclodextrin,[29,30] n-alcanoic acids[31] and cetyl-trimethylammonium bromide[32] have all been exploited for transferring nanocrystals into water. However, such encapsulated QDs are normally not stable enough if subjected to biological conditions.[33]

This limit can be pushed further by enhancing the entity of the intercalation between the hydrophobic moieties at the QD surface with amphiphilic polymers. Yu and co-workers[33] prepared QDs coated with a block copolymer such as PMAO-PEG (i.e., PMAO is poly(maleic anhydride-alt-1-octadecene and PEG is polyethylene glycol) exhibiting the same photophysical properties of the starting hydrophobic nanocrystals and, moreover, successfully recognizing the cancer cells with the Her2 receptor. The stability of amphiphilic polymer-encapsulated QDs can be further improved by covalently crosslinking the outmost layer.[34,35] The modular design of such coated QDs is represented in Figure 3.1:
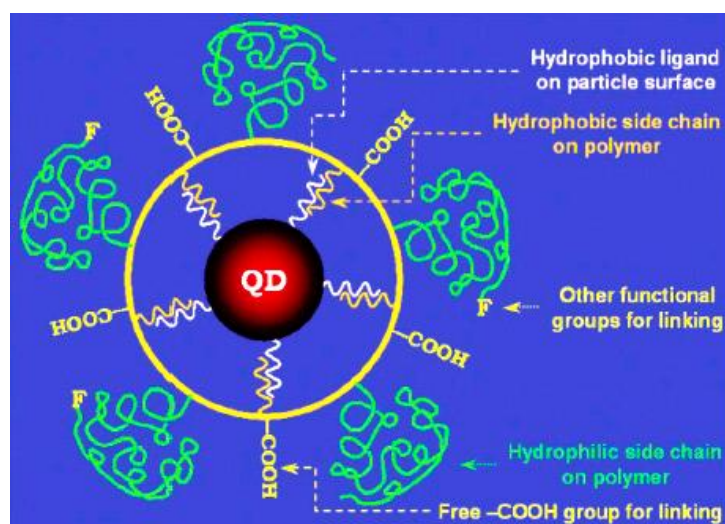
Figure 3.1. Schematic representation of an amphiphilic polymer-coated QD. Adapted from reference [33]. Copyright American Chemical Society 2007.

Overcoating QDs with an extra silica shell is a possible alternative method for producing biocompatible nanocrystals by taking advantage of the formation of a huge protective surface layer.

QDs may be coated through direct ligand exchange[36,37,38] as in the case of surface silanization, or indirect encapsulation[39-44] as in the case of sol-gel process, microemulsion and micellization of siloxane surfactants. In both cases the extra silica shell can be decorated with biomolecules.

Moreover, Gao and co-workers[45] observed that capping with both silica and amphiphilic polymers gives rise to a better passivation than that with either one alone. In this work, hydrophobic CdSe-ZnS Core-Shell QDs were incorporated into silica spheres via a reverse microemulsion process, functionalized with hydrophobic trimethoxy(octadecyl)silane (OTMS) and finally conjugated with amphiphilic polymer (1,2-distearoyl-snglycero-3-phosphoethanolamine-N-[carboxy(polyethylene glycol)-2000] (PE-PEG) as schematized in Figure 3.2:
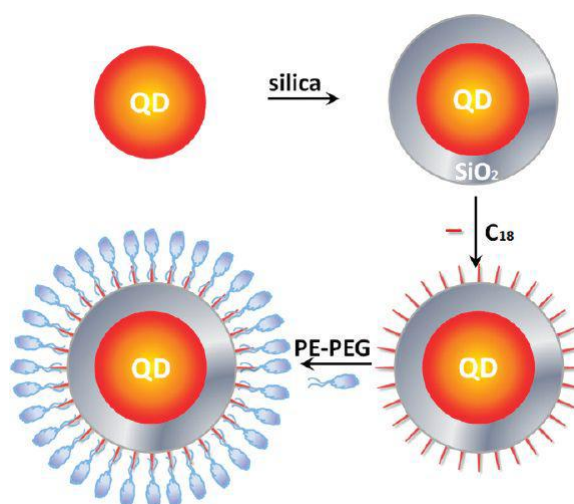
Figure 3.2 Scheme of the incorporation of a QD into SiO_2-PE-PEG sphere. Adapted from reference [45]. Copyright American Chemical Society 2010.

Despite the protocols described above, the most commonly performed strategy to make QDs soluble in polar media is the direct replacement of the native hydrophobic ligands with new hydrophilic ones, able to attach to the surface of nanocrystals and, at the same time, to provide a different solubility.

The most popular anchoring molecules bear thiol groups, several alternatives are amines, phosphonic acids and carboxylic acids.[46-49]

Nie and Chan[50] developed in 1998 one of the first protocols for preparing hydrophilic nanocrystals by coating CdSe-ZnS Core-Shell QDs with mercaptoacetic acid, which exploits the affinity of thiol moieties for the ZnS shell. After this pioneering work, many other monothiol ligands such as mercaptopropionic acid (MPA),[51,52,53] mercaptoundecanoic (MUA),[54] 4-mercaptobenzoic acid,[55] thiol-derivatized sugar,[56] thiolated derivative of diethyleneglycol,[57] dendrons,[58,59] cystamine,[60] cysteine[61] and related residues[62] have been exploited to provide water-soluble QDs.

Such an approach is still a popular method, owing to the ease of processing and the commercial availability of such ligands, but it is not free of disadvantages/limitations.

Firstly, QDs exhibit short shelf lives.[63] This is due to the dynamic binding interaction involving thiol moieties and ZnS shell; moreover, it is important to note that also the pH affects the thiolate ligand stability. The Peng group[64] found that if pH ranges between 2 and 7 then the thiol moiety becomes protonated and easily dissociates from the nanocrystal surface, which then precipitates. Another limitation is that thiols are able to quench QDs, since they can act as hole acceptors.[65]

Wang and co-workers[66] developed a new strategy giving rise to in situ shell formation and ligand capping in a single step, thus providing CdSe-ZnS Core-Shell QDs functionalized with MPA ligands. They have also observed that the as synthesized QDs exhibited an emission quantum yield comparable to that of starting hydrophobic QDs, while the direct ligand exchange resulted in significantly less luminescent QDs.

Bidentate ligands such as lipoic acid (LA) are very useful to make stronger interactions at the surface. Mattoussi and co-workers[67] decorated QDs with negatively charged dihydrolipoic acid (DHLA) to render them water-soluble and promote attachment of engineered recombinant proteins through electrostatic interactions.

However, DHLA negatively affects the luminescence of native QDs probably because of its lower coverage density, in addition to what has just said above for monodentate thiols. Moreover, this negatively charged capping ligand is only stable in basic conditions (i.e., pH $\geq$ 7) and may induce non-specific binding to positively charged proteins in cellular applications.

DHLA-coated QDs can be further modified by taking advantage of its carboxylic moiety which can be easily activated by an esterification reaction with N-hydroxysuccinimide,[68] thus introducing a new better leaving group to allow successive conjugation with new functional groups.

Mattoussi and co-workers[69] developed a new ensemble of water-soluble ligands consisting of DHLA, as surfactant; PEG, as hydrophilic bridge and terminal functional groups such as hydroxyl, carboxylic, amino and biotin ready to be conjugated with biomolecules, as shown in Figure 3.3:
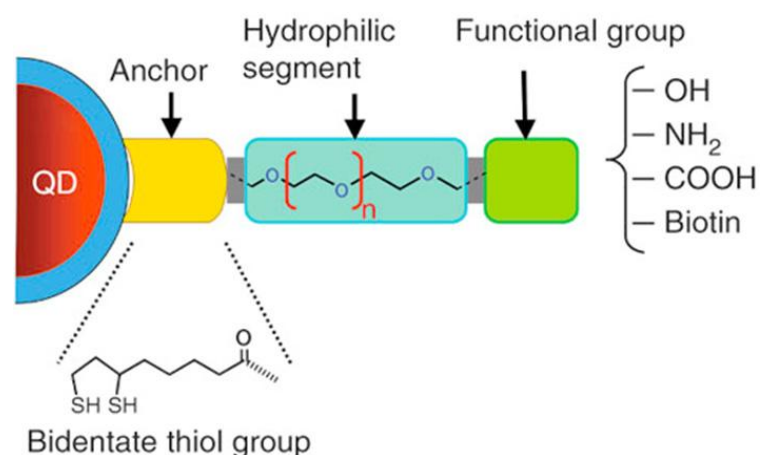
Figure 3.3. Modular design of a QD coated with hydrophilic ligands based on DHLA-PEG and bearing different terminal functional groups. Adapted from reference [69]. Copyright American Chemical Society 2007.

LA is commonly reduced to DHLA by a direct reaction in solution with sodium borohydride (NaBH$_4$).[70-76] However, this protocol requires careful preparation, handling and storage of the DHLA-based ligands under inert atmosphere to prevent reoxidation of the thiols to disulfide.[70-75] Moreover, ligands bearing moieties sensitive to Na$^+$ ions (e.g., receptors for metal ions) cannot be treated with NaBH$_4$. Mattoussi and co-workers[77] have recently published a method based on UV irradiation for breaking the disulfide S–S bond of LA-type ligands. Although this strategy avoids the use of chemical reductants and enables ligand activation as well as QDs functionalization to be performed in a single step, it requires a UV reactor and, more importantly, cannot be employed for reducing ligands bearing photosensitive units (e.g., anthracenyl moieties).

However, in our laboratories we have developed a new and advantageous methodology for efficiently activating and subsequently using LA to replace the native surfactants of QDs. The procedure enables the phase transfer of the nanocrystals in polar and aqueous media but also a simple modulation of their solubility in a wide range of differ polarity solvents (e.g., hexane and water). This protocol can be used with different types both of nanocrystals and of dithiolane-based ligands, and the resulting QDs maintain their optical properties as well as their colloidal stability.

3.2 Results and discussion

3.2.1 Activation of lipoic acid

Our method is based on the use of a borohydride-loaded ion-exchange resin (BER) for the reduction of the 1,2-dithiolane moiety, as shown in Scheme 3.1:
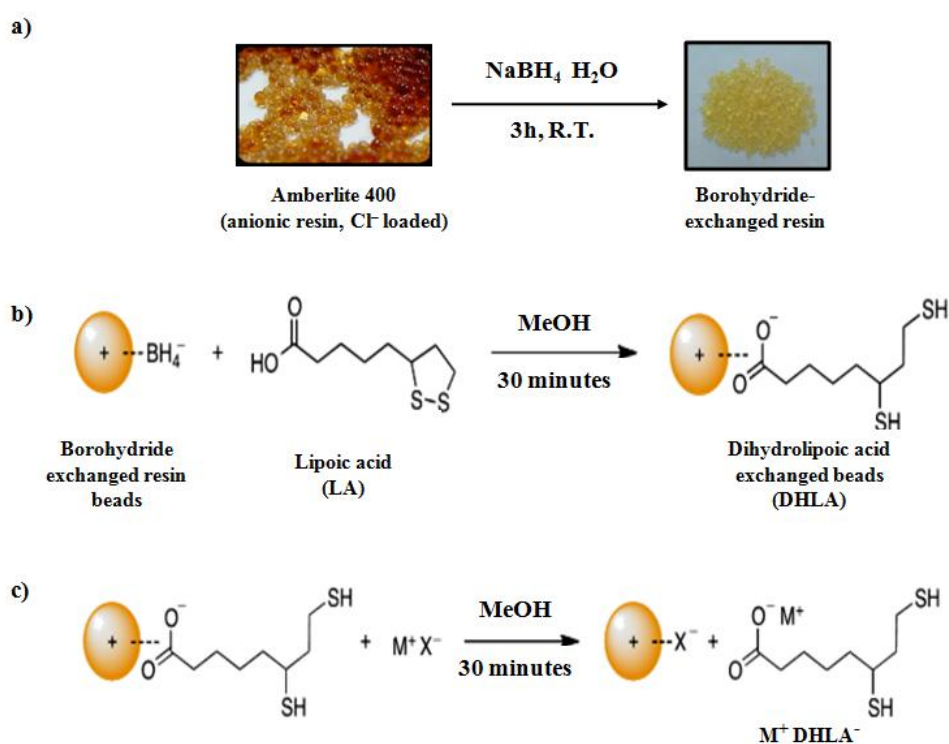
Scheme 3.1 Preparation of resin (a). Reduction of lipoic acid with a borohydride exchange resin (b). Extraction of dihydrolipoic acid from the resin beads (c). [†1]

The preparation of the BH_4 ion-loaded resin (Scheme 3.1 a) was carried out following the procedure developed by Yoon and coworkers.[78] Briefly, 4 g of commercially available Amberlite® IRA-400 (chloride form) resin were placed in a 100 mL one-neck round-bottom flask and mixed with a water solution of $NaBH_4$ (920 mg in 40 mL); the resulting suspension was stirred for at least 3 hours in order to allow the complete exchange of the chloride anions with borohydride ones.

[†1]Credi, A.; Silvi, S.; Avellini, T.; Lincheneau, C. Italian patent RM2013A000269; PCT/IB2014/061230[1]

The resin was filtered and washed with water up to reach a neutral pH, thus removing the excess of sodium borohydride and sodium chloride released during the exchange reaction. The resin beads were then dried under reduced pressure. The amount of BH_4^- per gram of resin was estimated via acid titration; in our case this amount was generally 2.5 mmol of anions per gram of resin. The resin could be successfully re-used for at least three new cap exchange reactions. Nevertheless, the resin beads can be re-loaded with borohydride anions after washing with a HCl solution in order to restore the original form.

The addition of the BER beads to a methanolic solution of lipoic acid (BH_4^-/LA ≈ 2:1 in terms of equivalents) provides, after half an hour of stirring, to the conversion of LA to the $DHLA^-$ anion, which remains bound to the cationic resin (see Scheme 3.1 b). The longer the time of stirring the higher the yield of such a conversion.

The process can be followed by electronic absorption spectroscopy simply monitoring the decrease of the disulfide absorption band of lipoic acid at 330 nm as well as of that in the 220-260 nm region, which is initially off-scale (see Figure 3.4). Such a decrease suggests that DHLA is physically adsorbed on the resin, owing to the electrostatic interaction between the carboxylate and the ammonium moieties of the resin (Scheme 3.1 b).
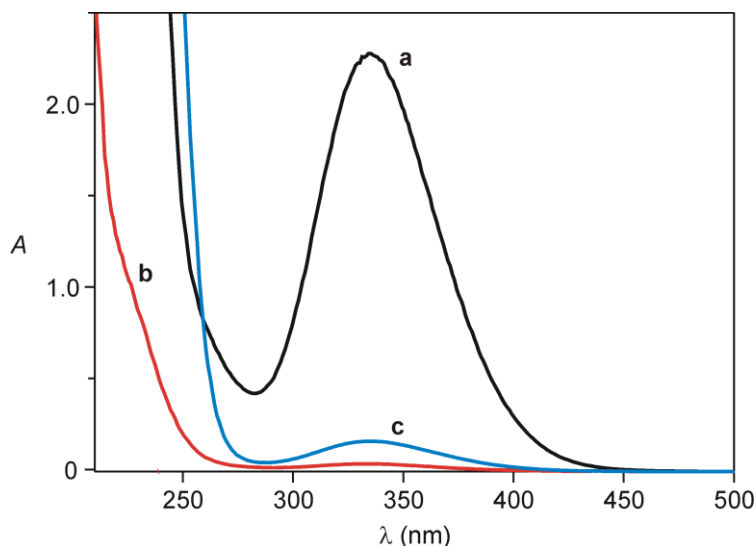
Figure 3.4. Absorption spectrum of 1.6 x 10^{-2} M solution of LA in MeOH before (a) and after (b) treatment with BER.

Absorption spectrum recorded after treating the mixture in (b) with NaOH (2 equivalents with respect to LA) and 30 minutes of stirring (c).

After removing the solvent layer, the beads were washed with fresh methanol to remove unreacted LA and borohydride products and treated with a methanolic solution of an excess of a salt M^+X^- (from 1.2 to 4 equivalents with respect to the BH_4^- content) in order to extract the activated ligands from the resin (see Scheme 3.1 c), by taking advantage of the anion exchange between X^- and $DHLA^-$ species. Finally a methanolic solution of the activated ligand as its M^+ salt is obtained.

We have found that sodium hydroxide (NaOH) is very suitable for extracting DHAL from the resin. More in detail, the addition of NaOH to the resin suspension gave rise to a substantial absorption enhancement between 220 and 250 nm (i.e., the DHLA band), while the signal at 330 nm (i.e., the LA band) was only slightly recovered (see Figure 3.4 c). These observations are consistent with the release of $DHLA^-$ from the resin, together with a minor amount of unreacted lipoic acid.

The increase of the absorption intensity at 330 nm was used to estimate the amount of unreacted lipoic acid, whereas the amount of $DHLA^-$ released in the solution was determined with Ellman's reagent. The yield of LA reduction is 29%, while the amount of unreacted LA is 7%, under the experimental conditions decribed in this paragraph.

It is important to point out that the purification procedures usually performed after the chemical reduction of lipoic acid are not required,[76] since the excess of reactant can be removed by decantation of the resin. The procedure is handy and only the amount of DHLA required for the ligand exchange needs to be prepared, thus avoiding the storage of a huge amount of reduced ligand under inert atmosphere at low temperature.

3.2.2 Ligand exchange and phase transfer of Quantum Dots

The cap exchange was performed by mixing a hexane solution of hydrophobic TOPO capped QDs with methanolic solution of activated ligands (from 1/20000 to 1/30000 QD/lipoic ligand equivalents ratio, depending on QDs size). A fast and efficient ligand exchange occurred, upon stirring this biphasic mixture, and a chromatic variation indicating the phase transfer[70-77] of the QDs from hexane to methanol was observed (see Figure 3.5). The biphasic system was then stirred for 2-3 hours or, in the case of larger QDs, overnight to allow a complete cap exchange to take place. Alternatively, hydrophobic QDs were added as a powder to the DHLA solution. In this case the cap exchange caused the rapid dissolution of the nanocrystals in the MeOH.
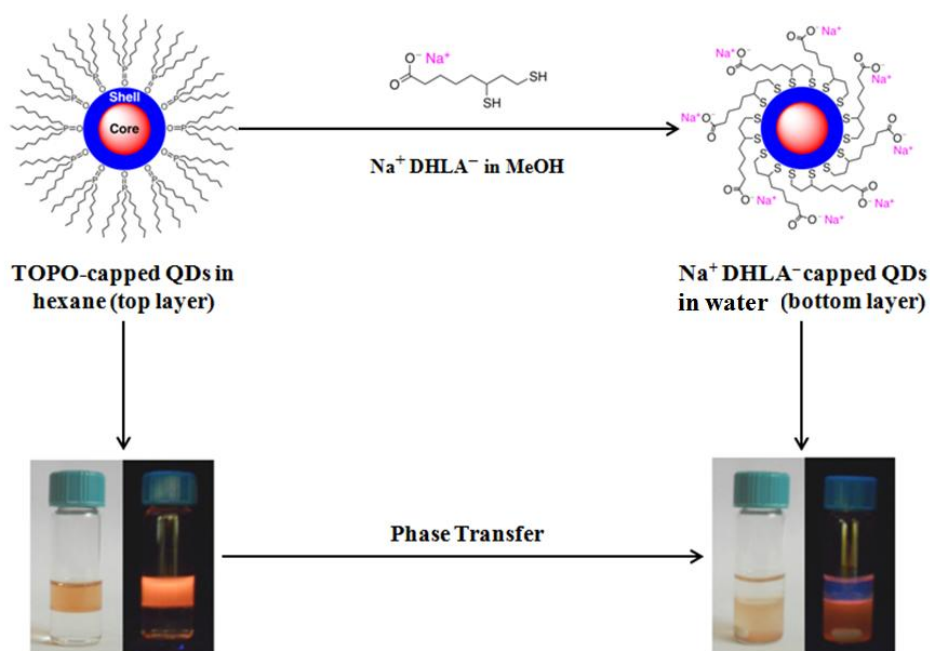
Figure 3.5. Phase transfer of hydrophobic QDs driven by ligand exchange with DHLA– ligands.

Then the starting hexane layer was removed and the MeOH suspension washed with fresh hexane to remove any trace of hydrophobic ligands and unreacted nanocrystals. The methanol was then evaporated under vacuum and the dried DHLA⁻Na⁺ capped QDs were dissolved in water.

Large aggregates were separated by using a syringe filter of 0.45 μm, and unreacted DHLA was removed trhough at least 3 cycles of dilution/concentration with centrifugal filters (Amicon Ultra-0.5 mL; 30 KD) at 7.000 rpm for 12 minutes at room temperature. Typically, a relatively concentrated (5-10 μM) solution of QDs in water is obtained.

This method has also been tested with nanocrystals of different structure and size (see Table 3.1). In all cases a complete phase transfer occurred. In particular, water solution of CdSe-ZnS core-shell QDs were stable for at least 3 months.

Table 3.1 Spectroscopic properties of different water solutions of DHLA⁻Na⁺ capped QDs.

	QD	D (nm)[a]	S (nm)[b]	λ_{abs} [$\Delta\lambda_{abs}$] (nm)[c]	λ_{em} [$\Delta\lambda_{em}$] (nm)[d]	ϕ^f	ϕ^g
1	CdSe	2.6	—	528 [0]	e		
2	CdSe	3.8	—	583 [0]	e		
3	CdSe-5ZnS	2.7	1.6	545 [+3]	562 [+2]	0.14	0.04
4	CdSe-3ZnS	3.4	0.9	562 [0]	586 [−1]	0.34	0.18
5	CdSe-5ZnS	3.6	1.6	572 [0]	597 [0]	0.23	0.08
6	CdSe-4ZnS	3.7	1.2	576 [−2]	606 [−1]	0.18	0.06
7	CdSe-3ZnS	4.1	0.9	587 [−1]	605 [0]	0.06	0.03

[a] Core diameter. [b] Shell thickness. [c] λ_{abs} = Wavelength of the lowest exciton absorption peak in H_2O; $\Delta\lambda_{abs} = \lambda_{abs}$ (H_2O) − λ_{abs} ($CHCl_3$). [d] λ_{em} = Wavelength of the luminescence band maximum in H_2O; $\Delta\lambda_{em} = \lambda_{em}$ (H_2O) − λ_{em} ($CHCl_3$). [e] Non luminescent. [f] Emission quantum yield of hydrophobic QDs with native ligands in $CHCl_3$ or hexane. [g] Luminescence quantum yield of QDs capped with DHLA⁻Na⁺ in water.

Only a slight shift both in the absorption and emission spectra was observed with respect to the starting QDs, indicating that no aggregation takes place and the spectroscopic properties of the final products are preserved (see Figure 3.6). However, the luminescence quantum yield of the final QDs in aqueous solution was 30-50% less with respect to that of the starting hydrophobic QDs, in agreement with data already reported in literature.[79,80] As observed in previous works[79,81,82,83] CdSe cores were not emissive after phase transfer.
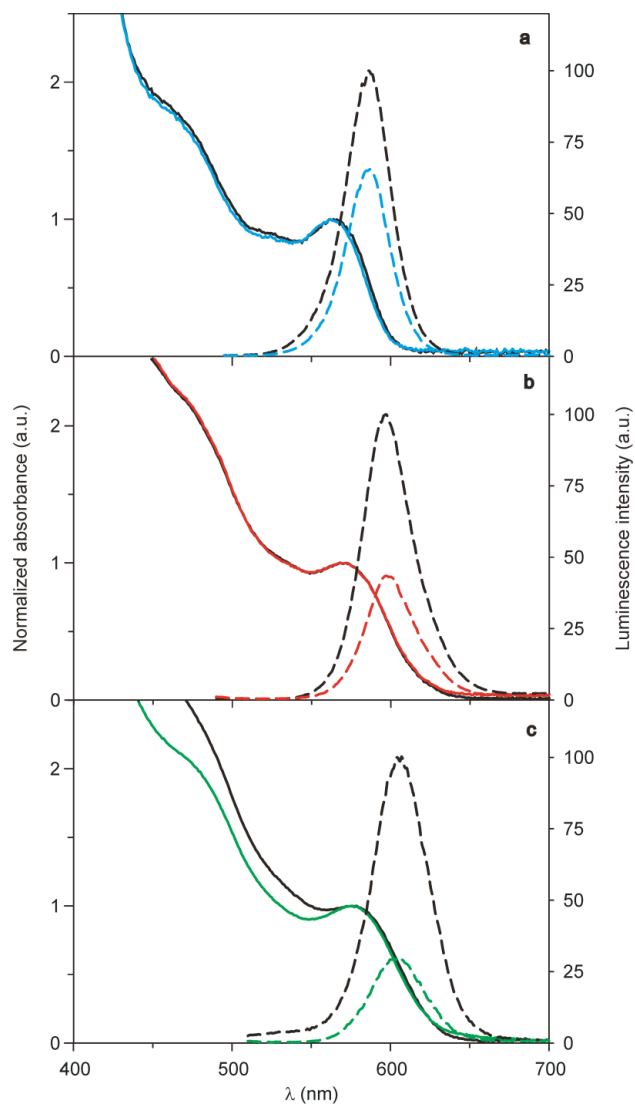
Figure 3.6. (a) Absorption (full line) and emission (λ_{exc} = 485 nm; dashed line) spectra of TOP/TOPO CdSe-3ZnS QDs (sample 4 in Table 1) in CHCl$_3$ (black) and DHLA$^-$Na$^+$ capped in H$_2$O (blue). (b) Absorption (full line) and emission (λ_{exc} = 480 nm; dashed line) spectra of TOP/TOPO CdSe-5ZnS QDs (sample 5 in Table 1) in CHCl$_3$ (black) and DHLA$^-$Na$^+$ capped in H$_2$O (red). (c) Absorption (full line) and emission (λ_{exc} = 450 nm; dashed line) spectra of TOP/TOPO CdSe-3ZnS QDs (sample 7 in Table 1) in CHCl$_3$ (black) and DHLA-PEG$_{400}$ capped in H$_2$O (green).

Moreover, TEM experiments have confirmed that the morphology (i.e., the size and shape) of such QDs is essentially unmodified by ligand exchange treatment (see figures 3.7 and 3.8).
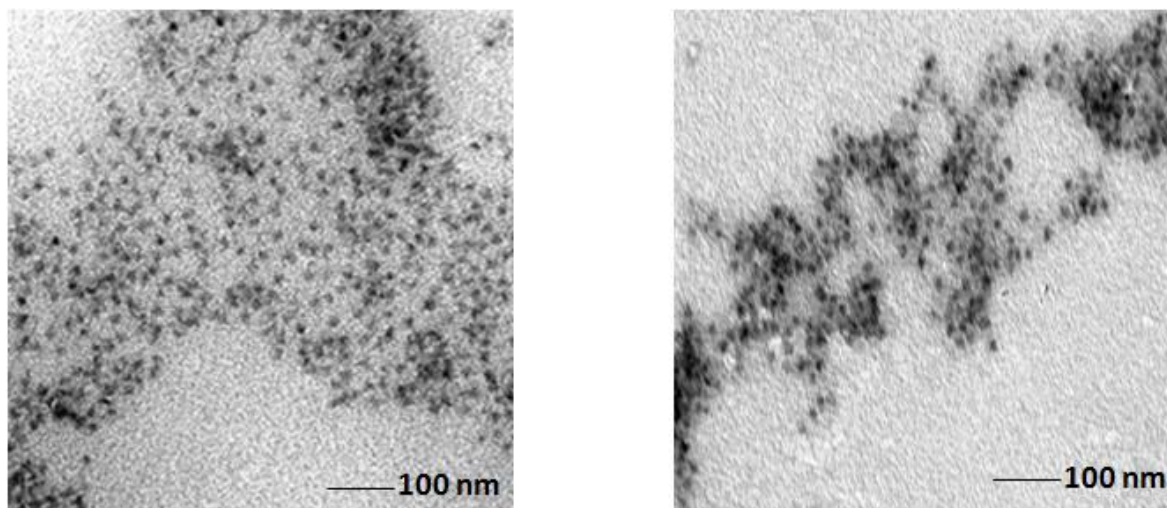
Figure 3.7. TEM images of CdSe-3ZnS QDs (sample 4 in Table 1) before (on the left) and after (on the right) ligand exchange with DHLA$^-$ Na$^+$.
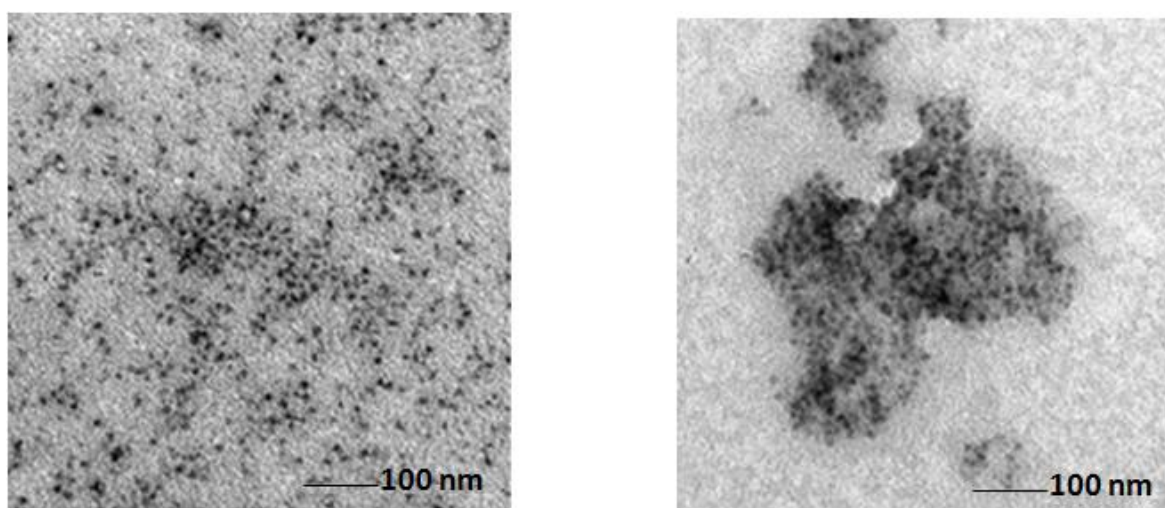
Figure 3.8. TEM images of CdSe-4ZnS QDs (sample 6 in Table 1) before (on the left) and after (on the right) ligand exchange with DHLA$^-$ Na$^+$.

Activation with the BER was also exploited for a ligand comprising a 1,2-dithiolane moiety attached to a hydrophilic poly(ethylene glycol) domain (LA-PEG$_{400}$)[71] and phase transfer of QDs was successfully achieved, as shown in Figure 3.6 c. In this case the DHLA-based ligand cannot bind to the resin since they have no ionizable moieties; then, the extraction step described in Scheme 3.1 b is not required.

The stability of as prepared DHLA⁻Na⁺ capped QDs was also investigated. For example, a water solution of sample 5 (130 nM) in Table 1 (or Figure 3.6 b) was stored at 5°C and the absorption and luminescence spectra were monitored over 3 weeks (see Figure 3.9). The emission quantum yield decreased from 0.081 to 0.05 during the first two weeks, as already observed for other DHLA-capped QDs[84] but no precipitation was observed.
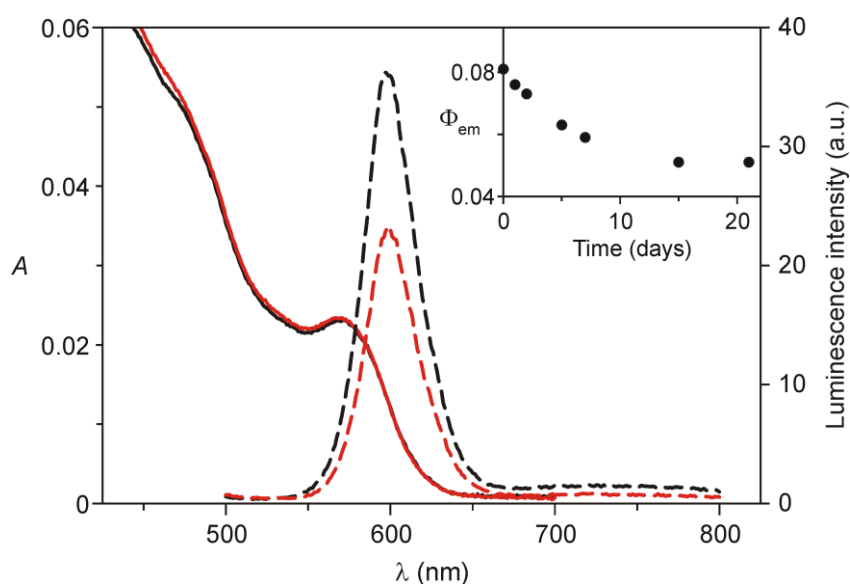
Figure 3.9. Absorption (full lines) and emission (λ_{exc} = 480 nm; dashed lines) spectra of CdSe-5ZnS QDs (sample 5 in Table 1, 130 nM) capped with DHLA⁻Na⁺ in water, freshly prepared (black) and after 21 days of storage at 5°C (red). The inset shows the evolution of the luminescence quantum yield over time.

3.2.3 Modulation of the solubility of the Quantum Dots

Interestingly we have also found that the MX species not only plays an important role for the extraction of reduced LA from the resin but also affects the solubility of final QDs. Many ligand exchange reactions have been performed with different salts, by following the aforementioned route, whose results are summarized in Table 3.2. The solubility of QDs can be essentially modulated by changing the counter ion (M^+) of the activated lipoic acid and/or the solvent chosen for the phase transfer. Although studies on counterion effects in nanocrystals capped with ionic ligands have been reported,[85,86,87] to our knowledge this is the first investigation highlighting the role of counterions for affecting the QD solubility in polar solvents.

Table 3.2 Solubility of CdSe-3ZnS QDs capped with $DHLA^-$ and different M^+ countercations in various solvents at room temperature.[a]

Solvent	Hexane	Toluene	CHCl$_3$	THF	Acetone	MeOH	MeCN	DMSO	Water
M^+ ε^b	1.89	2.38	4.81	7.58	20.7	32.7	35.9	46.5	80.2
Li^{+c}	✗	●	●	✗	✗	✗	✗	✗	●
Na^{+c}	✗	✗	●	●	✗	✗	✗	✗	●
K^{+c}	✗	✗	✗	✗	✗	●	✗	✗	●
TMA^{+c}	✗	✗	✗	✗	✗	●	✗	●	●
TEA$^{+d,e}$	✗	✗	✗	✗	✗	●	●	✗	●
TBA^{+c}	✗	✗	●	●	●	●	●	●	●
TOA^{+e}	✗	✗	✗	✗	✗	●	✗	✗	✗
CTA^{+f}	●	●	●	●	✗	✗	✗	✗	✗
TOPO/TOP^g	●	●	●	●	✗	✗	✗	✗	✗

[a] Green circles indicate that the QDs form homogeneous solutions at 0.5-1.0 µM concentrations; red crosses denote insoluble samples. TMA^+, tetramethylammonium; TEA^+, tetraethylammonium; TBA^+, tetra(*n*-butyl)ammonium; TOA^+, tetra(*n*-octyl)ammonium; CTA^+, cetyltrimethylammonium. [b] Relative dielectric constant. [c] $X^- = OH^-$. [d] $X^- = ClO_4^-$. [e] $X^- = NO_3^-$. [f] $X^- = Br^-$. [g] Native QDs TOP/TOPO capped.

The spectroscopic properties of the nanocrystals are maintained in all the dispersions listed in Table 2, with both the absorption and emission peaks shifting within 5 nm with respect to the native QDs. As an example, Figure 3.10 shows photographs of QDs capped with DHLA⁻TBA⁺ in different solvents.
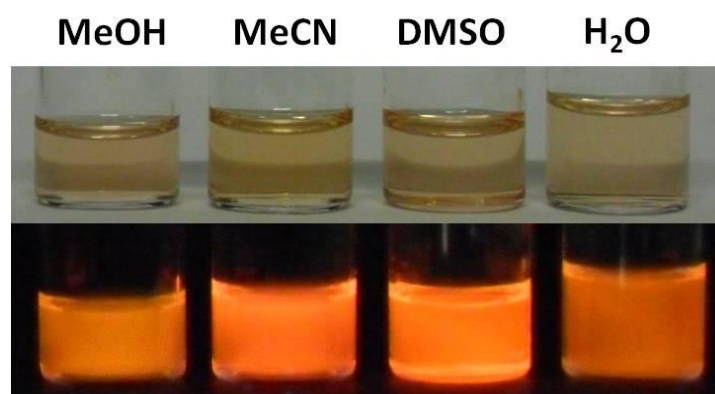
**Figure 3.10.** Photographs of 0.5 μM CdSe-5ZnS QDs solution (sample 5 in Table 1) capped with DHLA⁻TBA⁺ in different solvents under ambient light (top) and UV light (λ_{exc} = 365 nm, bottom).

It is not clear how to interpret the results shown in Table 3.2. It is known that the dissolution thermodynamics is a combination of endothermic (i.e., breaking of the interactions between QDs in the solid lattice and between solvent molecules) and exothermic (i.e., solvation of the anionic QDs and their counter cations) processes.

The solubility of the DHLA⁻M⁺ QDs in which M⁺ is an alkali cation or a quaternary ammonium ion with short alkyl substituents (e.g., TMA⁺) in methanol and/or water can be rationalized by considering the large solvation enthalpies of these cations in these solvents. Tetraalkylammonium ions with longer chains render the QDs more compatible with less polar organic solvents, probably due to Van der Waals forces involving the solvent molecules and the alkyl chains. Other interactions can be important in specific cases: for example, the solubility of DHLA⁻Li⁺ QDs in toluene could arise from favourable cation-π interactions of Li⁺ with the aromatic solvent molecules. It is noteworthy that TBA⁺ ions provide solubility of the anionic nanocrystals in a large variety of solvents (see Table 3.2 or Figure 3.10), suggesting that such cation can provide a good

compromise in terms of lattice and solvation energies in media as different as chloroform and water.

3.3 Conclusions

A new and general methodology for the chemical activation of lipoic acid and its successive utilization for phase transfer of colloidal semiconductor quantum dots in polar and aqueous solvents has been developed. This procedure has several practical advantages with respect to those already published: the resin can be separated from the reaction product simply by decantation or filtration; the reduction can be performed at room temperature and in aerated conditions; moreover, the time required is much shorter (ca. 1 h) than that required in the case of the direct reduction with $NaBH_4$ (ca. 5 h); the ligand can be quickly reduced, just in the amount necessary for the successive ligand exchange, thus avoiding the preparation of DHLA stock solutions and their storage at low temperature under inert atmosphere. Finally, our method enables the precise solubility modulation of the QDs in a wide range of differ polarity solvents by changing the countercation associated with the carboxylate moiety of DHLA-based surface ligands.

References

(1)   Callan, J.F.; de Silva, A.P.; Mulrooney, R.C.; McCaughan, B. *J. Incl. Phenom. Macroc. Chem.* **2007**, *58*, 257-262.

(2)   Raymo, F.M.; Yildiz, I. *Phys. Chem. Chem. Phys.* **2007**, *9*, 2036-2043.

(3)   Medintz, I.L.; Uyeda, H.T.; Goldman, E.R.; Mattoussi, H. *Nat. Mater.* **2005**, *4*, 435-447.

(4)   Somers, R.C.; Bawendi, M.G.; Nocera, D.G. *Chem. Soc. Rev.* **2007**, *36*, 579-591.

(5)   Gill, R.; Zayats, M.; Willner, I. *Angew. Chem. Int. Ed.* **2008**, *47*, 7602-7625.

(6)   Michalet, X.; Pinaud, F.F.; Bentolila, L.A.; Tsay, J.M.; Doose, S.; Li, J.J.; Sundaresan, G.; Wu, A.M.; Gambhir, S.S.; Weiss, S. *Science* **2005**, *307*, 538-544.

(7)   Zrazhevskiy, P.; Sena, M.; Gao, X. *Chem. Soc. Rev.* **2010**, *39*, 4326-4354.

(8)   Doane, T.L.; Burda, C. *Chem. Soc. Rev.* **2012**, *41*, 2885-2911.

(9)   Talapin, D.V.; Lee, J.S.; Kovalenko, M.V.; Shevchenko, E.V. *Chem. Rev.* **2010**, *110*, 389-458.

(10)   Bourvon, H.; Le Calvez, S.; Kanaan, H.; Meunier-Della-Gatta, S.; Philippot, C.; Reiss, P. *Adv. Mater.* **2012**, *24*, 4414-4418.

(11)   Shirasaki, Y.; Supran, G.J.; Bawendi, M.G.; Bulovic, V. *Nat. Photon.* **2013**, *7*, 13-23.

(12)   Kamat, P.V. *J. Phys. Chem. C* **2008**, *112*, 18737-18753.

(13)   Rühle, S.; Shalom, M.; Zaban, A. *ChemPhysChem* **2010**, *11*, 2290-2304.

(14)   Spanhel, L.; Haase, M.; Weller, H.; Henglein, A. *J. Am. Chem. Soc.* **1987**, *109*, 5649-5655.

(15)   Vinayaka, A.C.; Thakur, M.S. *Bioconjugate Chem.* **2011**, *22*, 968-975.

(16)   Talapin, D.V.; Rogach, A.L.; Shevchenko, E.V.; Kornowski, A.; Haase, M.; Weller, H. *J. Am. Chem. Soc.* **2002**, *124*, 5782-5790.

(17)   Rogach, A.L.; Harrison, M.T.; Kershaw, S.V.; Kornowski, A.; Burt, M.G.; Eychmüller, A.; Weller, H. *Phys. Stat. Sol. B* **2001**, *224*, 153-158.

(18)   Bao, H.; Wang, E.; Dong, S. *Small* **2006**, *2*, 476-480.

(19)   Rogach, A.L. (Ed.) *Semiconductor Nanocrystal Quantum Dots*; Springer-Verlag: Wien, 2008.

(20)   Yin, Y.; Alivisatos, A.P. *Nature* **2005**, *437*, 664-670.

(21)   Park, J.; Joo, J.; Kwon, S.G.; Jang, J.; Hyeon, T. *Angew. Chem. Int. Ed.* **2007**, *46*, 4630-4660.

(22)   Murray, C.B.; Norris, D.J.; Bawendi, M.G. *J. Am. Chem. Soc.* **1993**, *115*, 8706-8715.

(23)   Hines, M.A.; Guyot-Sionnest, P. *J. Phys. Chem.* **1996**, *100*, 468-471.

(24)   Peng, Z.A.; Peng, X. *J. Am. Chem. Soc.* **2001**, *123*, 183-184.

(25)   Li, J.J.; Wang, Y.A.; Guo, W.; Keay, J.C.; Mishima, T.D.; Johnson, M.B.; Peng, X. *J. Am. Chem. Soc.* **2003**, *125*, 12567-12575.

(26) Smith, A.M.; Duan, H.; Rhyner, M.N.; Ruan, G.; Nie, S. *Phys. Chem.Chem.Phys.* **2006**, *8*, 3895-3903.

(27) Dubertret, B. *Science* **2002**, *298*, 1759-1762.

(28) Fan, H.; Leve, E.W.; Scullin, C.; Gabaldon, J.; Tallant, D.; Bunge, S.; Boyle, T.; Wilson, M.C.; Brinker, C.J. *Nano Lett.* **2005**, *5*, 645-648.

(29) Lala, N.; Lalbegi, S.P.; Adyanthaya, S.D.; Sastry, M. *Langmuir* **2001**, *17*, 3766-3768.

(30) Wang, Y.; Wong, J.F.; Teng, X.; Lin, X.Z.; Yang, H. *Nano Lett*. **2003**, *3*, 1555-1559.

(31) Shen, L.; Laibinis, P.E.; Hatton, T.A. *Langmuir* **1999**, *15*, 447-453.

(32) Swami, A.; Kumar, A.; Sastry, M. *Langmuir* **2003**, *19*, 1168-1172.

(33) Yu, W.W.; Chang, E.; Falkner, J.C.; Zhang, J.; Al-Somali, A.M.; Sayes, C.M.; Johns, J.; Drezek, R.; Colvin, V.L. *J. Am. Chem. Soc.* **2007**, *129*, 2871-2879.

(34) Pellegrino, T.; Manna, L.; Kudera, S.; Liedl, T.; Koktysh, D.; Rogach, A.L.; Keller, S.; Rädler, J.; Natile, G.; Parak, W.J *Nano Lett.* **2004**, *4*, 703-707.

(35) Wu, X.; Liu, H.; Liu, J.; Haley, K.N.; Treadway, J.A.; Larson, J.P.; Ge, N.; Peale, F.; Bruchez, M.P *Nat. Biotech.* **2003**, *21*, 41-46.

(36) Gerion, D.; Pinaud, F.; Williams, S.C.; Parak, W.J.; Zanchet, D.; Weiss, S.; Alivisatos, A.P. *J. Phys. Chem. B* **2001**, *105*, 8861-8871.

(37) Fu, A.; Gu, W.; Boussert, B.; Koski, K.; Gerion, D.; Manna, L.; Le Gros, M.; Larabell, C.A.; Alivisatos, A.P. *Nano Lett.* **2007**, *7*, 179-182.

(38) Parak, W.J.; Gerion, D.; Zanchet, D.; Woerz, A.S.; Pellegrino, T.; Micheel, C.; Williams, S.C.; Seitz, M.; Bruehl, R.E.; Bryant, Z.; Bustamante, C.; Bertozzi, C.R.; Alivisatos A.P. *Chem. Mater.* **2002**, *14*, 2113-2119.

(39) Darbandi, M.; Thomann, R.; Nann, T. *Chem. Mater.* **2005**, *17*, 5720-5725.

(40) Kim, J.; Lee, J.E.; Lee, J.; Yu, J.H.; Kim, B.C.; An, K.; Hwang, Y.; Shin, C.-H.; Park, J.-G.; Kim, J.; Hyeon, *J. Am. Chem.Soc.* **2006**, *128*, 688-689.

(41) Yi, D.K.; Selvan, S.T.; Lee, S.S.; Papaefthymiou, G.C.; Kundaliya, D.; Ying, J.Y. *J. Am. Chem. Soc.* **2005**, *127*, 4990-4991.

(42) Nann, T.; Mulvaney, P. *Angew. Chem. Int. Ed.* **2004**, *43*, 5393-5396.

(43) Chen, Y.; Rosenzweig, Z. *Nano Lett.* **2002**, *2*, 1299-1302.

(44) Stöber, W.; Fink, A.; Bohn, E. *J. Colloid Interface Sci.* **1968**, *26*, 62-69.

(45) Hu, X.; Gao, X. *ACS Nano* **2010**, *4*, 6080-6086.

(46) Skaff, H.; Emrick, T. *Chem. Commun.* **2003**, *1*, 52-53.

(47) Locklin, J.; Patton, D.; Deng, S.; Baba, A.; Millan, M.; Advincula, R.C. *Chem. Mater.* **2004**, *16*, 5187-5193.

(48) Liu, Y.; Kim, M.; Wang, Y.; Wang, Y.A.; Peng, X. *Langmuir* **2006**, *22*, 6341-6345.

(49) Ren, T.; Mandal, P.K.; Erker, W.; Liu, Z.; Avlasevich, Y.; Puhl, L.; Müllen, K.; Basché, T. *J. Am. Chem. Soc.* **2008**, *130*, 17242-17243.

(50) Chan, W.C.W.; Nie, S. *Science* **1998**, *281*, 2016-2018.

(51) Tetsuka, H.; Ebina, T.; Mizukami, F. *Adv. Mater.* **2008**, *20*, 3039-3043.

(52) Mitchell, G.P.; Mirkin, C.A.; Letsinger, R.L. *J. Am. Chem. Soc.* **1999**, *121*, 8122-8123.

(53) Kirchner, C.; Liedl, T.; Kudera, S.; Pellegrino, T.; Muñoz Javier, A.; Gaub, H.E.; Stölzle, S.; Fertig, N.; Parak, W.J. *Nano Lett.* **2005**, *5*, 331-338.

(54) Hanaki, K.; Momo, A.; Oku, T.; Komoto, A.; Maenosono, S.; Yamaguchi, Y.; Yamamoto, K. *Biochem. Bioph. Res. Commun.* **2003**, *302*, 496-501.

(55) Chen, C.-C.; Yet, C.-P.; Wang, H.-N.; Chao, C.-Y. *Langmuir* **1999**, *15*, 6845-6850.

(56) Babu, P.; Sinha, S.; Surolia, A. *Bioconjugate Chem.* **2007**, *18*, 146-151.

(57) Charvet, N.; Reiss, P.; Roget, A.; Dupuis, A.; Grunwald, D.; Carayon, S.; Chandezon, F.; Livache, T. *J. Mater. Chem.* **2004**, *14*, 2638-2642.

(58) Wang, Y.A.; Li, J.J.; Chen, H.; Peng, X. *J. Am. Chem. Soc.* **2002**, *124*, 2293-2298.

(59) Guo, W.; Li, J.J.; Wang, Y.A.; Peng, X. *J. Am. Chem. Soc.* **2003**, *125*, 3901-3909.

(60) Resch-Genger, U.; Grabolle, M.; Cavaliere-Jaricot, S.; Nitschke, R.; Nann, T. *Nat. Methods* **2008**, *5*, 763-775.

(61) Liu, W.; Choi, H.S.; Zimmer, J.P.; Tanaka, E.; Frangioni, J.V.; Bawendi, M. *J. Am. Chem. Soc.* **2007**, *129*, 14530-14531.

(62) Sukhanova, A.; Venteo, L.; Devy, J.; Artemyev, M.; Oleinikov, V.; Pluot, M.; Nabiev, I. *Lab. Invest.* **2002**, *82*, 1259-1261.

(63) Parak, W.J.; Gerion, D.; Pellegrino, T.; Zanchet, D.; Micheel, C.; Williams, S.C.; Boudreau, R.; Gros, M.A.L.; Larabell, C.A.; Alivisatos, A.P. *Nanotechnology* **2003**, *14*, R15-R27.

(64) Aldana, J.; Lavelle, N.; Wang, Y.; Peng, X. *J. Am. Chem. Soc.* **2005**, *127*, 2496-2504.

(65) Breus, V.V.; Heyes, C.D.; Nienhaus, G.U. *J. Phys. Chem. C* **2007**, *111*, 18589-18594.

(66) Wang, Q.; Xu, Y.; Zhao, X.; Chang, Y.; Liu, Y.; Jiang, L.; Sharma, J.; Seo, D.-K.; Yan, H. *J. Am. Chem. Soc.* **2007**, *129*, 6380-6381.

(67) Mattoussi, H.; Mauro, J.M.; Goldman, E.R.; Anderson, G.P.; Sundar, V.C.; Mikulec, F.V.; Bawendi, M.G. *J. Am. Chem. Soc.* **2000**, *122*, 12142-12150.

(68) Liu, W.; Howarth, M.; Greytak, A.B.; Zheng, Y.; Nocera, D.G.; Ting, A.Y.; Bawendi, M.G. *J. Am. Chem. Soc.* **2008**, *130,* 1274-1284.

(69) Susumu, K.; Uyeda, H.T.; Medintz, I.L.; Pons, T.; Delehanty, J.B.; Mattoussi, H. *J. Am. Chem. Soc.* **2007**, *129*, 13987-13996.

(70) Aldana, J.; Wang, Y. A.; Peng, X. *J. Am. Chem. Soc.* **2001**, *123*, 8844-8850.

(71)   Uyeda, H.T.; Medintz, I.L.; Jaiswal, J.K.; Simon, S.M.; Mattoussi, H. *J. Am. Chem. Soc.* **2005**, *127*, 3870-3878.

(72)   Liu, W.; Howarth, M.; Greytak, A.B.; Zheng, Y.; Nocera, D.G.; Ting, A.Y.; Bawendi, M. G. *J. Am. Chem. Soc.* **2008**, *130*, 1274-1284.

(73)   Yildiz, I.; McCaughan, B.; Cruickshank, S.F.; Callan, J.F.; Raymo, F. M. *Langmuir* **2009**, *25*, 7090-7096.

(74)   Palui, G.; Na, H.B.; Mattoussi, H. *Langmuir* **2012**, *28*, 2761-2772.

(75)   Mei, B.C.; Susumu, K.; Medintz, I.L.; Delehanty, J.B.; Mountziaris, T.J.; Mattoussi, H. *J. Mater. Chem.* **2008**, *18*, 4949-4958.

(76)   Mattoussi, H.; Mauro, J.M.; Goldman, E.R.; Anderson, G.P.; Sundar, V.C.; Mikulec, F. V.; Bawendi, M.G. *J. Am. Chem. Soc.* **2000**, *122*, 12142-12150.

(77)   Palui, G.; Avellini, T.; Zhan, N.; Pan, F.; Gray, D.; Alabugin, I.; Mattoussi, H. *J. Am. Chem. Soc.* **2012**, *134*, 16370-16378.

(78)   Yoon, N.M.; Lee, H.J.; Ahn, J.H.; Choi, J. *J. Org. Chem.* **1994**, *59*, 4687-4688.

(79)   Kloepfer, J.A.; Bradforth, S.E.; Nadeau, J.L. *J. Phys. Chem. B* **2005**, *109*, 9996-10003.

(80)   Susumu, K.; Oh, E.; Delehanty, J.B.; Blanco-Canosa, J.B.; Johnson, B.J.; Jain, V.; Hervey IV, W.J.; Algar, W.R.; Boeneman, K.; Dawson, P.E.; Medintz, I.L. *J. Am. Chem. Soc.* **2011**, *133*, 9480-9496.

(81)   Xie, R.; Kolb, U.; Li, J.; Basché, T.; Mews, A. *J. Am.Chem.Soc.* **2005**, *127*, 7480-7488.

(82)   Kloepfer, J.A.; Bradforth, S.E.; Nadeau, J.L. *J. Phys. Chem. B* **2005**, *109*, 9996-10003.

(83)   Bullen, C.; Mulvaney, P. *Langmuir* **2006**, *22*, 3007-3013.

(84)   Liu, D.; Snee, P.T. *ACS Nano* **2011**, *5*, 546-550.

(85)   Kovalenko, M.V.; Bodnarchuk, M.I.; Talapin, D.V. *J. Am. Chem. Soc.* **2010**, *132*, 15124-15126.

(86)   Feng, Q.; Dong, L.; Huang, J.; Li, Q.; Fan, Y.; Xiong, J.; Xiong, C. *Angew. Chem. Int. Ed.* **2010**, *49*, 9943-9946.

(87)   Nag, A.; Chung, D.S.; Dolzhnikov, D.S.; Dimitrijevic, N.M.; Chattopadhyay, S.; Shibata, T.; Talapin, D.V. *J. Am. Chem. Soc.* **2012**, *134*, 13604-13615.

Chapter 4
Implementation of chiroptical properties of Quantum Dots

4.1 Introduction

In 1980 James Clerck Maxwell[1] postulated that light can be referred to as a pair of oscillating electric and magnetic fields orthogonal each to one another and to the propagation direction of light. The term *oscillating* means that the intensity of these two vectors changes with the time by following a sinusoidal function, as represented in Figure 4.1:
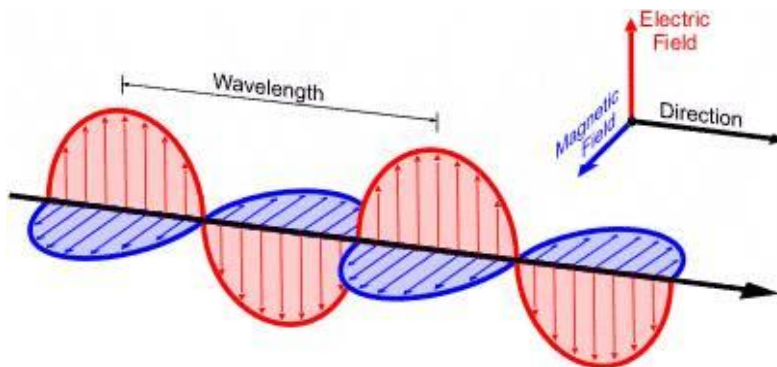

Figure 4.1 Representation of light as an electromagnetic radiation.

The light, as any wave, can be described in terms of length, λ (i.e., the distance between two consecutive maximum or minimum), and frequency, υ (i.e., the number of oscillations per time unit) which are correlated by Equation 4.1:

$$\lambda = v/\upsilon \qquad \text{(Eq.4.1)}$$

where v is the speed of the wave in a medium.

Maxwell's theory has also established the value of light speed in the vacuum through by Equation 4.2:

$$C = \frac{1}{\sqrt{\varepsilon_0 \mu_0}} \approx 3 \times 10^8 \text{ m/s} \qquad \text{(Eq. 4.2)}$$

Where ε_0 is the permittivity of free space and is referred to the electrical interaction between two charged particles in a vacuum; while μ_0 is the permeability of free space and it describes the entity of the magnetic interaction acting on an object in a magnetic field, so it is the magnetic analogue of ε_0.

Such a value was extremely close to those determined by Roemer[2] with astronomical observations and by Michelson and Morley[3] with the interferometer experiment, respectively before and after Maxwell's equations had been formulated. These coincidental values were sufficient enough to recognize that light was an electromagnetic wave and thus part of the electromagnetic spectrum.

The limits of Maxwell's model, as well as of the classical physics, became evident at the beginning of 20th century, since it could not provide a reasonable explanation of the black body radiation phenomenon. Such a problem was then resolved by Max Planck[4] by introducing the new "revolutionary" concept of light interacting with matter only with discrete amount of energy which Planck called a quantum of energy. It is known that, in principle, this was just a mathematical assumption introduced to justify what have been experimentally-observed concerning the blackbody radiation, but also that a few years later Albert Einstein[5] confirmed, by investigating the photoelectric effect, without no more doubts that light consists actually of energy packets, which will be finally defined photon by Lewis[6] in 1926 and whose magnitude depends on the frequency of light by following equation 4.3:

$$\Delta E = hv = h\left(\frac{c}{\lambda}\right) \qquad \text{(Eq 4.3)}$$

Where h is Planck's constant, h= 6.626×10^{-34} J.s.

This simple relationship is the *conditio sine qua non* of matter-light interaction since each transition between two discrete states of matter can occur only if light provides exactly the amount of energy ΔE corresponding to the difference between the states involved.

In the case of UV-vis absorption spectroscopy the electronic states of matter are involved, as shown in Figure 4.2:
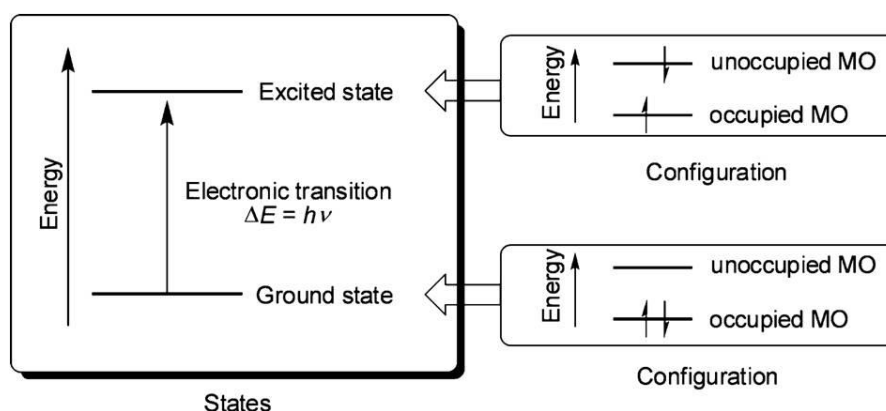
Figure 4.2 Schematic representation of an electronic transition. Adapted from reference [7]. Copyright Royal Society of Chemistry 2012.

However the behaviour of light in interacting with matter can be affected by its oscillation plane, also defined polarization plane. In UV-vis absorption spectroscopy the light source typically provides an isotropic beam, consisting of waves with all possible polarization planes.

If such a plane is fixed then it is possible to distinguish between linearly and circularly polarized light. The difference between them is due to the behaviour of the electric field vector. In the case of circularly polarized light there is no oscillation of the intensity with time but the direction of the vector rotates perpendicularly to the propagation axis. Linearly and circularly polarized light are represented in Figure 4.3:
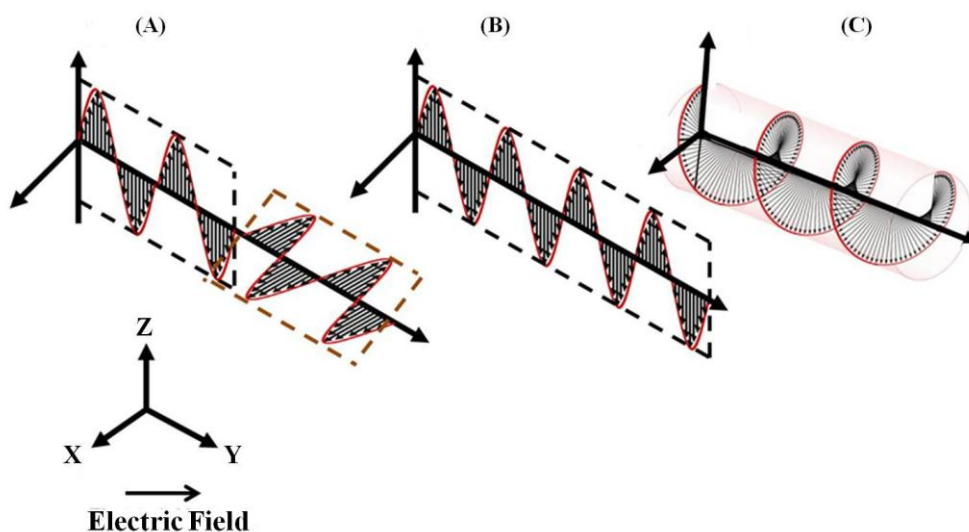
Figure 4.3 Schematic representation of unpolarized light (A), linearly polarized light (B) and circularly polarized light (C).

4.1.1 Circular Dichroism and Optical Rotation Dispersion

Linearly polarized light can be obtained by combining the vectors of two circularly polarized components, respectively right (R) and left (L), having the same intensity. The orientation of the polarization plane of the resulting linearly polarized light wave depends on the phase difference between the R and L circularly polarized components.

When a linearly polarized light beam interacts with a chiral species or simply passes through a chiral environment, the two components will be subjected to a different refractive index, so their relative speed will be different. Such a difference produces a phase shift that ultimately results in the rotation of the polarization plane. The light is still linearly polarized but the polarization plane has now a different orientation that depends on the entity of the phase difference between R and L. The investigation of the orientation angle variation of the polarization plane is referred as optical rotation dispersion (ORD).

Moreover, the two circularly polarized components can be also differently absorbed. In this case the difference between their relative intensities provides a new resulting vector, whose projection into a plane orthogonal to the direction is no longer a circle but an ellipse. The light is now said to be elliptically polarized (see Figure 4.4).
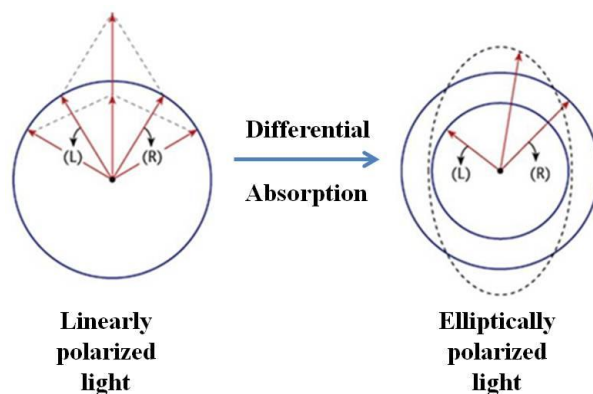
Figure 4.4 Schematic representation of the elliptical distortion of the polarization plane of the linearly polarized light due to the differential absorption of its component R and L.

The degree of such an ellipticity (θ) corresponds to the angle whose tangent is equal to the ratio of the minor over the major axes as shown in the Equation 4.4:

$$\theta = \arctan (m/M) \quad [\text{mdeg}] \quad (\text{Eq.4.4})$$

where m and M are the minor and the major axes, respectively.

Linearly polarized light has $0°$ of ellipticity, while fully left or right circularly polarized light has $+45°$ or $-45°$. The ability of the medium to exhibit different absorption for the two components R and L gives rise to the circular dichroism (CD).

CD spectra are differential spectra showing ΔA or θ values as function of the wavelength. ΔA is the difference in the absorption values of the left-handed and right-handed components, while θ is the ellipticity as defined above. The relationship between them is provided by Equation 4.5:

$$\theta = 32.98 \times \Delta A \quad (\text{Eq.4.5})$$

θ is mostly used by biologists, while chemists prefer ΔA which is correlated to the differential absorption coefficient Δε simply by the Lambert-Beer's law.

The analogue of Δε is the molar ellipticity [θ] given by Equation 4.6:

$$[\theta] = \frac{\theta}{c\,l} \qquad \text{(Eq.4.6)}$$

Then their relationship is provided by Equations 4.7:

$$\Delta\varepsilon = \frac{[\theta]}{32.98} \qquad \text{(Eq.4.7 a)}$$

$$\Delta\varepsilon = \frac{[\theta]}{3298} \qquad \text{(Eq.4.7 b)}$$

If [θ] is provided in [deg M^{-1}.cm^{-1}] then Δε will be calculated by Eq. 4.7 a; otherwise if [θ] is provided in [deg dmol^{-1}.cm^{2}] then Eq. 4.7 b will be used.

CD is a phenomenon dependent on the presence of a chiral environment or species; moreover, it is important to underline that the two enantiomers of the same species show CD spectra which mirrors one to another, but also that a racemic mixture of the same species does not show any CD bands as well as any achiral species.

An example of CD spectra of two enantiomers of the same species is represented in Figure 4.5:
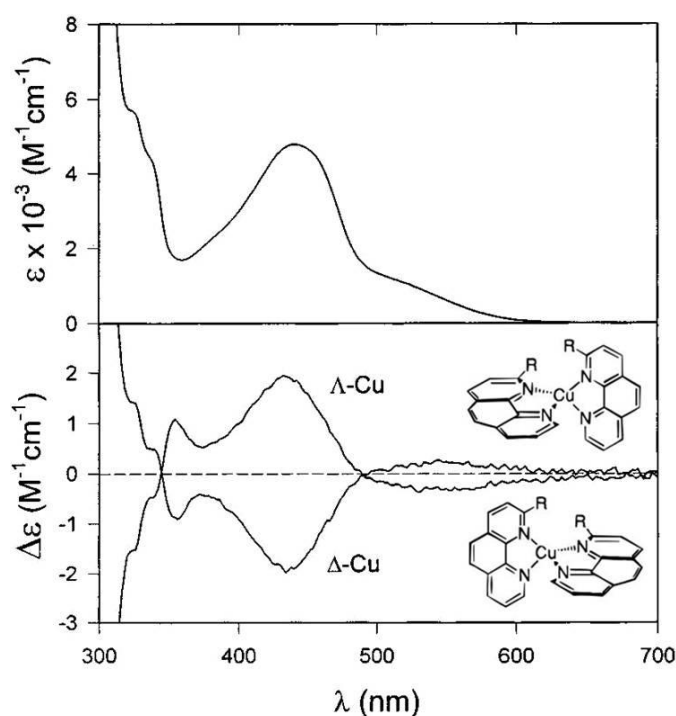
Figure 4.5 Absorption (top) and circular dichroism (bottom) spectra of Λ and Δ [Cu(2-R-phen)$_2$]$^+$ in CH$_2$Cl$_2$ solution at 298 K. Adapted from reference [8]. Copyright American Chemical Society 1998.

It is important to point out that CD is observed only at wavelengths corresponding to the absorption of light, as shown in Figure 4.5, while ORD is observed at any wavelength; meaning that if CD signals can be recorded then ORD must necessarily be detected, while the reverse is not a sufficient condition. Moreover CD and ORD spectral data can be directly related to each other by the Kramers-Kronig[9] transformations.

The relationship between isotropic absorption and ORD spectra, in correspondence to an absorption band, is essentially the same of that between the isotropic absorption and the variation of the refractive index with wavelength. In particular such a behavior is defined at the Cotton Effect and can be positive or negative. Briefly, the ORD increases up to a maximum with decreasing wavelength; then in correspondence of the maximum absorption the optical rotation decreases very fast to reach a minimum and, finally, it increases once again. More in detail such a trend is defined as positive Cotton Effect, while the exact opposite is defined negative Cotton Effect.

Moreover, positive CD bands correspond to a positive Cotton Effect, while negative ones correspond to a negative Cotton Effect.

All these relationships are represented in Figure 4.6, and it is interesting to note that at the wavelength corresponding to the maximum value of ellipticity there is no optical rotation.
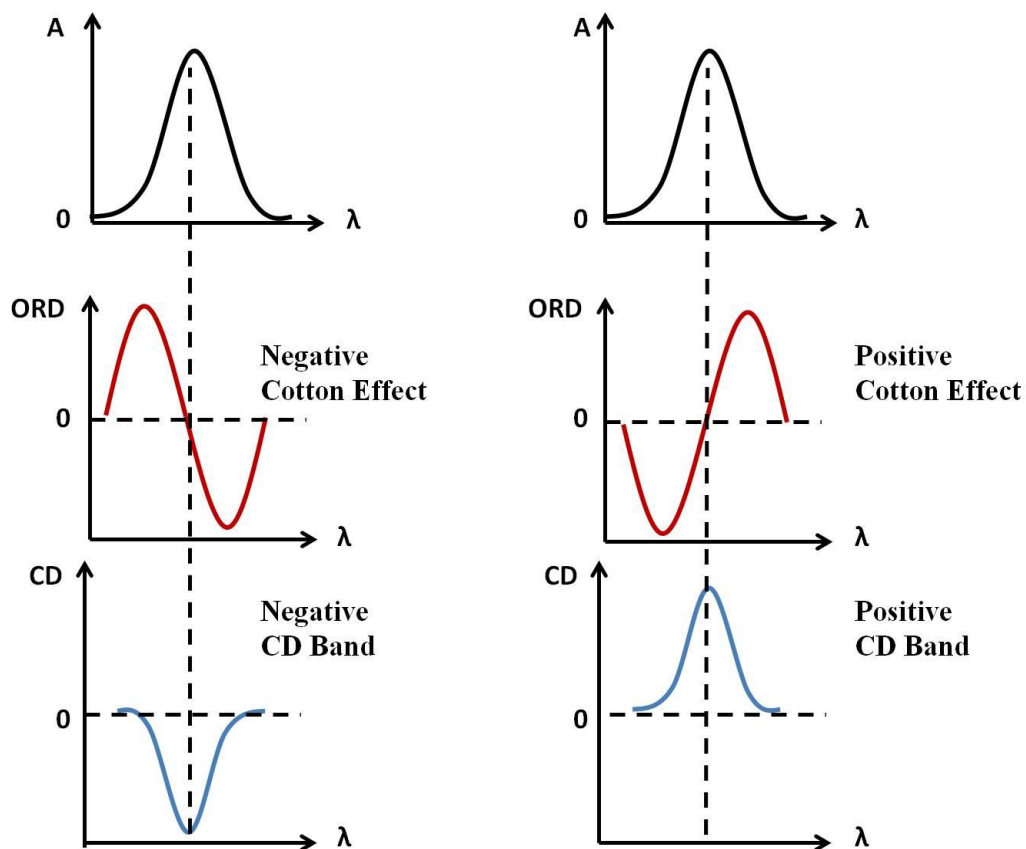
Figure 4.6 Relationships between the isotropic absorption (at the top), the optical rotation dispersion (in the middle) and circular dichroism (at the bottom) bands.

Finally, it is known that for an electronic transition to occur its transition electric dipole (μ) must be different from 0 (i.e., $\mu \neq 0$); however this condition is necessary but not sufficient in the case of circular dichroism, whose band intensities also depends on the rotational strength (R).

R is the scalar product between μ and m vectors, where m is the transition magnetic dipole. Essentially μ describes the net displacement of charge occurring during a transition, while m describes the net circulation of charge during the same transition.

In the case of isotropic absorption spectroscopy m can be neglected with respect to μ, while in the case of CD spectroscopy it plays a fundamental role; in fact, if m is orthogonal to μ then R is zero and no CD bands can be observed.

4.1.2 Induced Circular Dichroism

While CD arises from the interaction between circularly polarized light and chiral species, another possibility is that an achiral species is dispersed in a chiral environment or connected to a chiral moiety. This case can give rise to the Induced Circular Dichroism (ICD).

ICD has been first observed whit an achiral substrate dissolved in an enantiomerically pure solvent,[10,11,12] but it is also frequent in host-guest interaction between an achiral guest complexed by a chiral host, such as in the case of β-cyclodextrin and 4-benzylbenzoic acids,[13] or vice versa such as in the case of achiral pyridino- or phenazino-18-crown-6 ligands with chiral organic ammonium salts[14].

It is difficult to understand the origin of such an effect but the most reasonable explanation concerns an asymmetric perturbation of the achiral component induced by the conjugation with the chiral species as well as the fact that this two partners are close enough for an efficient coupling between the respective transition electric dipoles to occur.

One of the most exciting challenge of nanotechnology is to provide nanostructured materials with improved chiroptical properties to be applied in a wide range of fields from asymmetric catalysis[15] and enantioseparation[16] to enantioselective sensing[17,18] or in spintronic processes.[19]

The possibility of enhancing chiroptical properties of QDs has been first shown by Gun'ko and Moloney.[20] In such a work CdS QDs have been functionalized with L- or D-penicillamine and CD bands corresponding to the exciton transition have been successfully recognized. This pioneering work has been followed by others on CdS,[21,22,23] CdSe,[24,25] CdTe[26,27] and ZnSe[28] QDs exhibiting CD activity at wavelengths corresponding to electronic (or electron-hole) transitions of the dots. Very recently Gun'ko and co-workers[29] have developed a protocol to synthesize chiral CdSe, CdS and CdTe quantum dots.

Examples of QDs with chiroptical properties are represented in Figure 4.7 and 4.8.
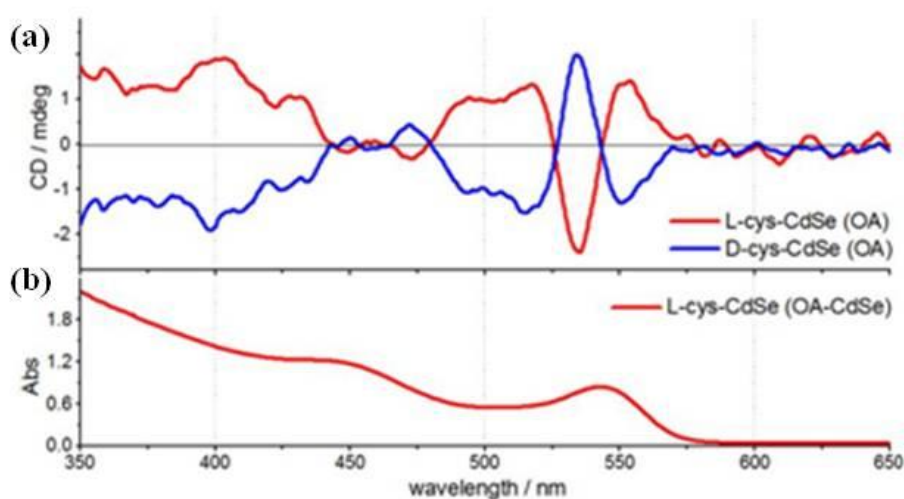
Figure 4.7 (a) CD spectrum of CdSe coated by L-Cysteine (red line) and D-Cysteine (blue line). (b) Isotropic absorption of CdSe QDs coated by L-Cysteine. Adapted from reference [25]. Copyright American Chemical Society 2011.
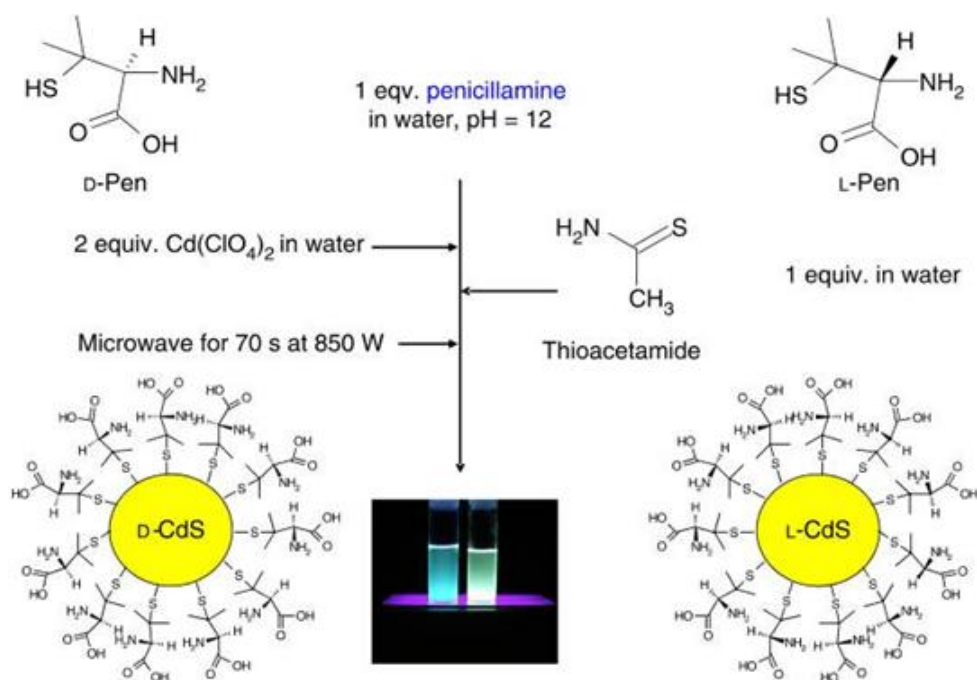
Figure 4.8 Schematic representation of the synthesis of chiral CdS QDs. Adapted from reference [29]. Copyright Nature Publishing Group 2015.

As discussed in the previous Chapter, lipoic acid is a very suitable surfactant for transferring QDs in wide range of solvents and, as shown in Figure 4.9, it is also a chiral species. So a possible induced dichroism effect has been investigated for different QDs as well as its dependence on the size of nanocrystals.
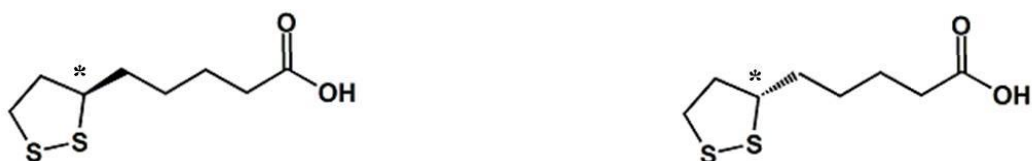
Figure 4.9 The two enantiomers of lipoic acid: the R-(+) on the left and the S-(-) on the right.

4.2 Results and discussion

Three different batches of CdSe and CdS QDs have been synthesized by following the protocols reported in Chapter 2. The absorption spectra and the main properties of such batches are reported in Figure 4.10, Table 4.1 and in Figure 4.11, Table 4.2, respectively.
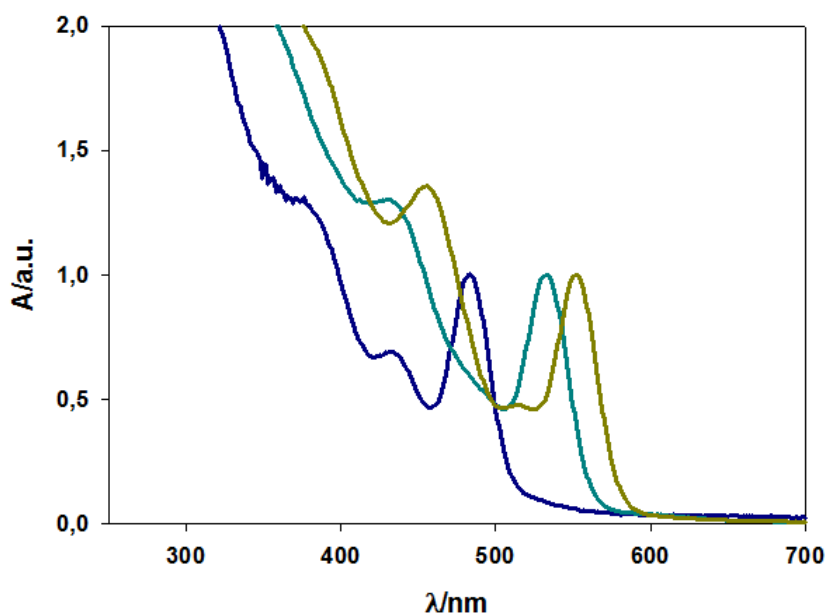
Figure 4.10 Normalized absorption spectra of CdSe QDs samples 1 (dark blue line), 2 (dark cyano line) and 3 (dark yellow line) recorded in $CHCl_3$.

QD	λ exciton peak ε/M^{-1} cm^{-1}	Diameter
CdSe-1	484 nm 47600	2.20 nm
CdSe-2	533 nm 84800	2.74 nm
CdSe-3	552 nm 115600	3.08 nm

Table 4.1 Spectroscopic and dimensional data of CdSe 1-3 QDs.
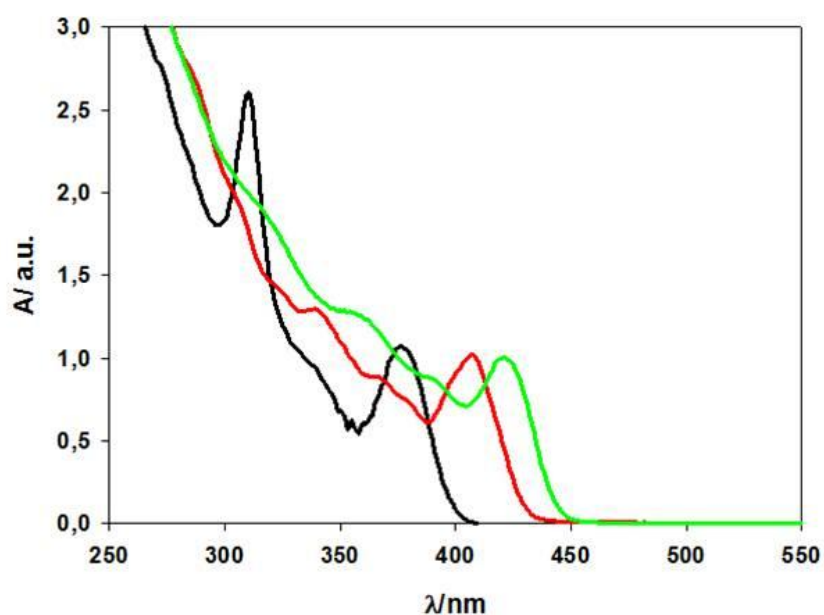
Figure 4.11 Normalized Absoprtion spectra of CdS QDs samples 1 (black line), 2 (red line), 3 (green line) recorded in CHCl$_3$.

QD	λ exciton peak ε/M^{-1} cm^{-1}	Diameter
CdS-1	381 nm 233000	2.81 nm
CdS-2	409 nm 431660	3.68 nm
CdS-3	420 nm 544250	4.07 nm

Table 4.1 Spectroscopic and dimensional data of CdS 1-3 QDs.

The synthesized CdS QDs are coated by oleic Acid and trioctyl phospine ligands while CdSe QDs are coated by trioctyl phospine oxide, hexadecylamine and trioctyl phospine ligands.

Each sample has been decorated with the enantiopure R-(+)-lipoic acid by following the protocol of the borohydride ion-loaded resin as discussed in Chapter 2. In this case the solvent for the phase transfer is water and the counter cation of the reduced lipoic acid is Na$^+$.

4.2.1 Induced Circular Dichroism on CdS QDs
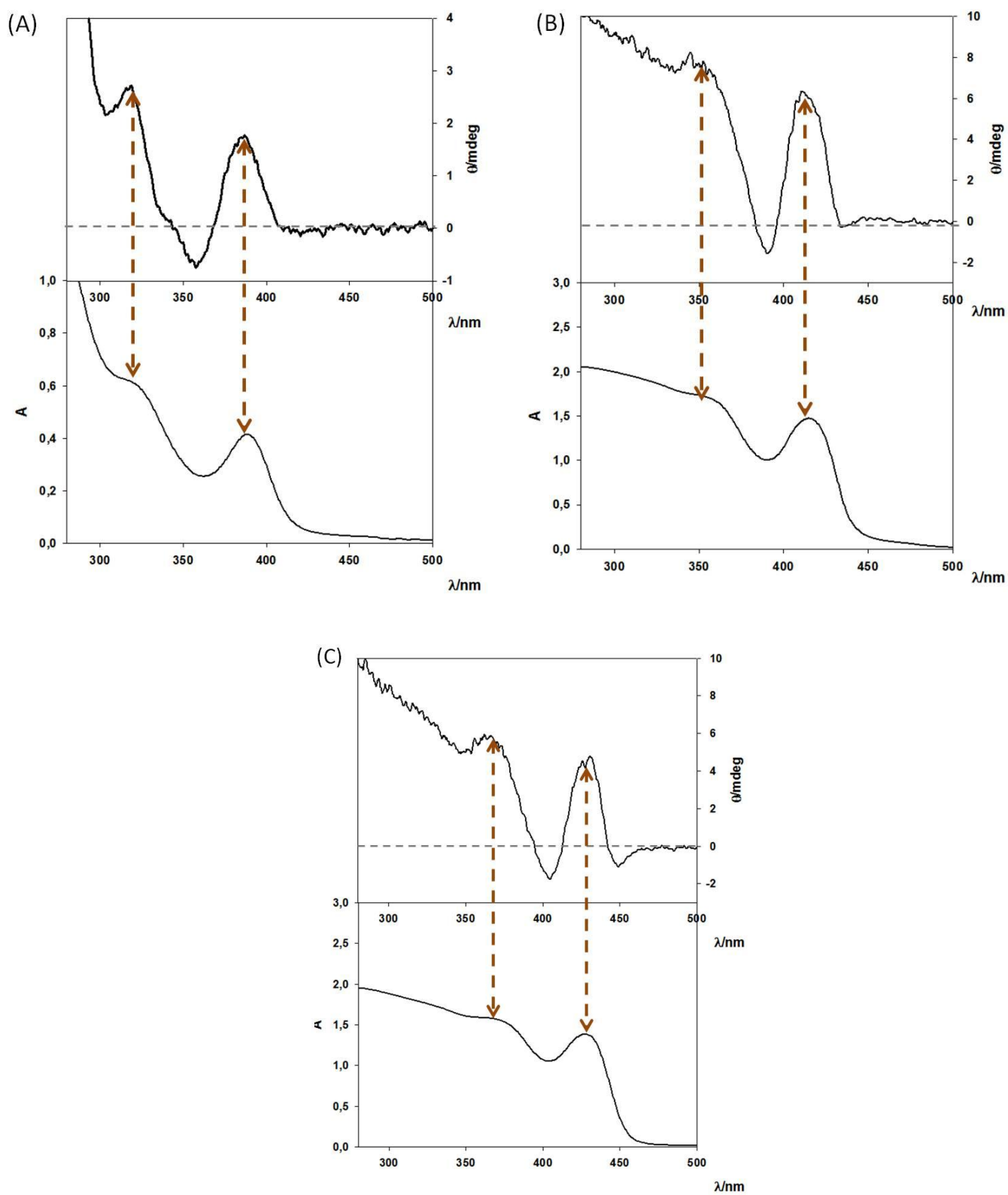
**Figure 4.12** CD (at the top) and Isotropic (at the bottom) Absoprtion Spectra of CdS QDs samples 1 (A); 2 (B) and 3 (C).

For each sample the position of the first and second bands in the CD spectra correspond to those appearing in the absorption spectra (see Figure 4.12). In particular the position of the first CD band corresponds to that of the lowest exciton peak, thus suggesting that such a CD band arises from the electronic transitions of QDs.

Moreover, by normalizing CD and isotropic absorption spectra it is possible to see no shift of CD bands with respect to those in absorption, as shown in Figure 4.13:
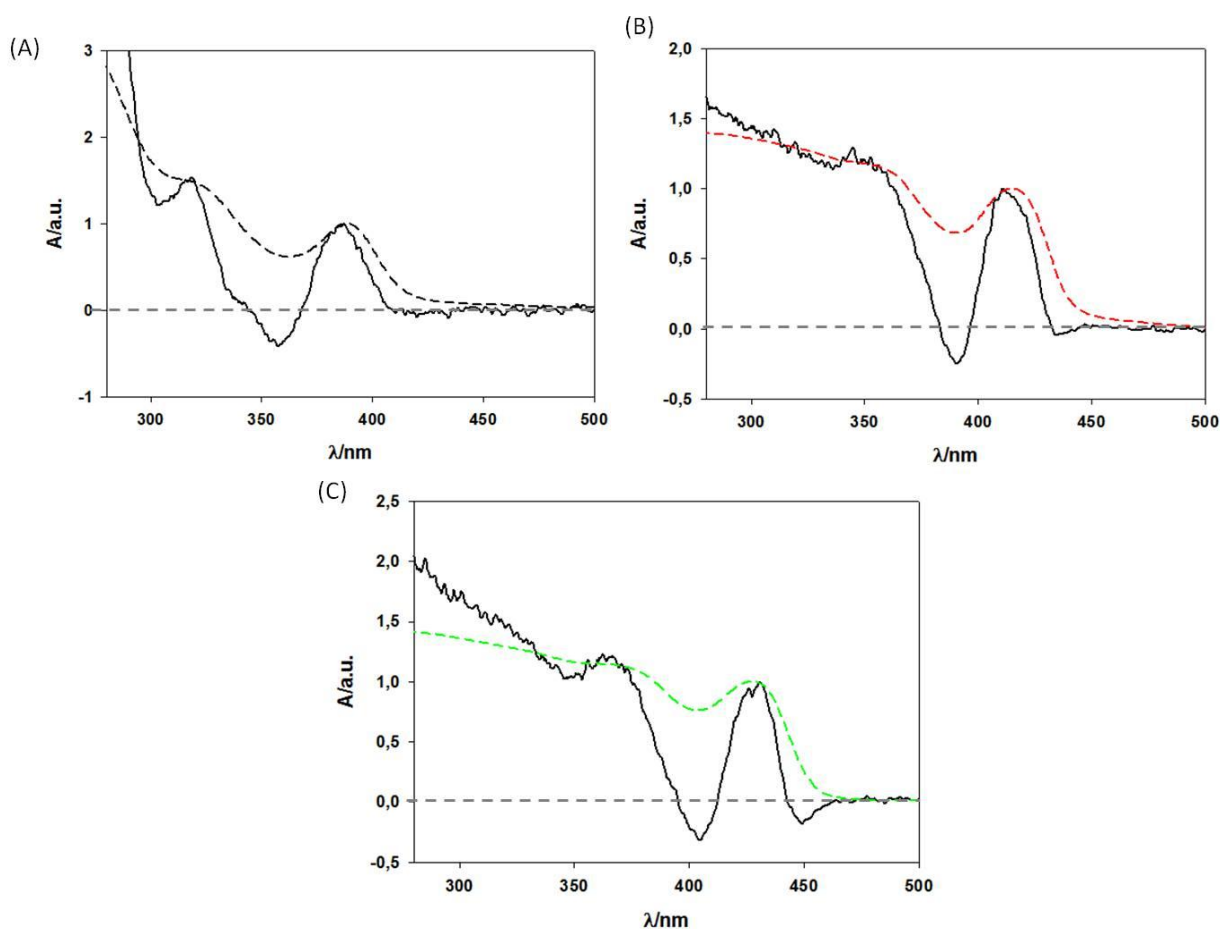

Figure 4.13 Normalized CD (black solid line) and isotropic spectra (dashed lines) at the first exciton transition of CdS samples 1 (A), 2 (B) and 3 (C).

The CD spectra have been also converted in the corresponding differential absorption coefficient spectra simply by using the equations reported above and by taking account of the sample concentrations and the optical length of the cell used (see Figure 4.14):
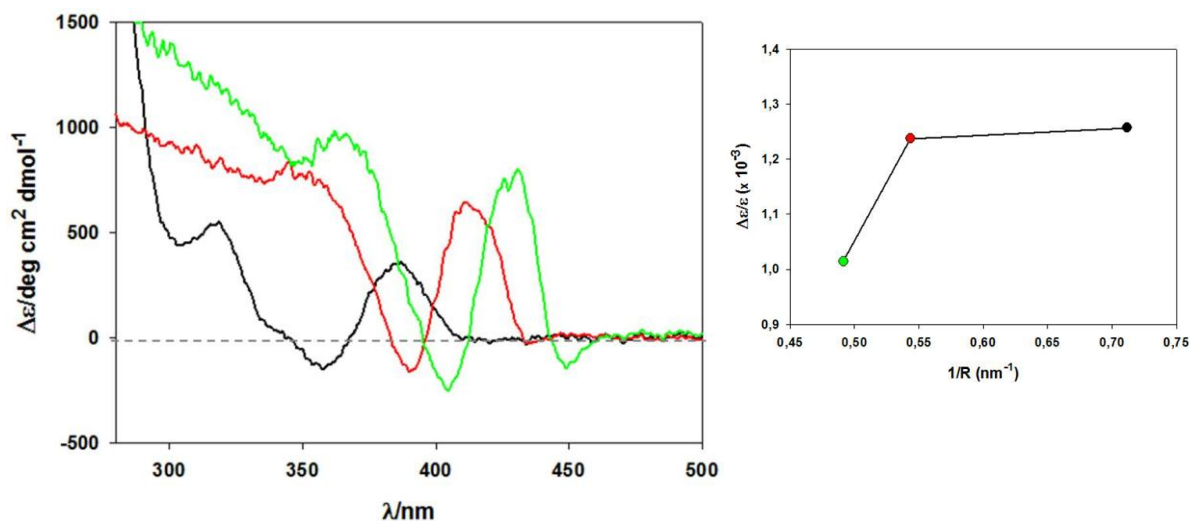

Figure 4.14 Differential Absorption Coefficient Spectra of CdS QDs samples 1 (black line), 2 (red line) and 3 (green line). In the inset the dissymmetry factor is reported as function of the size of QDs.

Figure 4.14 clearly shows that the bigger is the size of QDs the higher are the $\Delta\varepsilon$ values. This is probably due to the fact that by increasing the size of the nanocrystals the average amount of chiral ligands per QD increases, thus resulting in a higher probability for an efficient dichroism induction to occur.

The dissymmetry factor ($\Delta\varepsilon/\varepsilon$) has also been calculated, as shown in the inset; however, surprisingly it does not show the same behavior of $\Delta\varepsilon$.

4.2.2 Induced Circular Dichroism on CdSe QDs
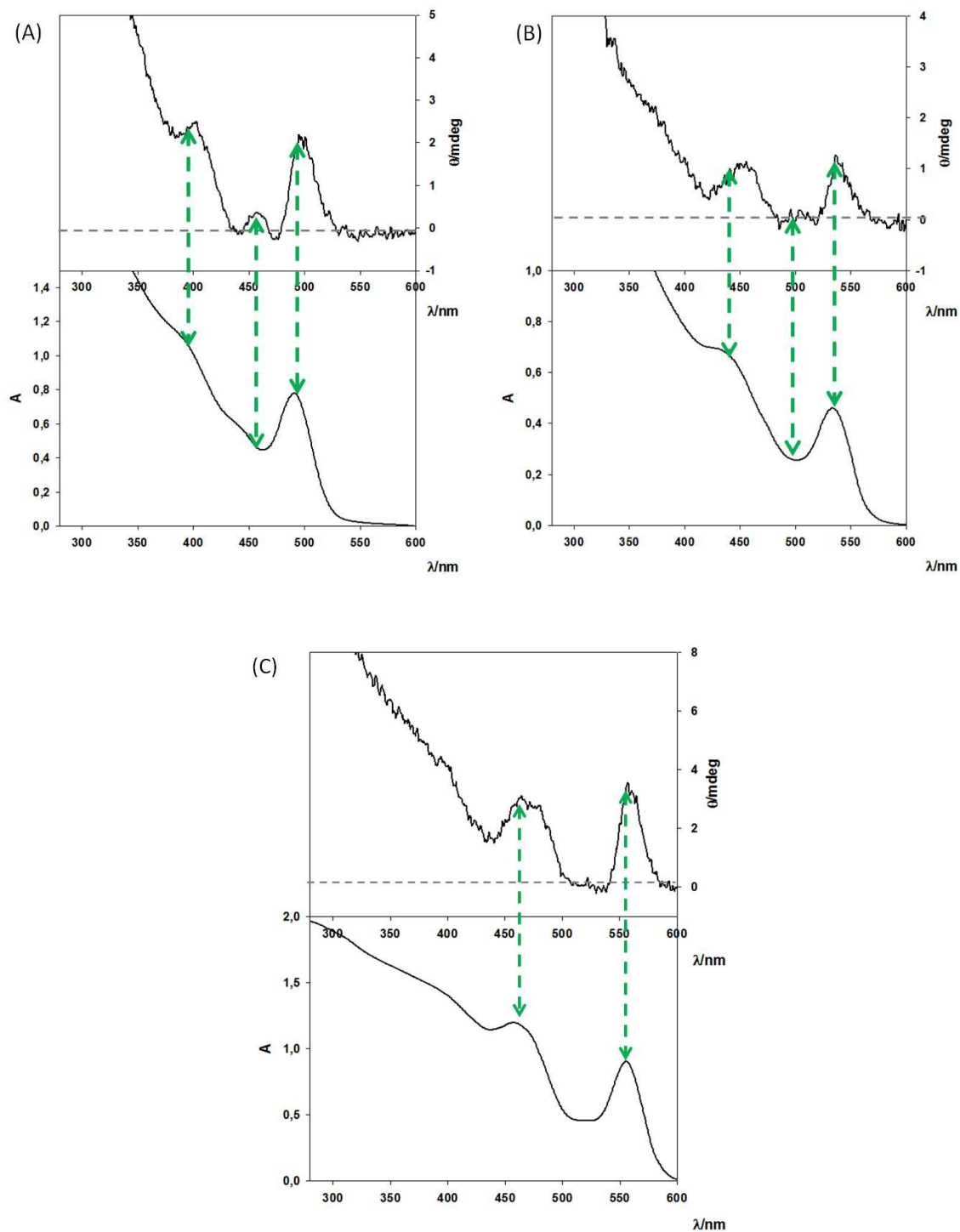
Figure 4.15 CD (at the top) and Isotropic (at the bottom) Absorption spectra of CdSe QDs samples 1 (A); 2 (B) and 3 (C).

CdSe QDs also exhibit CD bands, as well as in the case of CdS QDs. Moreover in this case it is possible to distinguish CD bands which do not have corresponding ones in the absorption spectra.
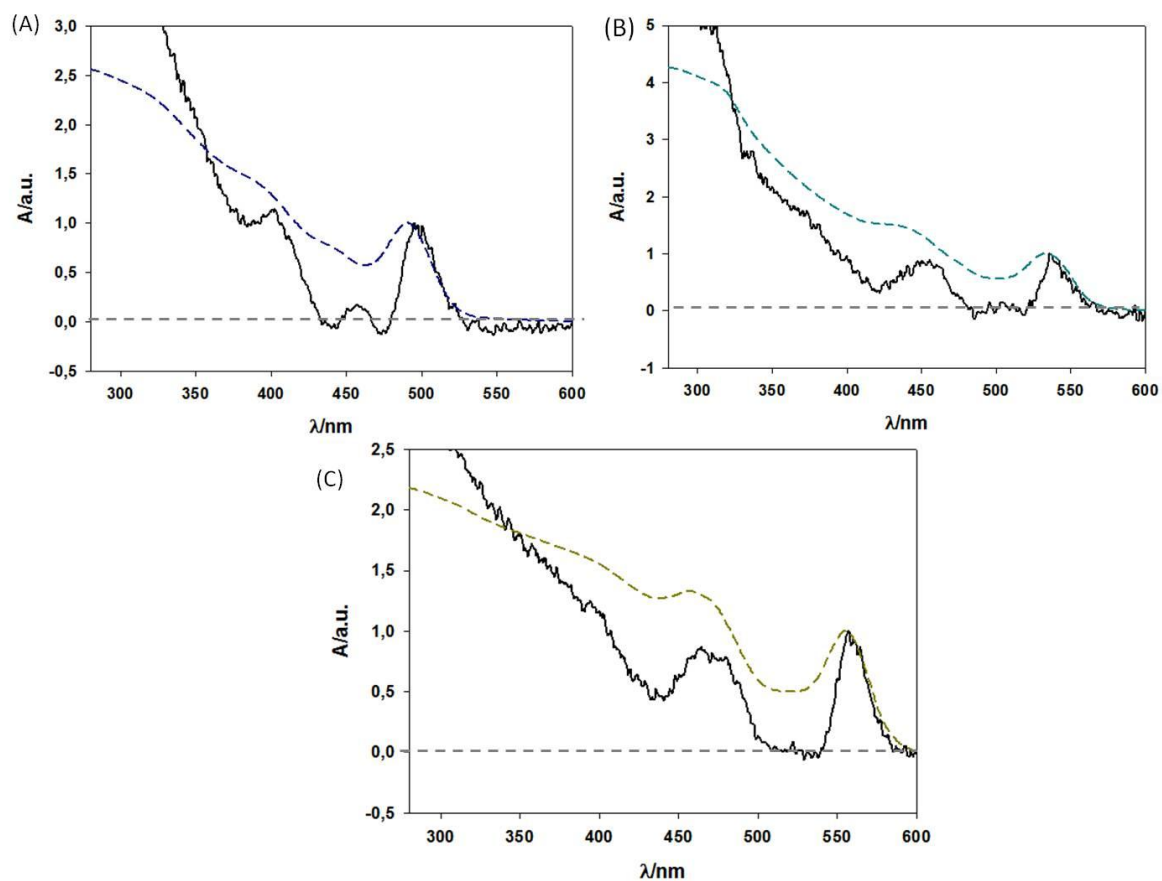
Figure 4.16 Normalized CD (black solid line) and isotropic spectra (dashed lines) at the first exciton transition of CdSe samples 1 (A), 2 (B) and 3 (C).

The CD spectra have been also converted in the corresponding Differential Absorption Coefficient ones by using the equations reported above and by taking account of the sample concentrations and the optical length of the cell used (see Figure 4.17).
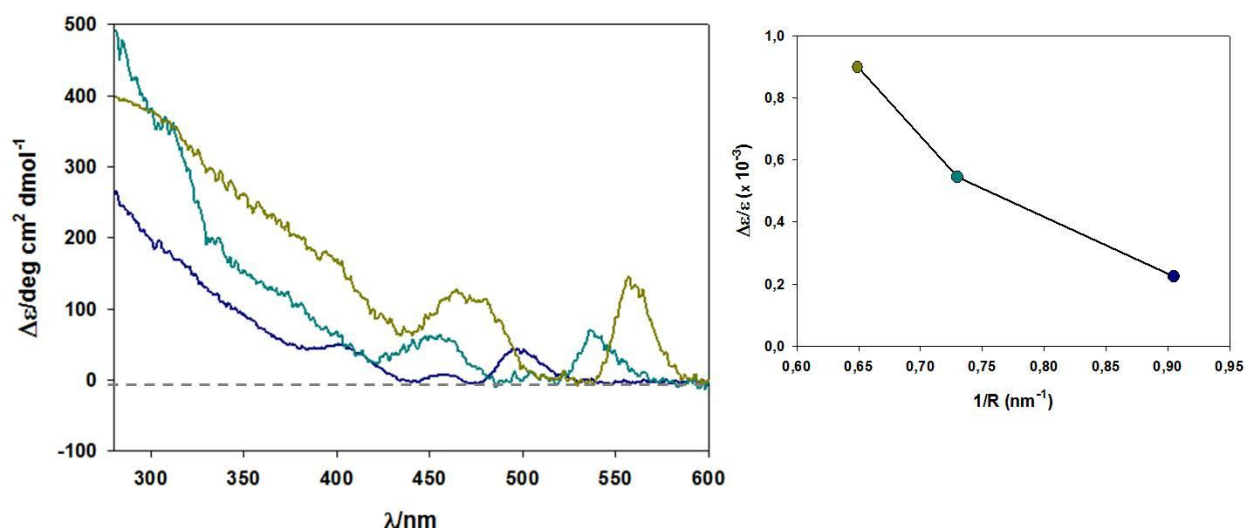
Figure 4.17 Differential Absorption Coefficient Spectra of CdSe QDs samples 1 (dark blue line), 2 (dark cyano line) and 3 (dark yellow line). In the inset the dissymmetry factor is reported as function of the size of QDs.

Figure 4.17 clearly shows that by increasing the size of QDs there is a significant increase of the $\Delta\varepsilon$ values, however such an increase is lower than that observed for CdS QDs. Such an effect is evidently dependent on the nature of QDs. In this case the dissymmetry factor increases with the increasing of the size so it follows the same behaviour of $\Delta\varepsilon$, as shown in the inset.

4.3 Conclusions

QDs showing new chiroptical properties have been successfully developed. The circular dichroism induced effect, due to enantiopure ligands attached on the surface of QDs, has been demonstrated, as well as its dependence on the nature and size of the QDs. Such an effect can be rationalized by considering an effective coupling between the transition moments of chiral ligands and QDs.

As expected there is a clear dependence of such an effect on both the nature and the size of colloidal nanocrystals. Moreover, the possibility to tune simultaneously the absorption and CD bands of such particles in water might be useful for biosensing applications.

References

(1) Hall, G. *Phil. Trans. R. Soc. A* **2008***, 366,* 1849-1860.

(2) Roemer, M. *Journal des Sçavans* **1676**, 276-279.

(3) Michelson, A.A.; Morley, E.W. *Sidereal Messenger* **1887**, *6*, 306-310.

(4) Planck, M. *The theory of the heat radiation* **1914** Philadelphia, P. Blakinston's Son & Co.

(5) Einstein, A. *Annalen der Physik* **1905**, *17*, 132-148.

(6) Lewis, G.N. *Nature* **1926**, *118*, 874-875.

(7) Kobayashi, N.; Muranaka, A. *Circular Dichroism and Magnetic Circular Dichroism Spectroscopy for Organic Chemists* 2012 RSC Publishing.

(8) Riesgo, E.C.; Credi, A.; De Cola, L.; Thummel R.P. *Inorg. Chem.* **1998**, 37, 2145-2149.

(9) Lucarini, V.; Saarinen, J.J.; Peiponen, K.E. *Kramers-Kronig relations in Optical Materials Research* 2005 Springer.

(10) Bosnich B. *J Am Chem Soc* **1966**, *88,* 2606-2607.

(11) Hayward, L.D., Totty, R.N. *Can J Chem* **1971**, *49*, 624-631.

(12) Norden, B. *Chem Scr* **1975**, *8*, 20-22.

(13) Takenaka, S.; Matsuura, N.; Tokura, N *Tetrahedron Lett.* **1974**, *19*, 2325-2328.

(14) Somogyi, L.; Samu, E.; Huszthy, P.; Lázár, A.; Aángyán, J.G.; Surján MD, P.R.; Miklós, H. *Chirality* **2001**, *13,* 109-117.

(15) Shah, E.; Soni, H.P. *RSC Adv.* **2013**, *3*, 17453-17461.

(16) Wang, H.S.; Wei, J.P. *Nanoscale* **2015**, *7*, 11815-11832.

(17) Han, C.P.; Li, H.B. *Small* **2008**, *4*, 1344-1350.

(18) Delgado-Pèrez, T.; Bouchet, L.M.; de la Guardia, M.; Galian,, R.E.; Pèrez-Prieto, J *Chem. Eur. J.* **2013**, *19*, 11068-11076.

(19) Dor, O.B.; Morali, N.; Yochelis, S.; Baczewski, L.T.; Paltiel, Y. *Nano Lett.* **2014**, *14*, 6042-6049.

(20) Moloney, M.P.; Gun'ko, Y.K.; Kelly, J.M. *Chem. Commun.* **2007**, *38*, 3900-3902.

(21) Elliott, S.D.; Moloney, M.P.; Gun'ko, Y.K. *Nano Lett.* **2008**, *8*, 2452-2457.

(22) Naito, M.; Iwahori, K.; Miura, A.; Yamane, M.; Yamashita, I. *Angew. Chem., Int. Ed.* **2010**, *49*, 7006-7009.

(23) Moshe, A.B.; Szwarcman, D.; Markovic, G. *ACS Nano* **2011**, *5*, 9034-9043.

(24) Gallagher, S.A.; Moloney, M.P.; Wojdyla, M.; Quinn, S.J.; Kelly, J.M.; Gun'ko, Y.K. *J. Mater. Chem.* **2010**, *20*, 8350-8355.

(25) Tohgha, U.; Deol, K.K.; Porter, A.G.; Bartko, S.G.; Choi, J.K.; Leonard, B.M.; Varga, K.; Kubelka, J.; Muller, G.; Balaz, M. *ACS Nano* **2013**, *7,* 11094-11102.

(26)   Zhou, Y.; Yang, M; Sun, K.; Tang, Z.; Kotov, N.A. *J. Am. Chem. Soc*. **2010**, *132*, 6006-6013.

(27)   Zhou, Y.; Zhu, Z.; Huang, W.; Liu, W.; Wu, S.; Liu, X.; Gao, Y.; Zhang, W.; Tang, Z. *Angew. Chem. Int. Ed*. **2011**, *50*, 11456-11459.

(28)   Moshe, A.B.; Markovich , G. *Isr. J. Chem.* **2012***, 52,* 1104-1110.

(29)   Moloney, M.P.; Govan, J.; Loudon, A.; Mukhina, M.; K Gun'ko, Y. *Nat.Prot.* **2015**, *10,* 558-573.

Chapter 5
Quantum Dots with long-lived luminescence as result of reversible electronic energy transfer

5.1 Introduction

Electronic energy transfer is a process involving a donor in its lowest excited state (D*) and an acceptor in its ground state (A), as represented by Equation 5.1:

$$D^* + A \rightarrow D + A^* \qquad \text{(Eq. 5.1)}$$

Such a process is referred to as bimolecular if D and A are two independent species or intramolecular if D and A are connected in a supramolecular approach. The electronic energy transfer processes can essentially occur through two different mechanisms, one radiative and the other one non radiative.

5.1.1. Radiative Electronic Energy Transfer

The radiative mechanism (also called trivial) is the direct absorption by A of the photon emitted by D. This mechanism is the simplest one and can be schematized by equations 5.2 and 5.3:

$$D^* \rightarrow D + h\nu \qquad \text{(Eq. 5.2)}$$
$$h\nu + A \rightarrow A^* \qquad \text{(Eq. 5.3)}$$

The efficiency of such a process essentially depends on the emission quantum yield of the donor, the concentration and the molar absorption coefficient of the acceptor but mainly by the overlap of the emission spectrum of D and the absorption spectrum of A.

This last factor can be quantified by the spectral overlap integral J, as represented in Figure 5.1:
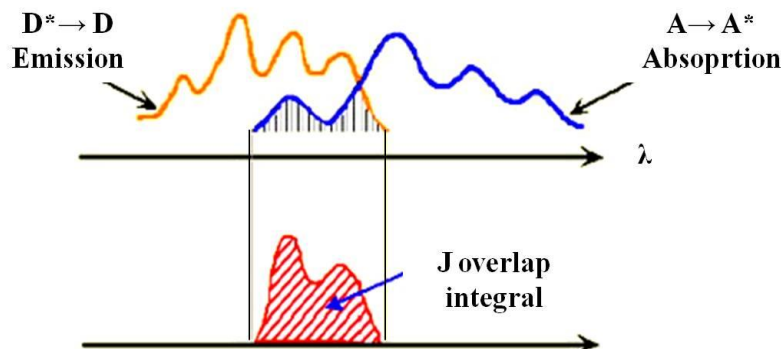
Figure 5.1 Schematic representation of J integral.

The transition A → *A must be spin allowed for the radiative mechanism to occur; so, by assuming that the ground state of the acceptor is of singlet-type, processes involving the lowest singlet (or triplet) excited state of the donor and the lowest singlet excited state of the acceptor, which are referred to as Singlet-Singlet (or Triplet-Singlet) energy transfer, are allowed:

<table>
<tr><td>Singlet-Singlet</td><td>Triplet-Singlet</td></tr>
<tr><td>$^1D^* \rightarrow {}^1D + h\nu$</td><td>$^3D^* \rightarrow {}^1D + h\nu$</td></tr>
<tr><td>$h\nu + {}^1A \rightarrow {}^1A^*$</td><td>$h\nu + {}^1A \rightarrow {}^1A^*$</td></tr>
</table>
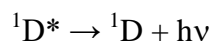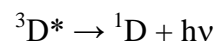
while processes such as Singlet-Triplet and Triplet-Triplet are forbidden:

<table>
<tr><td>Singlet-Triplet</td><td>Triplet-Triplet</td></tr>
<tr><td>$^1D^* \rightarrow {}^1D + h\nu$</td><td>$^3D^* \rightarrow {}^1D + h\nu$</td></tr>
<tr><td>$h\nu + {}^1A \rightarrow {}^3A^*$</td><td>$h\nu + {}^1A \rightarrow {}^3A^*$</td></tr>
</table>
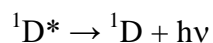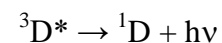
5.1.2 Non Radiative energy transfer

The energy transfer process can be referred to as the transition from the state "*D + A" to the state "D + *A"; then it can be described by the Fermi's Golden Rule, as shown in Equation 5.4:

$$\text{Probability }_{(*D + A \rightarrow D + *A)} = [(\frac{2\pi}{h})\,(\rho) <\psi_i|H|\psi_f>^2] \qquad \text{(Eq. 5.4)}$$

where ψ_i is the wavefunction of the starting state while ψ_f is the wavefunction of the final state, ρ is the density of interacting states and H is the operator corresponding to the perturbation coupling ψ_i and ψ_f. Moreover, since such a transition can occur through two different radiationless mechanisms, the operator H can be split in two different contributions: H_C for the Coulombic interaction and H_S for the exchange interaction. Finally the transition matrix element can be factorised as follows:

$$<\psi_i|H|\psi_f>^2 \rightarrow <\psi_i|H_c|\psi_f>^2 <\psi_i|H_s|\psi_f>^2 \qquad \text{(Eq. 5.5)}$$

The Coulombic mechanism consists of a classical interaction between two charged particles. The electrical field arising from an excited electron can be referred to as generated by an oscillating dipole which can affect the electron clouds of nearby molecules.

In other words, an excited molecule can induce the oscillation of the electrons of another molecule, in its ground state, in the same way as an electrical field of an electromagnetic radiation if a resonance condition is satisfied.

It is known that such a resonance condition is $\Delta E_{(A \rightarrow *A)} = h\nu$ for direct light absorption but also that a coupling between electrons of A and the oscillating field of light occurs in this case, while $\Delta E_{(*D \rightarrow D)} = \Delta E_{(A \rightarrow *A)}$ is the condition to be satisfied for the photoinduced energy transfer to occur and for the coupling between the oscillating electron of *D and electrons of A to be established.

The nature of perturbation Hc can be represented in terms of interaction between the electron d standing on the LUMO of the excited donor and the electron a of the HOMO of the acceptor, as represented in Figure 5.2:
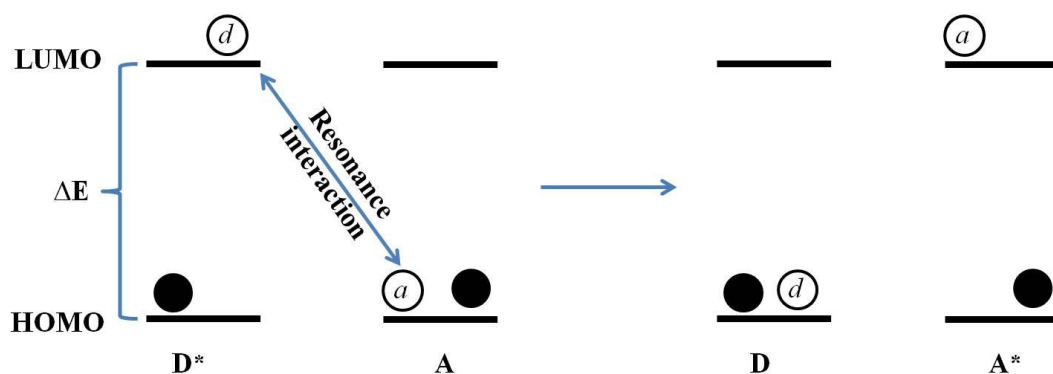
Figure 5.2 Schematic representation of Coulombic mechanism of energy transfer.

The energy of two interacting dipoles, from a classical point of view, is directly correlated to their magnitude, μD and μA, but inversely correlated to their distance R_{DA} as shown in Eq.5.6:

$$E(*D \text{ dipole- } A \text{ dipole}) = \frac{\mu D \mu A}{R_{DA}^3} \qquad \text{(Eq. 5.6)}$$

Förster[1] associated μD and μA to the oscillator strength of radiative transitions $*D \rightarrow D$ and $A \rightarrow *A$, respectively. These values depend on several factors such as vibrations and spin. So, since they can be determined experimentally, it is possible to predict the entity of such an interaction.

Förster's theory establishes that the kinetic constant of the resonance energy transfer (FRET) is proportional to the square of μD and μA but also to inversely to the sixth power of their distance $R_{DA,}$ as shown in equation 5.7:

$$k_{FRET} \sim E^2 \sim \left(\frac{\mu D \mu A}{R_{DA}^3}\right)^2 = (\mu D \mu A)^2 / R_{DA}^6 \qquad \text{(Eq 5.7)}$$

Moreover Equation 5.7 can be modified[2] by introducing the experimental parameters correlated to μD and μA:

$$k_{FRET} = \left(\frac{1}{\tau_D}\right)\left(\frac{R_0}{R_{DA}}\right)^6 \qquad \text{(Eq.5.8)}$$

with $R_0^6 = \dfrac{\phi_D \, \kappa^2 \, 9000 \, (\ln 10)}{n^4 N_A \, 128 \, \pi^5} J = \dfrac{\phi_D \, \kappa^2 \, 9000 \, (\ln 10)}{n^4 N_A \, 128 \, \pi^5} \int_0^\infty F_D(\lambda)\varepsilon_A(\lambda)\lambda^4 d\lambda$

(Eq. 5.8.1)

Where Q_D and τ_D are the emission quantum yield and lifetime of donor in the absence of the acceptor, respectively; n is refractive index of the medium; N_A is Avogadro number; R_{DA} = donor-acceptor distance, $F_D(\lambda)$ is the emission intensity of the donor in the range from λ to $(\lambda + d\lambda)$, with total intensity normalized to 1; $\varepsilon_A(\lambda)$ is the molar absorption coefficient of the acceptor in $M^{-1}cm^{-1}$; κ is the orientation factor between the donor and acceptor dipoles. It follows that the most important factors affecting the probability for FRET to occur are Q_D, τ_D and ε_A as well as the overlap integral and the distance between the donor and the acceptor.

FRET can be finally referred as to a long-range mechanism not requiring a physical contact between the donor and the acceptor and, as any transition between two quantum states, it must obey the spin selection rules. Such rules are based on the conservation of the spin within each molecule; so both of transitions $D^* \rightarrow D$ and $A \rightarrow {}^*A$ must be spin allowed, then processes such as Singlet-Singlet and Singlet-Triplet are allowed:

Singlet-Singlet   Singlet- Triplet

${}^1D^* + {}^1A \rightarrow {}^1D + {}^1A^*$ ${}^1D^* + {}^3A \rightarrow {}^1D + {}^3A^*$
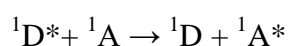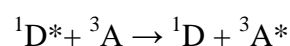
while processes such as Triplet-Singlet and Triplet-Triplet are forbidden:

Triplet-Singlet   Triplet- Triplet

${}^3D^* + {}^1A \rightarrow {}^1D + {}^1A^*$ ${}^3D^* + {}^1A \rightarrow {}^1D + {}^3A^*$
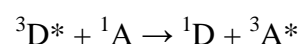
A classical example of singlet-singlet FRET is the one occurring in light harvesting systems of photosynthetic organisms.[3] In the case of metal complexes the lowest excited state with a significant lifetime is usually spin forbidden, then it would be rare to observe FRET in such a system.

Many examples of chemosensors consisting of QDs decorated with functional molecules and based on FRET mechanism, either from the photoexcited QD to the chromophore or in the opposite way, are available.

For example QD-based pH sensors, wherein QDs act as donor and the absorption of the chromophoric acceptor depends on the pH, have been reported. The energy transfer efficiency depends, as already discussed previously, on the spectral overlap between the donor emission and the acceptor absorption, then pH-dependent spectral shifts of the dye absorption will result in different energy transfer efficiencies.

The first ratiometric QD-based pH sensor have been developed by Nocera[4] and consists of CdSe–ZnS Core-Shell QDs encapsulated within an amphiphilic polymer conjugated with a squaraine dye. The emission profile of such nanohybrids is pH dependent. In particular at low pH values the absorption band of the dye matches the emission band of QDs, so the energy transfer is efficient and QDs are quenched. The emission spectrum is dominated by the band of the squaraine dye. Conversely at high pH values the spectral overlap is small, the energy transfer is inefficient and the emission spectrum shows only the QD band. The behaviour of such a chemosensor is represented in Figure 5.3:
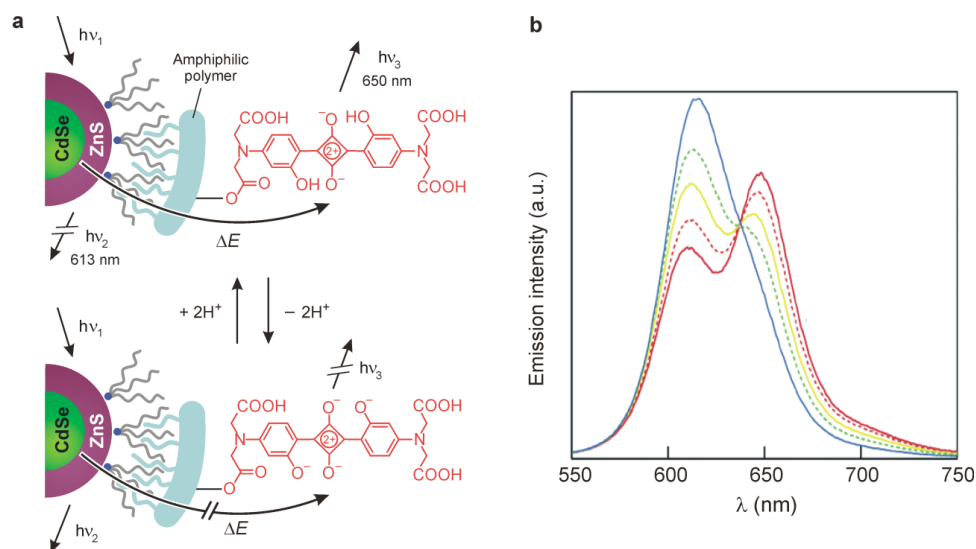
Figure 5.3 (a) Scheme of a luminescent pH sensor composed of CdSe-ZnS QDs functionalized with a pH-sensitive squaraine. (b) Emission spectra of the QD-squaraine conjugate at different pH values (H$_2$O, λ_{exc} = 380 nm): 6.0 (red solid line); 7.0 (orange dotted line); 8.0 (yellow solid line); 9.0 (green dotted line); 10 (blue solid line). Adapted by permission from reference [4].Copyright Springer 2016.

The pH-triggered modulation of the overlap of QD and chromophore emission and absorption spectra was also investigated in the case of CdTeSe-ZnS QDs functionalized with near infrared (NIR) fluorescent probes such as carbocyanines.[5] Such probes are very suitable for sensing in biological environment, since NIR light has the maximum depth of penetration in tissues. Moreover the control of pH is fundamental for many cellular processes, then its measurement has a relevant biological importance.

QDs can also play the role of acceptors in energy transfer processes. For example, it has been observed that QDs are efficient energy acceptors in combination with long-lived lanthanide-based donors.[6] Five different QDs decorated with biotin were modified with a luminescent Terbium complex conjugated to streptavidin for multiplexed diagnostics. CdSe-ZnS or CdSeTe-ZnS nanocrystals with emission maxima at 529, 565, 604, 653 and 712 nm have been selected to fit within the gaps of the terbium complex emission bands. A simple scheme of such nanohybrids is reported in Figure 5.4.
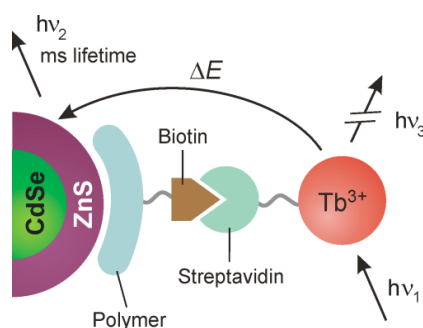
Figure 5.4 A nanohybrid consisting of a surface-biotinylated QD bound to a terbium complex-streptavidin conjugate. Upon light excitation of the lanthanide complex in the UV, energy is transferred to the QD, thus resulting in luminescence quenching of Tb and the appearance of a long-lived QD luminescence with millisecond decay times. Adapted by permission from reference [6].Copyright Springer 2016.

The nature of the exchange perturbation Hs can be described in terms of an overlap between the electron cloud standing on the LUMO of D* and the LUMO of A and of another overlap between the electron cloud standing on the HOMO of A and the HOMO of D* thus providing a double electron transfer as represented in figure 5.5
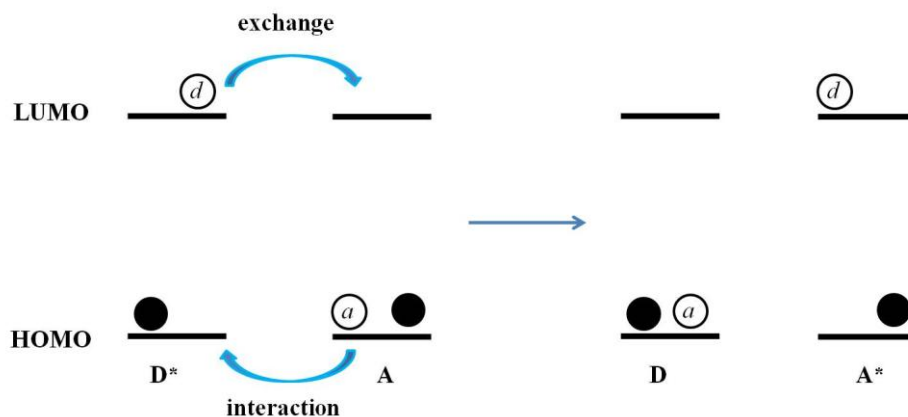
Figure 5.5 Schematic representation of exchange mechanism of energy transfer.

The exchange mechanism is a short-range interaction requiring a physical contact between the donor and the acceptor for electron cloud overlapping to occur.

The theory of Exchange energy transfer has been developed by Dexter[7] and provides the following equation for calculating the kinetic constant:

$$k_{\text{Dexter ET}} = (\frac{2\pi}{h}) \, K \, J \, \exp(-2R_{DA}/L) \qquad \text{(Eq. 5.9)}$$

where $J = \int_0^\infty F_D(\lambda) \varepsilon_A(\lambda) d\lambda$

K is related to specific orbital interaction, J is a spectral overlap integral normalized for the extinction coefficient of the acceptor ε_A and R_{DA} is the donor-acceptor separation relative to the sum of their van der Walls radii, L.

It is important to note that in this case J is normalized for ε_A so it does not depend on the magnitude of ε_A, then $k_{ET(\text{exchange})}$ is expected to be independent on the absorption characteristic of the acceptor, differently from $k_{ET(\text{Coulombic})}$ thus implying that excited states spin-forbidden can be involved in such a process.

Since the exchange mechanism can be considered as a collisional interaction, the spin selection rules arise from the necessity to conserve the total spin of such a collisional complex, meaning that processes such as singlet-singlet and triplet-triplet are allowed:

Singlet-Singlet $\qquad\qquad$ Triplet- Triplet

$$^1D^* + {}^1A \rightarrow {}^1D + {}^1A^* \qquad\qquad ^3D^* + {}^1A \rightarrow {}^1D + {}^3A^*$$
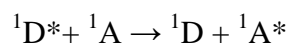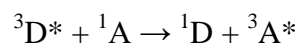
while processes such as singlet-triplet and triplet-singlet are forbidden:

Singlet-Triplet $\qquad\qquad$ Triplet- Singlet

$$^1D^* + {}^1A \rightarrow {}^1D + {}^3A^* \qquad\qquad ^3D^* + {}^1A \rightarrow {}^1D + {}^1A^*$$
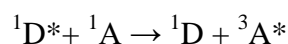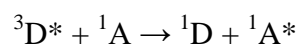
Triplet-Triplet Dexter energy transfer was observed for the first time by Terenin and Ermolaev.[8] In their work the lowest triplet state of naphthalene was sensitized by the excited triplet of benzophenone in rigid matrix at 77 K. The first example of triplet-triplet energy transfer in solution has been provided by Backstrom and Sandros.[9]

Triplet-Triplet energy transfer is also important for selectively triplet quenching as well as for sensitizing triplet states in organic reactions.[10]

A particular Triplet-Singlet allowed process $^3D^* + {}^3A \rightarrow {}^1D + {}^1A^*$ is the one involving the formation of singlet oxygen of $^1O_2$ from a photosensitizer such a polypyridyl ruthenium (II) complex in its lowest excited triplet state. This sensitization process is also a basis of photodynamic therapy (type II).

Dexter-like triplet-triplet energy transfer from QDs to suitable organic surfactants has been recently observed by Castellano and co-workers.[11]

CdSe QDs with a diameter of 2.4 nm were decorated with 9-anthracenecarboxylic acid or 1-pyrenecarboxylic acid (see Figure 5.6). Once photoexcited the QDs are quantitatively quenched and ultrafast transient absorption spectra showed that the decay of the QD excited state occurs on a timescale coinciding with the growth of the $T_1 \rightarrow T_n$ transition of 9-anthracenecarboxylic acid, thus confirming that an energy transfer from the QD to the organic surface ligand is occurring.

The same results were achieved in the case of QDs decorated with 1-pyrenecarboxylic acid but with different kinetics.

Moreover, both the energy transfer from the long-lived triplets localized on the surfactants to suitable acceptors (e.g., 2-chloro-9,10-bisphenylethynylanthracene) free in solution and the photosensitization of oxygen, as indicated by the typical phosphorescence spectrum centered at 1270 nm, were successfully demonstrated. These results suggest that quantum dots can be useful photosensitizers for applications in optoelectronics, solar energy conversion, and medicine.
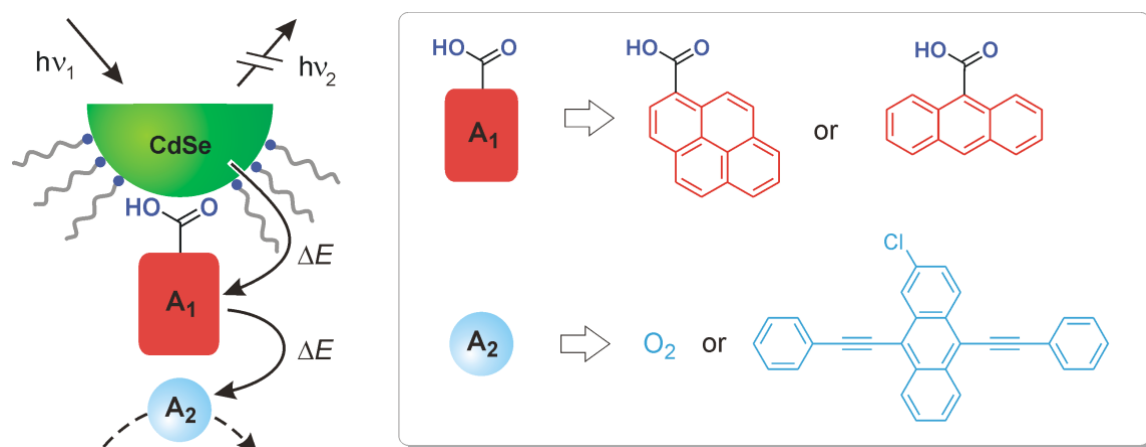
Figure 5.6. Schematic representation of nanohybrids composed of CdSe QDs and surface-adsorbed organic molecules acting as triplet energy acceptors (A_1). Triplet-triplet energy transfer from the organic ligands to secondary molecular acceptors (A_2) freely diffusing in solution is also shown. Adapted from reference [11]. Copyright Springer 2016.

5.1.3 Reversible Electronic Energy transfer

Electronic energy transfer is typically considered a unidirectional process from the donor to the acceptor independently of the mechanism. However, if the energy levels involved in such a process are very close to one another then the forward energy transfer can be followed by a back energy transfer from the acceptor to the donor, thus resulting in the equilibration between these two states or in other words in a reversible energy transfer (REET). Moreover if the lifetime of one of these two excited states involved is much longer than the other one then an elongation of the shorter lifetime is observed. Such an elongation is normally the consequence of reversible Dexter type Triplet-Triplet energy transfer.

As well as previously discussed mechanisms also the REET must satisfy proper conditions to occur. These conditions can be identified by considering the prototypical example of supramolecular system showing REET. Such a system has been developed by Ford and Rodgers[12] and consists of a polypyridyl ruthenium (II) complex connected to a pyrenyl moiety through a flexible bridge. The energy levels of these two components as well as the energetic and kinetic parameters are schematized in Figure 5.7.
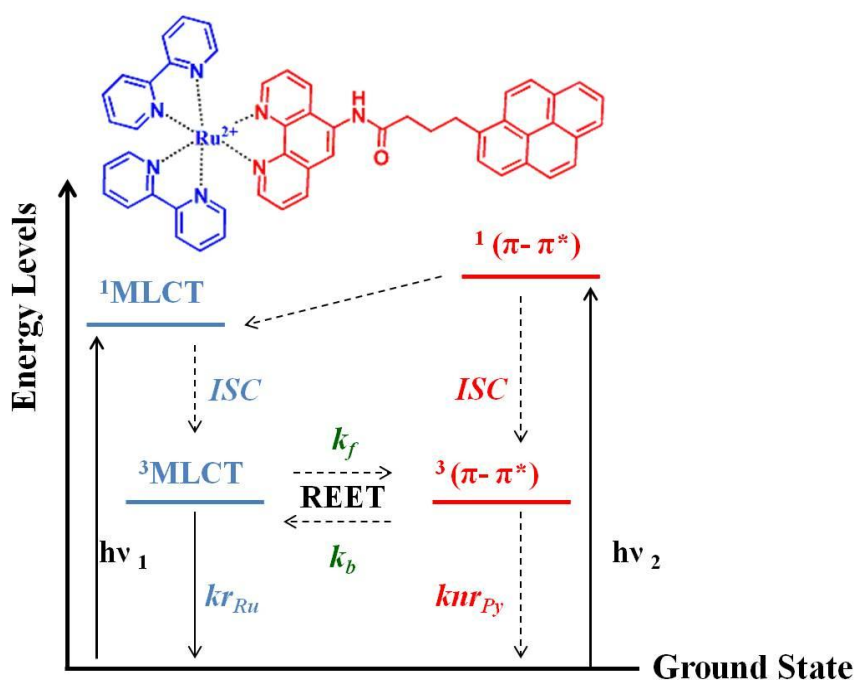

Figure 5.7 Schematic representation of REET occurring after selectively exciting the polypyridyl ruthenium (II) complex or the pyrenyl moiety.

ISC= intersystem crossing;

k_f = rate constant for direct energy transfer from Ru(II) complex to pyrenyl moiety;

k_b= rate constant for back energy transfer;

kr_{Ru} and knr_{Py} are the intrinsic rate deactivation constant of ^{3}MLCT and $^3\pi$-π* states, respectively

In such a system the two lowest triplet excited states (i.e. the emitting ^{3}MLCT of the polypyridyl ruthenium (II) complex and the $^3\pi$-π* of the pyrenyl moiety) are so close in terms of energy ($\Delta E < 0.1$ eV) that, for example, if the Ru(II) moiety is selectively excited then the forward energy transfer from its ^{3}MLCT to the $^3\pi$-π* of the pyrenyl moiety is followed by a back energy transfer.

Moreover the rate constant for the direct, k_f, and back, k_b, energy transfer are, respectively, 1.3 x 10^8 s^{-1} and 7.2 x 10^6 s^{-1} so 2-3 times bigger than the intrinsic deactivation rate constants kr_{Ru} and knr_{Py} which are typically around 10^6 s^{-1} for Ru(II) moiety[13] and 10^3 s^{-1} for pyrenyl moiety. Consecutively an excited-state equilibration is established with the pyrene chromophore playing the role of energy reservoir.

The rate for reaching such an equilibrium is the sum of k_f, and k_b while the ratio of k_f over k_b is the equilibrium constant.

After the equilibration, the two components will decay with a common rate, which is the weighted linear combination of kr_{Ru} and knr_{Py}, giving rise to a unique lifetime. From an experimental point of view, the most important evidence of such an equilibration is the elongated lifetime of ruthenium complex, which corresponds to roughly 11 μs, with respect to the one measured in the absence of the pyrenyl moiety and corresponding to less than 1 μs.

Another condition for the excited states equilibration to occur is to avoid any interferences from oxygen, meaning that a deareated environment is required. In fact in aerated conditions the triplet state sensitized by the direct energy transfer will be immediately quenched by free oxygen, so that the equilibration cannot occur anymore.

After Ford's and Rodgers's pioneering work, REET has been exhaustively investigated.

Wilson and co-workers[14,15] pointed out the importance of the energy difference between the triplet states involved by replacing the pyrenyl moiety of Ford's and Roger's system with homologous naphthalene or anthracene moieties. In the case of pyrene the two lowest triplet states are almost isoenergetic, while in the cases of naphthalene and anthracene the organic triplet is higher and lower, respectively, with respect to the ^{3}MLCT, meaning that REET cannot take place anymore. Supramolecular systems consisting of a polypyridyl ruthenium (II) complex connected to anthracenyl[16] or naphtalenyl[17] moieties and showing REET have been developed just by modulating properly the position of the organic triplet.

Castellano and co-workers[18] have investigated first if the presence of more than one chromophore with respect to the Ru(II) complex can affect the excited state equilibration. They observed that the higher is the number of organic chromophores the higher is the value of the equilibrium constant, simply because the higher is the number of acceptors the more favored is the direct energy transfer so the higher is the value of k_f while it is reasonable to assume constant k_b since the forward process always involves only one ^{3}MLCT state.

The solvatochromic effect on REET have been also investigated by studying the behaviour of a tetracyano ruthenate(II) pyrenyl complex[19] in different solvents. By changing solvent the excited states stabilization will be modulated then the triplet states will be differently shifted so that the energy transfer process can occur as uni- or bidirectional or be suppressed.

REET has been recently observed in other different type of supramolecular architectures such as a pseudorotaxanes[20] consisting of a central electron-rich dialkoxynaphthalene unit, as a thread, and a tetracationic cyclophane, as a cage; and a foldaxane[21] consisting of a helical foldamer arranged around a linear molecular axis in analogy to rotaxanes. Such systems are schematized in Figures 5.8 and 5.9, respectively.
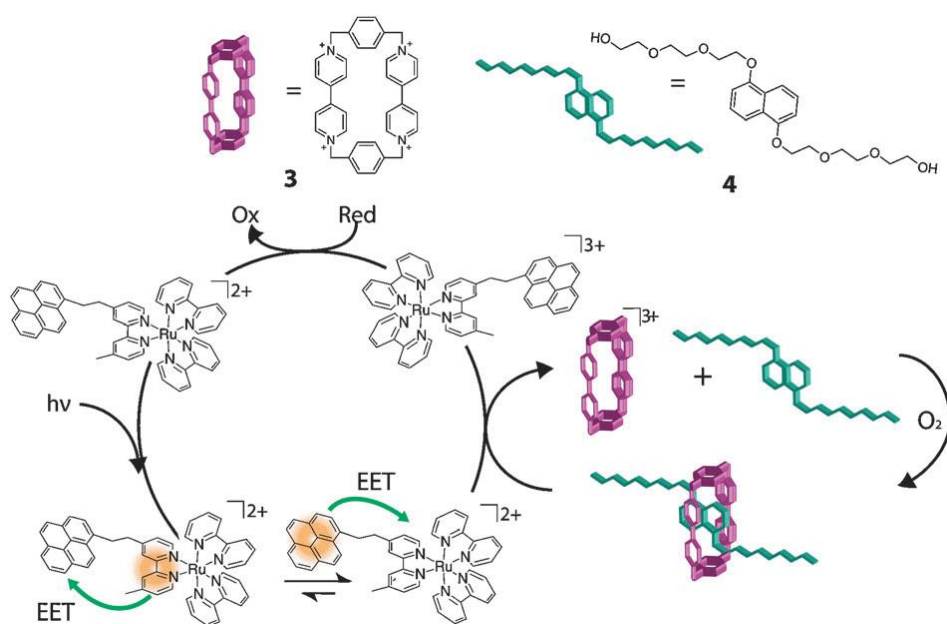
Figure 5.8 Schematic representation of REET occurring in photocatalytic electron pumping driving a molecular piston. The irradiation of a suitable external photosensitizer, in the presence of a sacrificial reductant, induces reduction and disassembly of the pseudorotaxane, while reassembly of the molecular piston is restored in the presence of oxygen. Adapted from reference [20]. Copyright RSC publishing 2012.

The system shown in Figure 5.8 was already developed by Balzani and Stoddart in 1998[22] and concerns the photochemically driven threading and dethreading of the pseudorotaxane by exploiting an external electron-transfer photosensitizer such as a polypyridyl ruthenium complex (e.g., $[Ru(bipy)_3]^{2+}$) in the presence of a large excess of a suitable sacrificial reductant (e.g., triethanolamine) to prevent undesired back electron transfer. If the "simple" $Ru(bipy)_3]^{2+}$) is replaced with another one showing REET, such as ruthenium complex bearing a pyrenyl moiety, then a more efficient dethreading is achieved, by taking advantage of both long-lived excited state and the nature of the donor. As already said, if REET is occurring then the energy is prevalently localized on the aromatic triplets, which have seen to be better electron donors than MLCT states for spin-orbit factors.
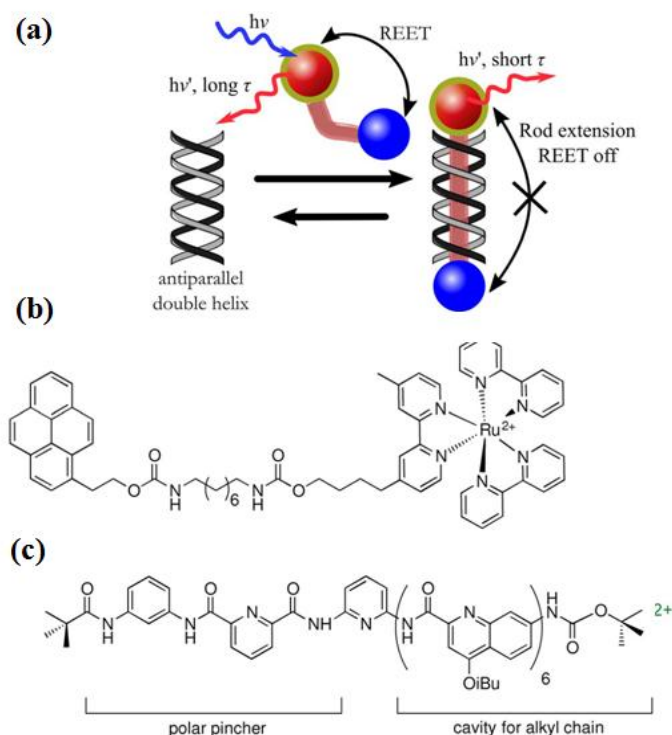
Figure 5.9 Modulation of REET in a dynamic foldaxane (a); molecular structures of molecular thread (b) and foldamer (c), which dimerizes in solution giving (c)$_2$.

Adapted from reference [21]. Copyright Wiley-VCH 2016.

A foldamer is an artificial discrete chain molecule/ oligomer (see Figure 5.9 c), which can self-assemble into a conformationally-ordered configuration in solution (e.g., a double helix) which can host a bichromophoric thread (see Figure 5.9 b) in its central cavity (see Figure 5.9 a). REET can occur only in the case of such a thread free in solution; while, once these two components have arranged in a more rigid supramolecular architecture, the two chromophoric units of the thread are so far apart that a significant decoupling is established and REET cannot occur anymore. Such a conformation-dependent reversible electronic energy transfer can provide a new tool for the investigation of the geometry on the molecular scale.

It is important to note that all the REET examples already published concerns molecular entities connected in a more complex supramolecular architecture, but there is no example reported in literature of REET occurring in nanohybrids consisting of QDs and suitable chromophoric units.

Moreover, the QDs have the enormous advantage that their emitting state can be tuned by manipulating their size, thus providing a significant accuracy in projecting and developing of REET-based systems. The experiments described in the next paragraph provide the first evidence of the elongation of lifetime of colloidal luminescent nanocrystals.

5.2 Results and discussion

5.2.1 First strategy: QDs coated with lipoic acid based surfactants

The strategy initially adopted concerned the development of QDs decorated with lipoic acid based ligands bearing chromophoric units such as pyrene, naphthalene imide and a Ru(II) based metal complex. (Note: See chapter 2 for synthetic procedures of developed ligands).

As discussed above, for REET to occur it is necessary that the energetic levels involved are as close as possible. By taking advantage of the synthetic procedures which allows us to prepare QDs with an accurate control of their dimension, suitable nanohybrids consisting of CdSe-4ZnS Core-Shell quantum dots functionalized with lipoic acid based surfactants have been prepared and investigated. The structure of such ligands are represented in Figure 5.10:
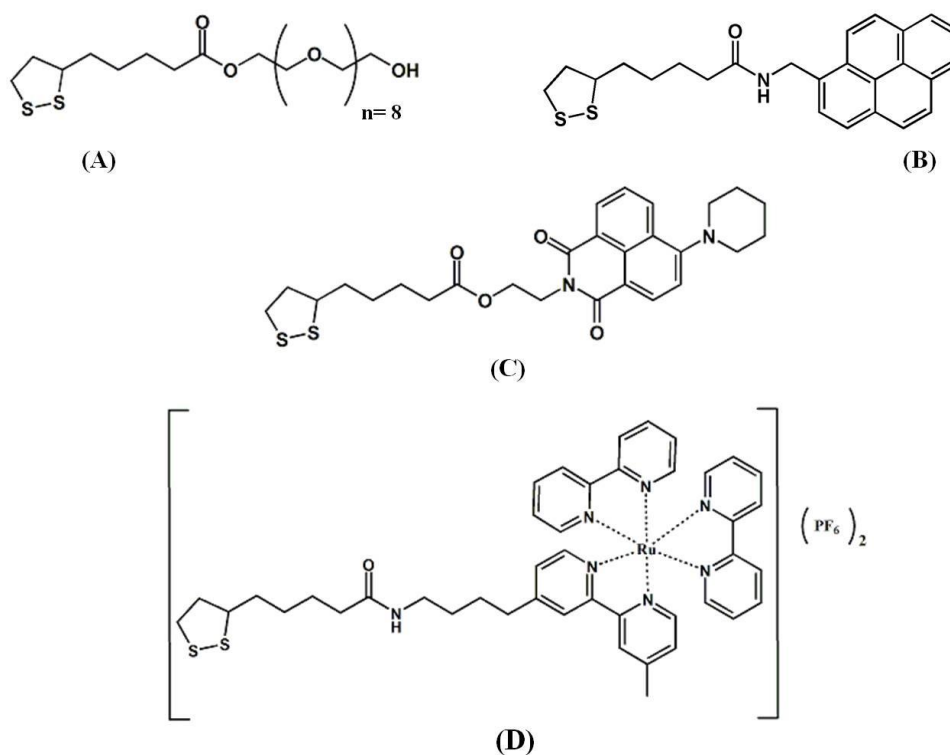
Figure 5.10 Molecular structure of (A) LA-PEG$_{400}$; (B) LA-PYR; (C) LA-NAP; (D) LA-Ru.

CdSe-4ZnS Core-Shell Quantum Dots have been prepared according to Peng's protocol described in Chapter 2, then ligand exchange has been performed by adding to a methanolic solution of lipoic acid derivatives such as LA-PEG400 and LA-Pyr or LA-Nap or LA-Ru (0.024 mmol; 95% of LA-PEG$_{400}$ and 5% of lipoic acid conjugated with a chromophore) the hexane solution of TOPO/TOP coated QDs (1:30000 QD/Lipoic Ligands ratio). Once an excess of TBABH$_4$ had been added, the disulfide bridges of the ligands have been broken so immediately that, upon stirring the biphasic mixture, a fast and efficient ligand exchange occurred.

After removing the colorless hexane layer the methanolic phase was washed with fresh hexane to remove unreacted nanocrystals. Large aggregates were separated by using a syringe filter (0,45 μm pore size), and unreacted DHLA ligands were removed by three cycles of dilution/concentration with centrifugal filter (Amicon Ultra-0.5 mL, 30 kDa, 7000 rpm, 25°C, 12 minutes).

All the samples have been then characterized and investigated in deareated conditions, as shown in the next figures:
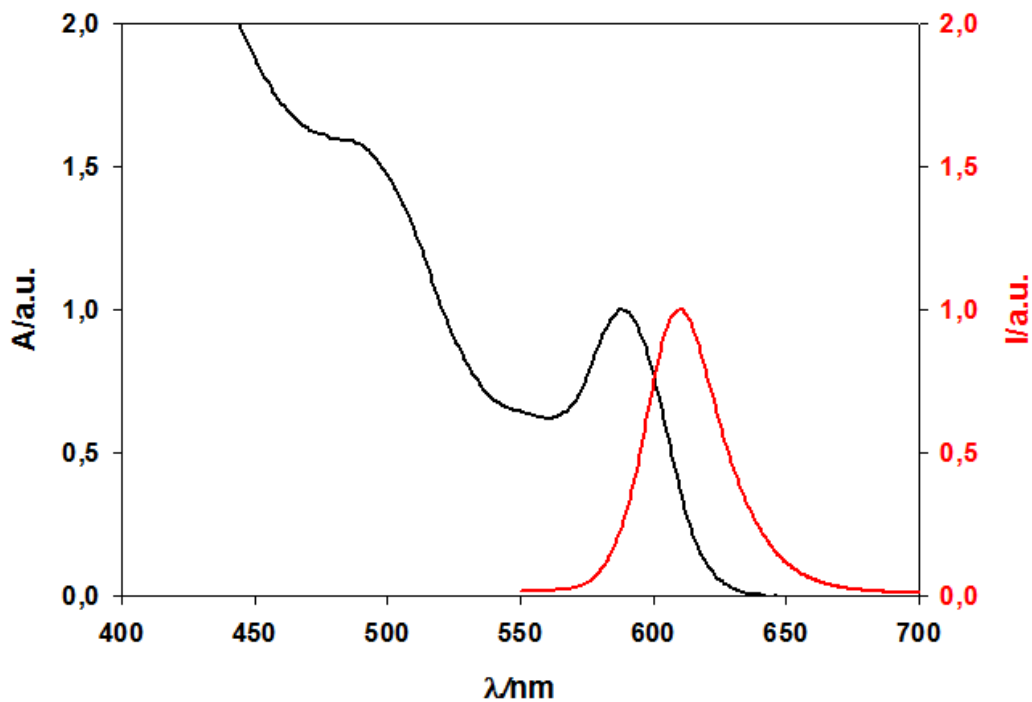
Figure 5.11 Normalized absorption (black line) and emission (red line) spectra in MeOH of CdSe-4ZnS QDs functionalized with LA-PEG$_{400}$.
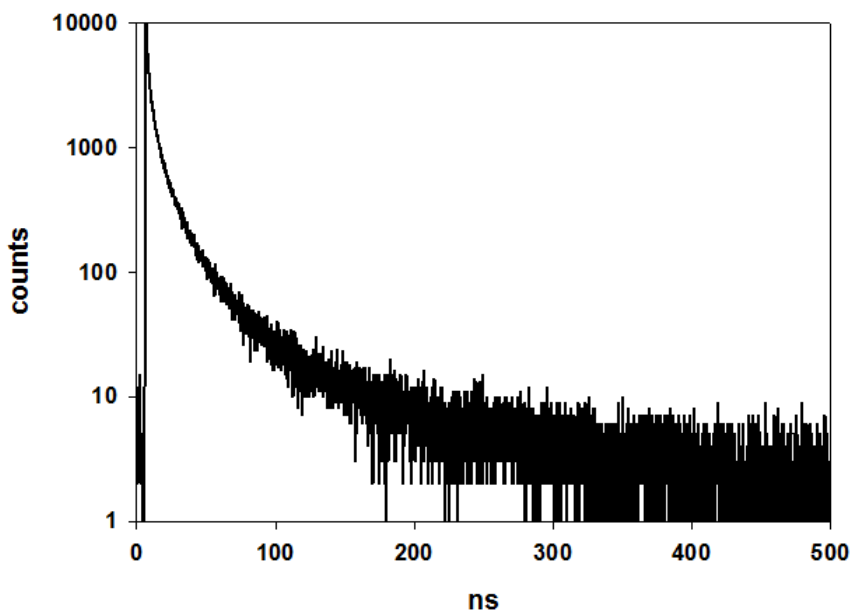

Figure 5.12 Luminescence lifetime of CdSe-4ZnS functionalized with LA-PEG$_{400}$ recorded in deareated MeOH by exciting QDs at 405 nm.The time scale is 500 ns while the 10000 counts detected at 615 nm are reported in logarithmic scale.

λ exciton peak	λ emission maximum	φ	τ			
586 nm	615 nm	30 %	τ_1=3 ns	B_1= 1895	22%	χ^2= 1,17
			τ_2=13 ns	B_2= 1152	52%	
			τ_3=47 ns	B_3= 147	26%	

Table 5.1 Photophysical properties of CdSe-4ZnS QDs functionalized with LA-PEG$_{400}$.
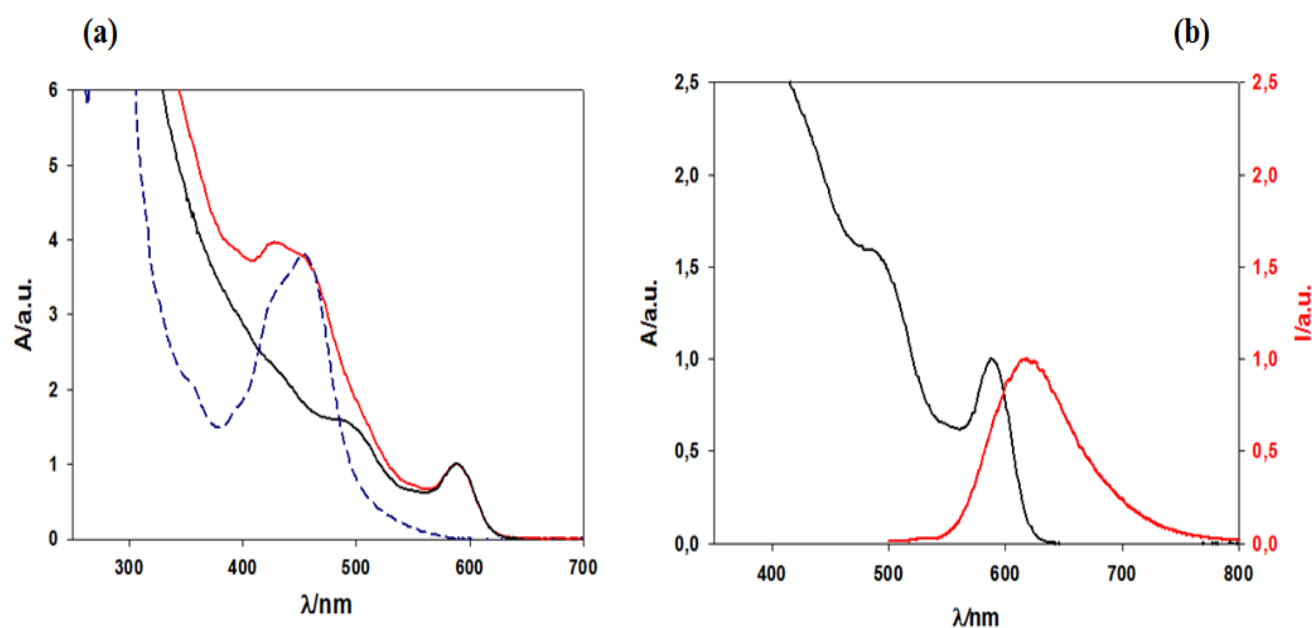
Figure 5.13 (a) Normalized absorption spectra of CdSe-4ZnS decorated with LAPEG$_{400}$ (black line), LAPEG$_{400}$ /LA-Ru (red line), and only LA-Ru (dashed blue line) in MeOH. (b) Normalized absorption spectra of LAPEG$_{400}$ decorated CdSe-4ZnSQ Ds in MeOH (black line) and triplet emission spectrum of LA-Ru (red line) recorded in MeOH by exciting at 450 nm.
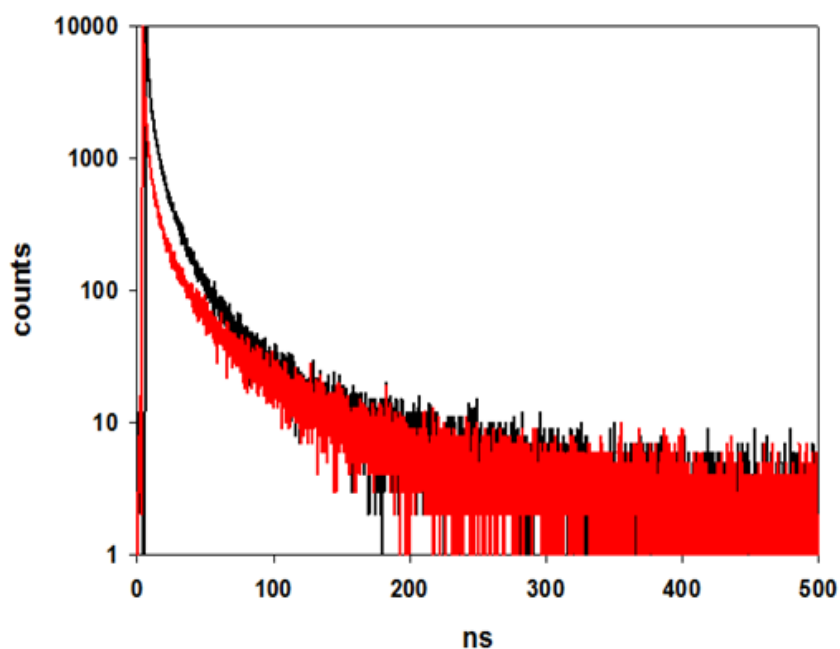
Figure 5.14 Luminescence lifetimes of CdSe-4ZnS decorated with LAPEG$_{400}$ (black decay), LAPEG$_{400}$/LA-Ru (red decay) recorded in deareated MeOH by exciting selectively QDs at 600 nm. The time scale is 500 ns while the 10000 counts detected at 615 nm are reported in logarithmic scale.

ϕ	τ				ϕ	τ			
	τ_1=3 ns	B$_1$= 1895	22%			τ_1=2 ns	B$_1$= 2152	25%	
30 %	τ_2=13 ns	B$_2$= 1152	52%	χ^2= 1,17	26 %	τ_2=11 ns	B$_2$= 670	42%	χ^2= 1,17
	τ_3=47 ns	B$_3$= 147	26%			τ_3=54 ns	B$_3$= 106	33%	

Table 5.2 Lifetimes and emission quantum yields values of CdSe-4ZnS functionalized with LA-PEG$_{400}$ (in black) and with LAPEG$_{400}$/LA-Ru (in red).
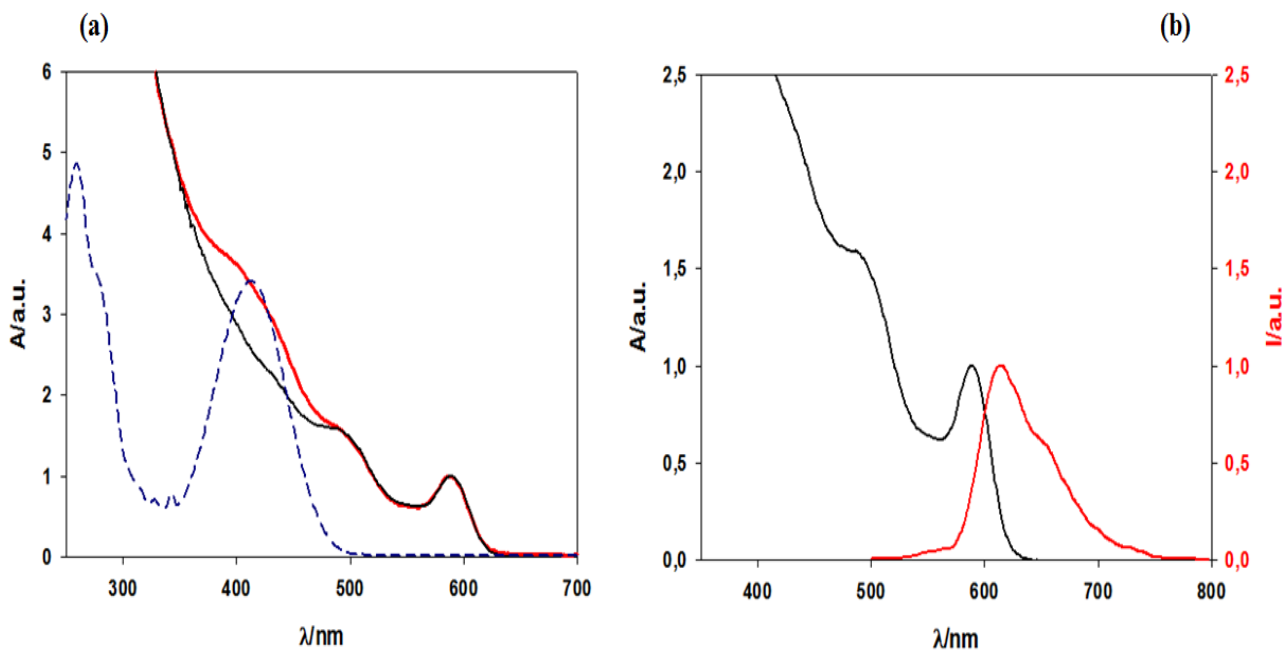
Figure 5.15 (a) Normalized absorption spectra of CdSe-4ZnS decorated with LAPEG$_{400}$ (black line), LAPEG$_{400}$ /LA-NAP (red line) and only LA-NAP (dashed blue line) in MeOH.

(b) Normalized absorption spectra of LAPEG$_{400}$ decorated CdSe-4ZnSQ Ds in MeOH (black line) and triplet emission spectrum of LA-NAP (red line) recorded in CHCl$_3$/ CH$_2$Cl$_2$ (1:1, v:v) at 77 K by exciting at 410 nm (time delay = 0.04 ms; gate = 2 ms; cycle = 20 ms; fòash count = 1).
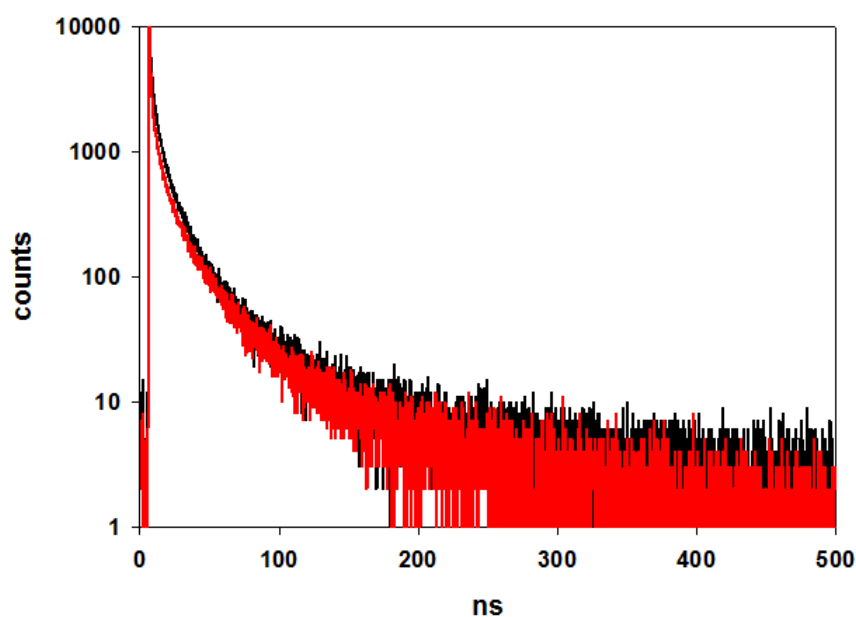
Figure 5.16 Luminescence lifetimes of CdSe-4ZnS decorated with LAPEG$_{400}$ (balck decay), LAPEG$_{400}$ /LA-NAP (red decay) recorded in deareated MeOH by exciting selectively QDs at 600 nm. The time scale is 500 ns while the 10000 counts detected at 615 nm are reported in logarithmic scale.

ϕ	τ			
30 %	τ_1=3 ns	B_1= 1895	22%	χ^2= 1,17
	τ_2=13 ns	B_2= 1152	52%	
	τ_3=47 ns	B_3= 147	26%	

ϕ	τ			
28 %	τ_1=2 ns	B_1= 2142	19%	χ^2= 1,17
	τ_2=10 ns	B_2= 1072	47%	
	τ_3=40 ns	B_3= 197	34%	

Table 5.3 Lifetime and emission quantum yields values of CdSe-4ZnS functionalized with LA-PEG$_{400}$.(in black) and with LAPEG$_{400}$/LA-NAP (in red).

121
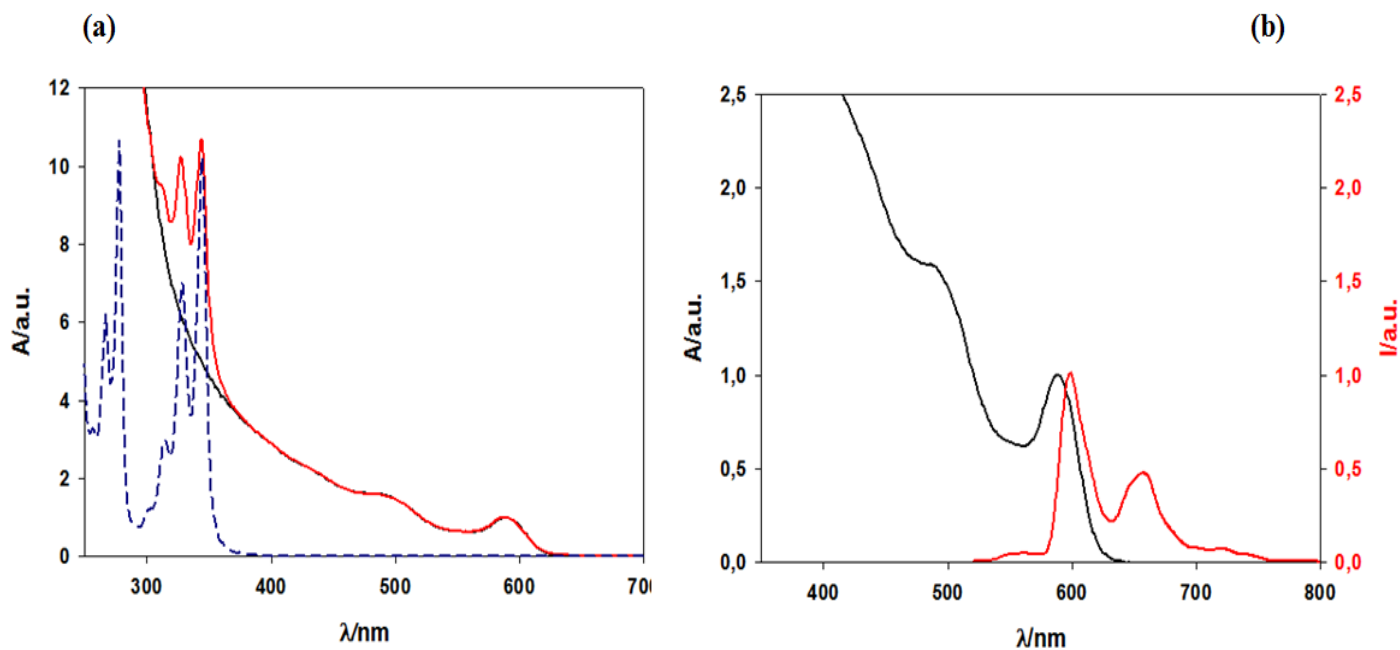
Figure 5.17 (a) Normalized absorption spectra of CdSe-4ZnS decorated with LAPEG$_{400}$ (black line), LAPEG$_{400}$/LA-PYR (red line) and only LA-PYR (dashed blue line) in MeOH. (b) Normalized absorption spectra of LAPEG$_{400}$ decorated CdSe-4ZnSQ Ds in MeOH (black line) and triplet emission spectrum of LA-PYR (red line) recorded in CHCl$_3$/CH$_2$Cl$_2$ (1:1, v:v) at 77 K by exciting at 410 nm (time delay = 0.04 ms; gate = 2 ms; cycle = 20 ms; fòash count = 1).
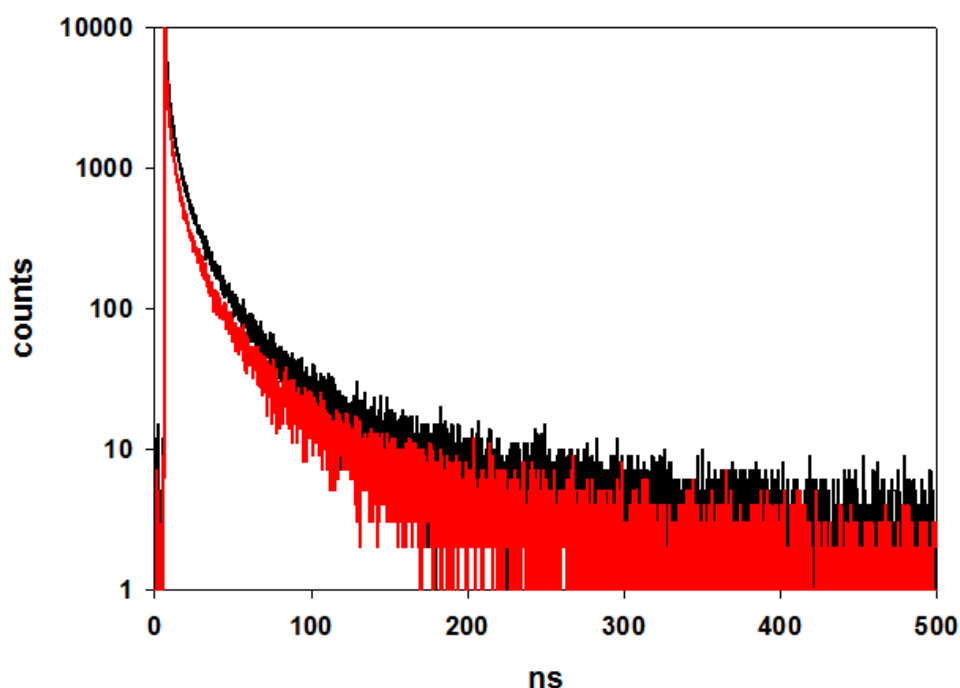
Figure 5.18 Luminescence lifetimes of CdSe-4ZnS decorated with LAPEG$_{400}$ (balck decay), LAPEG$_{400}$ /LA-PYR (red decay) recorded in deareated MeOH by exciting selectively QDs at 405 nm. The time scale is 500 ns while the 10000 counts detected at 615 nm are reported in logarithmic scale.

φ	τ				φ	τ			
	τ_1=3 ns	B_1= 1895	22%			τ_1=2 ns	B_1= 3214	22%	
30 %	τ_2=13 ns	B_2= 1152	52%	χ^2= 1,17	24 %	τ_2=9 ns	B_2= 1408	50%	χ^2= 1,12
	τ_3=47 ns	B_3= 147	26%			τ_3=37 ns	B_3= 174	28%	

Table 5.4 Lifetimes and emission quantum yields values of CdSe-4ZnS functionalized with LA-PEG$_{400}$.(in black) and with LAPEG$_{400}$/LA-PYR (in red).

The strategy initially adopted concerned essentially to position as close as possible the exciton level of QDs to the triplet states of chromophores attached on their surface, as shown by the previous figures. However, very minor modifications in the emission decay were observed and no elongation of the luminescence lifetime took place.

5.2.2 First strategy: QDs coated with 1-pyrenecarboxylic acid

After these disappointing results, another strategy was adopted. Lipoic acid based ligands were replaced by 1-Pyrene Carboxylic Acid (1-PCA) which is known to act as an energy acceptor in Dexter's type Energy Transfer with QDs, as previously mentioned. Since such a process is intrinsically a short-range interaction involving a physical contact between the two components, then it is reasonable to assume that the shell can prevent this interaction. For this reason QDs consisting only of a CdSe Core were selected for subsequent experiments.

Four different batches of QDs were synthesized by following Maitra's protocol described in Chapter 2. The absorption spectra and main properties of such batches are reported in figure 5.19 and table 5.5 respectively, while the molar absorption spectrum of 1-PCA is reported in Figure 5.20.
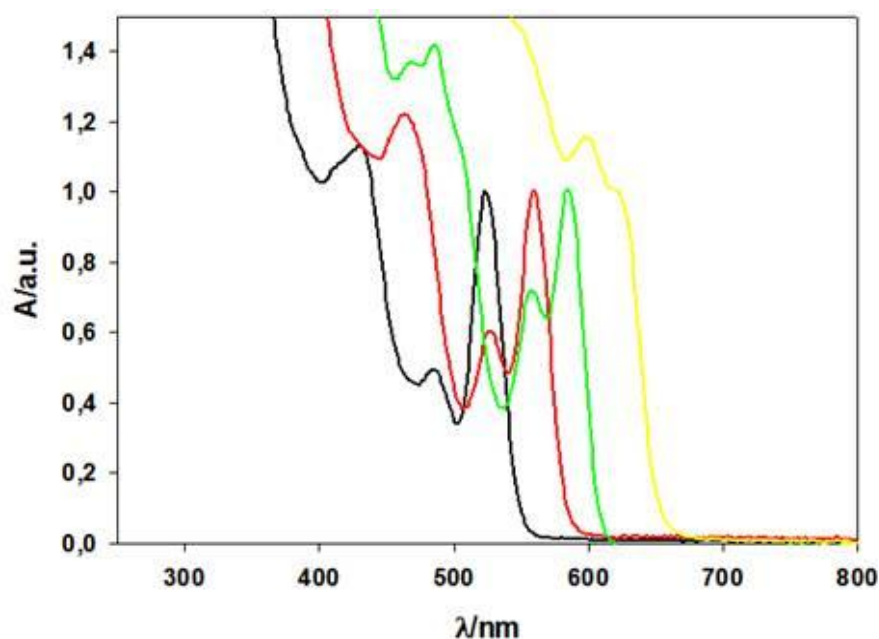

Figure 5.19 Normalized absorption spectra of CdSe 1 (black line), CdSe 2 (red line), CdSe 3 (green line) and CdSe 4 (yellow line) recorded in heptane.

QD	λ exciton peak (Diameter)	QY
CdSe 1	524 nm (2.61 nm)	0.18
CdSe 2	560 nm (3.26 nm)	0.16
CdSe 3	586 nm (4.02 nm)	0.57
CdSe 6	622 nm (5.72 nm)	0.03

**Table 5.5** Spectroscopic and dimensional data of CdSe 1-4 samples.
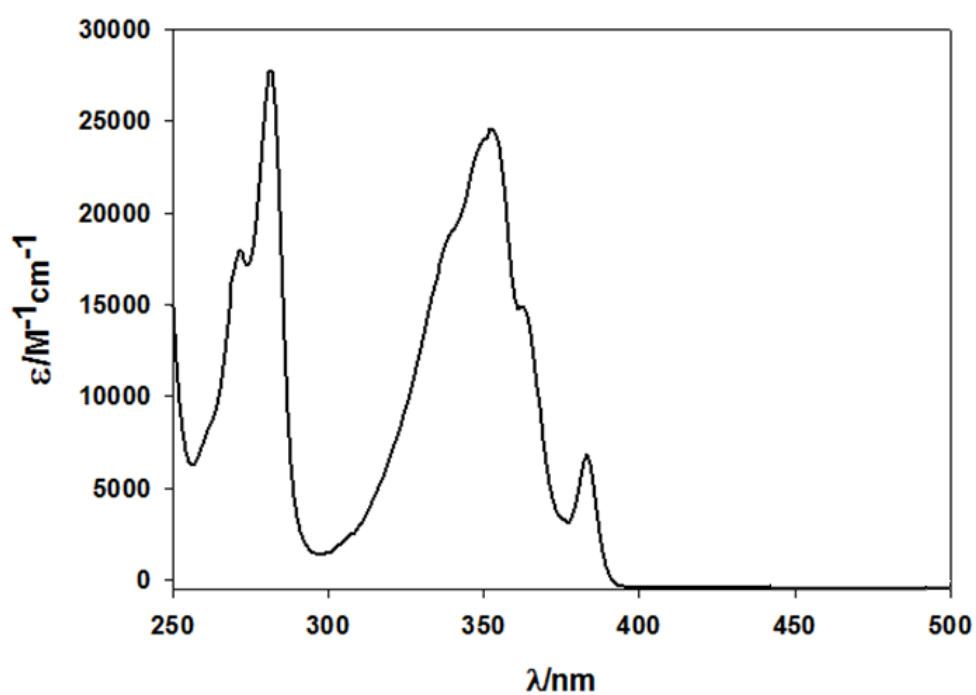
Figure 5.20 Molar Absorption Spectrum of 1-PCA recorded in THF.

The QDs have been re-dissolved in heptane and mixed with 1-PCA, which is not soluble in such a solvent. During the stirring the formation of a white precipitate was observed. Such a precipitate can be attributed to the deoxycholic acid and 1-hexadecylamine ligands, which are not soluble in heptane, indicating that a surface modification has occurred. After one hour of stirring at room temperature, the mixture was filtered to remove both precipitated ligands and undissolved 1-PCA. The absorption spectra of such a filtrate has confirmed that the functionalization with 1-PCA had been successfully achieved, as shown in figure 5.21:
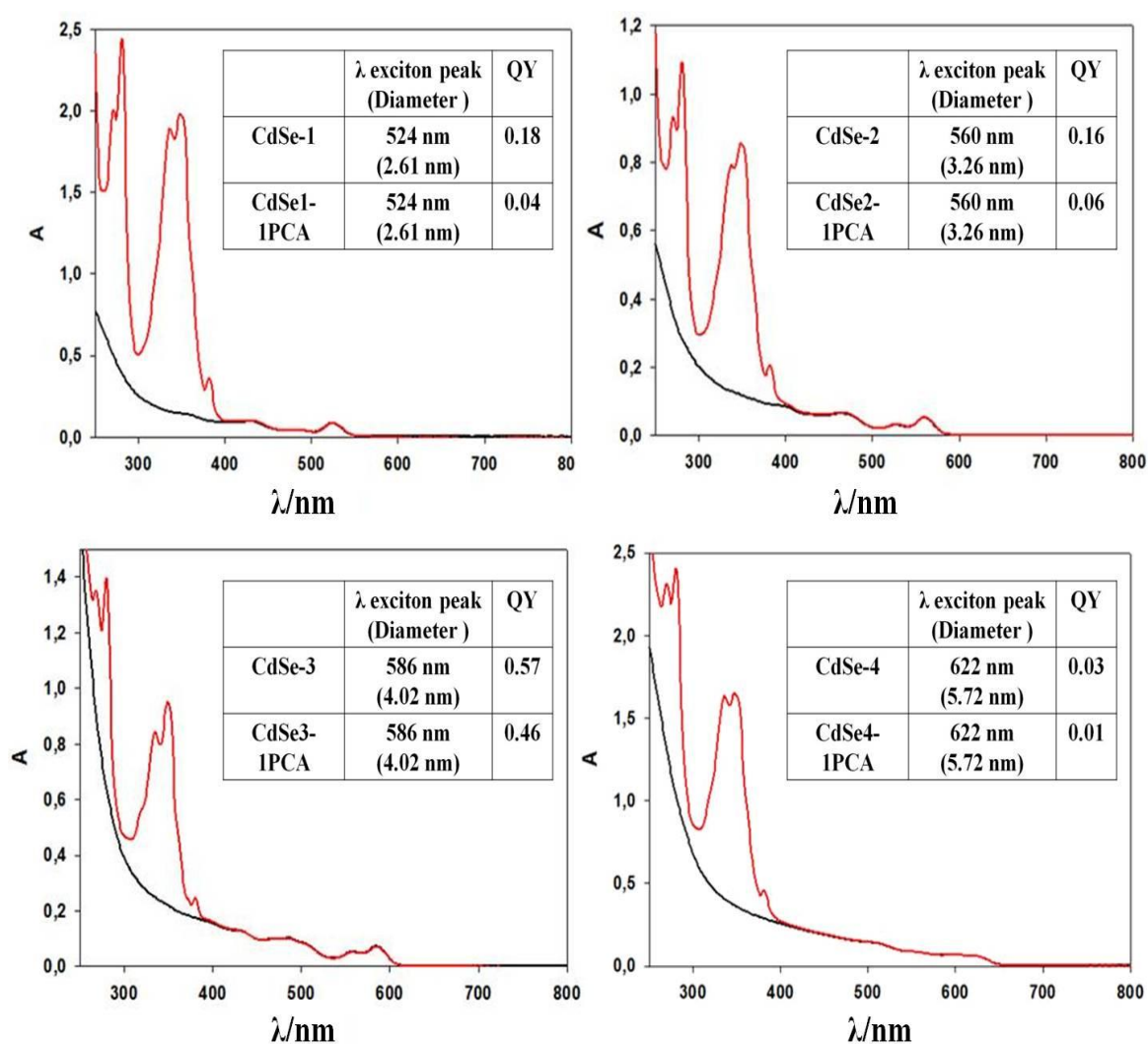
Figure 5.21 Absorption spectra of CdSe QDs before (black lines) and after (red lines) functionalization with 1-PCA, recorded with same absorbance value at the exciton peak.

In the insets the photophysical and dimensional properties of each sample, with and without 1-PCA, are reported.

126

CdSe3 and CdSe3-1PCA have been first investigated both in deareated and air-equilibrated conditions. It is important to note that all the following experiments were performed by exciting selectively the QDs. Since the main evidence of REET is the elongation of the lifetime, the next discussion arises from the comparison between the lifetimes of CdSe3 and CdSe3-1PCA in deareated conditions, as shown in Figure 5.22:
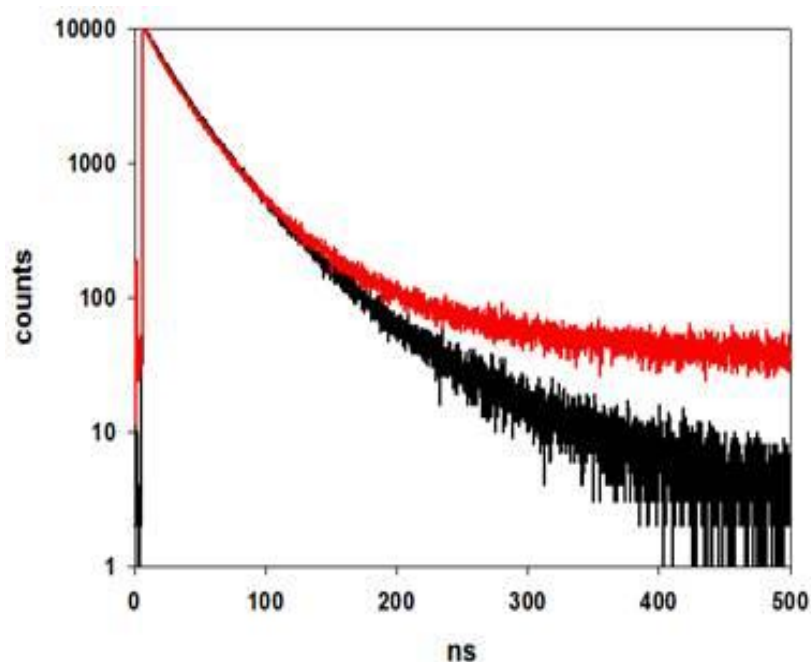

Figure 5.22 Luminescence lifetimes of CdSe3-1PCA (red decay) and CdSe3 (black decay) recorded in deareated heptane by exciting selectively QDs at 405 nm.
The time scale is 500 ns while the 10000 counts detected at 600 nm are reported in logarithmic scale.

Lifetimes measurements reported in Figure 5.22 clearly show a significant elongation of the longer component of the decay of CdSe3-1PCA compared to that of CdSe3, while the shorter component is not sensitive to the presence of pyrene based ligands on the surface.

Further experiments with streak camera detection were performed in order to quantify such an elongation, as shown in Figure 5.23:
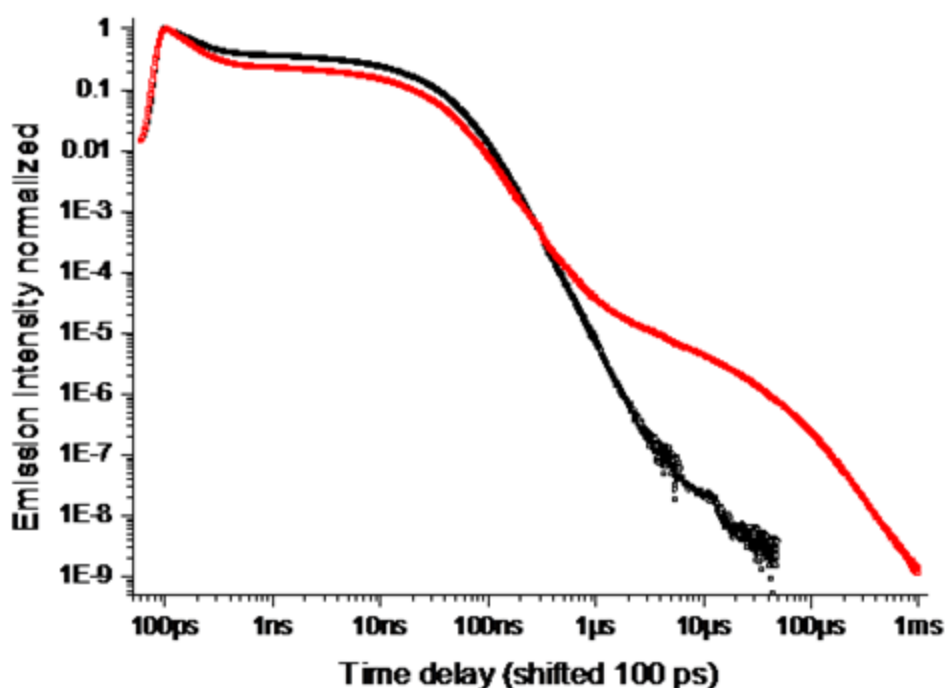
Figure 5.23 Emission decay of CdSe3 (black line) and CdSe3-1PCA (red line) in deareated heptane; recorded with a streak camera and by exciting at 465 nm.

Figure 5.23 provides another evidence of the elongation of the decay of CdSe3-1PCA QDs with respect to CdSe3 not functionalized QDs, as well as the shortening of the ns QD emission component, consistent with an initial sensitization of the lower-lying pyrene triplet.

Moreover, the integral of emission decay in the range 0.5 μs-1 ms represents 3.5% of overall emission intensity of CdSe3-1PCA, and its slowest decay time constant is in the range 25-80 μs.

Then it was decided to record the emission of both CdS3-1PCA and CdSe3 QDs at different time delays with respect to the excitation pulse, in order to investigate better such a preliminary result.
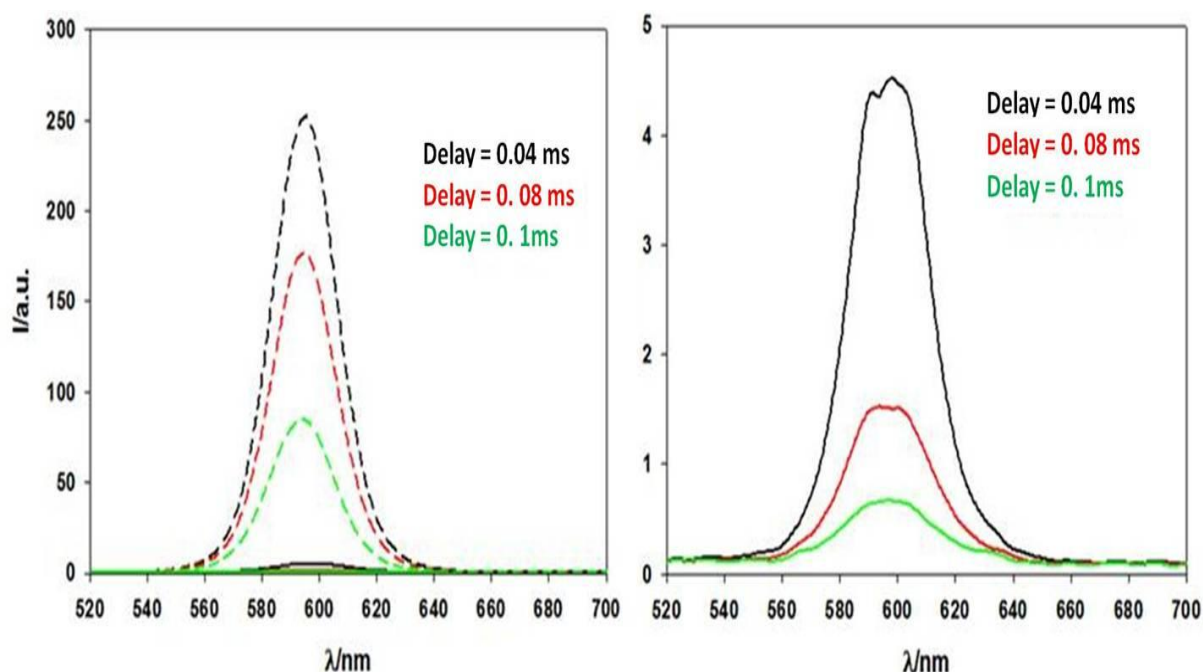
Figure 5.24 Phosphorescence emission spectra recorded at different time delays of CdSe3-1PCA (dashed lines) and CdSe3 (solid lines) on the left.

For clarity only phosphorescence spectra of CdSe3 are reported on the right.

All the spectra have been recorded in deareated heptane and by exciting selectively QDs at 500 nm. Other instrumental conditions are: gate 2 ms; cycle=20 ms and flash count=1.

The phosphorescence spectra show a huge difference between the signals arising from CdSe3-1PCA and CdSe3. It is important to point out that CdSe3-1PCA shows a real emission at the same time intervals that does not allow to record a significant emission for CdSe3; although, as shown on the left of figure, a weak emission signal is still detectable for CdSe3.

The excitation spectra of such emissions have then been recorded to clarify the origin of these signals.
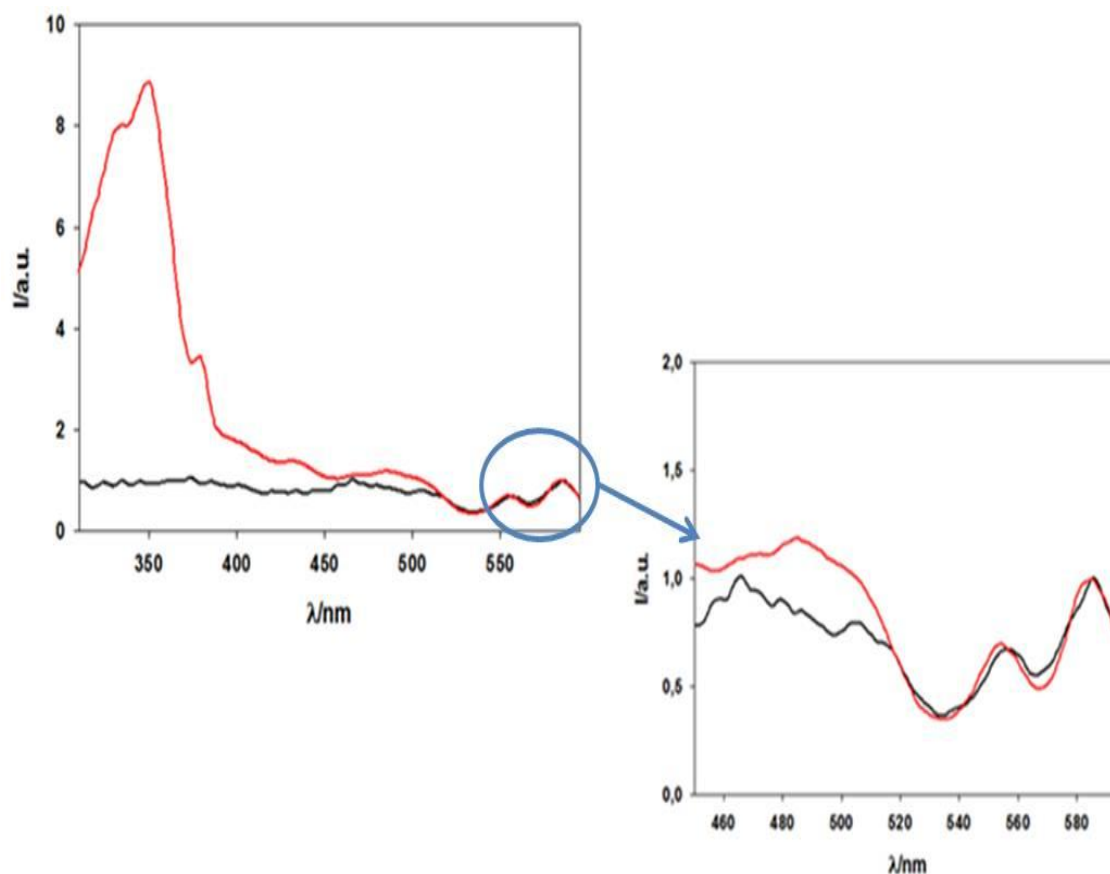

Figure 5.25 Phosphorescence excitation spectra of CdSe3-1PCA (red line) and CdSe3 (black line). The spectra are recorded in the same experimental conditions: 600 nm as emission wavelength, delay time 0.04 ms, gate 2 ms, cycle 20 ms, flash count 1.

The phosphorescence excitation spectra exhibit a perfect match in the region of the exciton peak, indicating that both the signals showed in the previous figure arise from QDs. These results indicate that the luminescence lifetime of CdSe3-1PCA has been actually elongated while CdSe3 is still emitting but very weakly.

More in detail, it is possible to correlate such a signal to intrinsic processes of QDs, from the data reported in literature.[23]

Moreover it is possible to refer the excitation band centered at around 360 nm in the case of CdSe3P as an evidence of the energy transfer process occurring from the lowest excited singlet state of 1-PCA to QDs. The efficiency of such a process has been estimated to be about 30% from excitation spectra recorded at 0 delay.

After these experiments the solutions were re-equilibrated with air in order to investigate if the oxygen can affect such a process. Luminescence lifetimes and delayed emission spectra of air-equilibrated solution of both CdSe3-1PCA and CdSe3 are reported in figures 5.26 and 5.27, respectively. A comparison between the decay of CdSe3-1PCA in deareated and air-equilibrated heptane is reported in Figure 5.28; the same comparison for CdSe3 is reported in Figure 5.29:
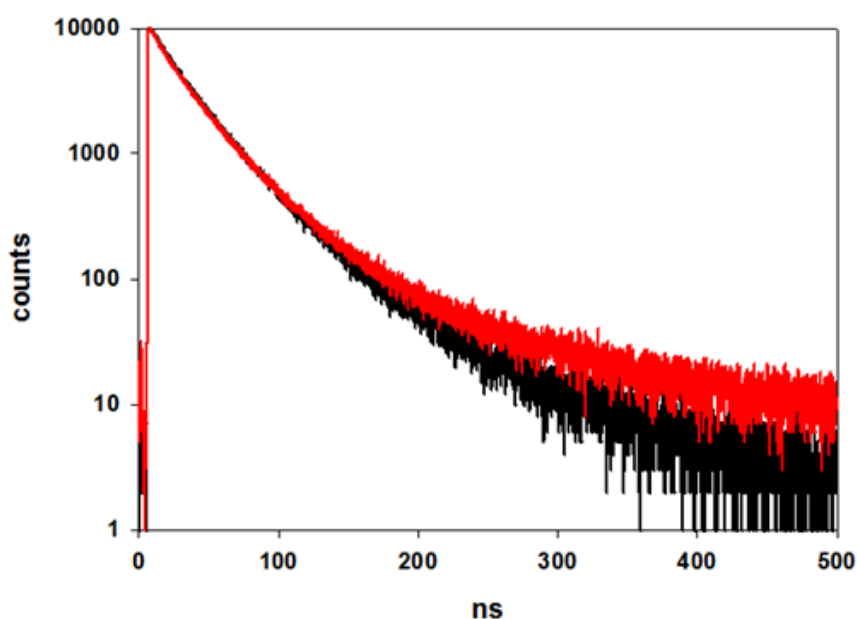

Figure 5.26 Luminescence lifetimes of CdSe3-1PCA (red decay) and CdSe3 (black decay) recorded in air-equilibrated heptane by exciting selectively QDs at 405 nm.
The time scale is 500 ns while the 10000 counts detected at 600 nm are reported in logarithmic scale.

τ			
τ_1=16 ns	B_1= 3400	18%	
τ_2=32 ns	B_2= 6600	72%	χ^2= 1,15
τ_3=84 ns	B_3= 351	10%	

τ			
τ_1=16 ns	B_1= 4408	25%	
τ_2=34 ns	B_2= 5427	64%	χ^2= 1,17
τ_3=104 ns	B_3= 303	11%	

Table 5.6 Lifetime values of CdSe3 (in black) and CdSe3-1PCA (in red) in air-equilibrated heptane.
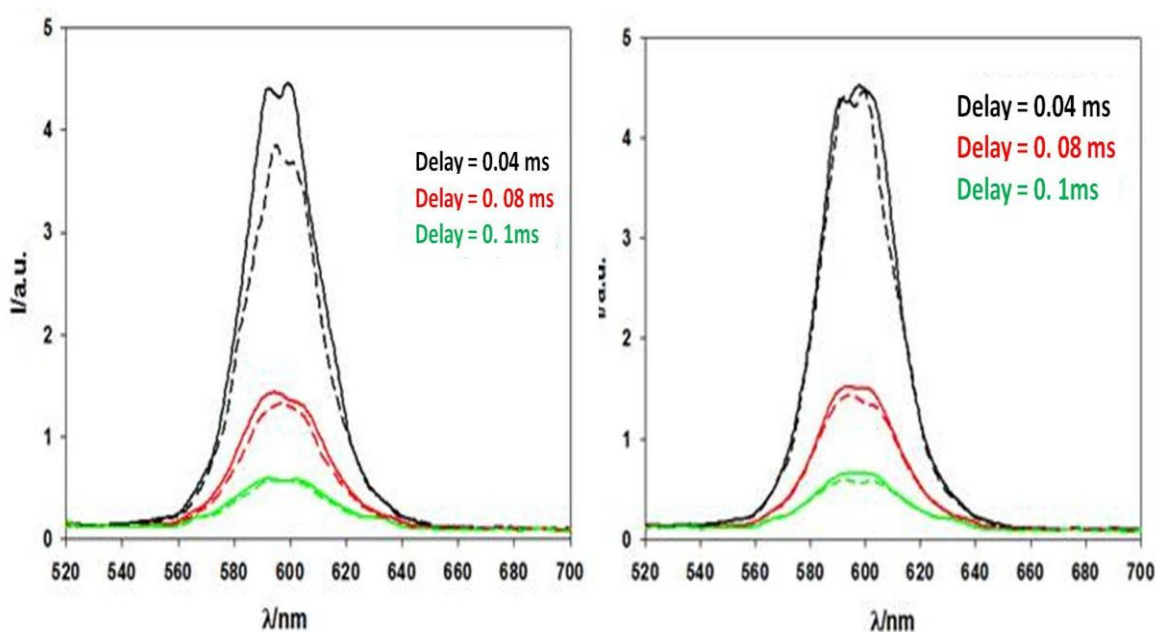

Figure 5.27 Phosphorescence emission spectra recorded at different time delays of CdSe3-1PCA (dashed lines) and CdSe3 (solid lines) on the left.

Comparison between phosphorescence spectra of CdSe3 (dashed lines are referred to deareated conditions, solid lines to air-equilibrated ones) on the right.

All the spectra have been recorded in air-equilibrated heptane and by exciting selectively QDs at 500 nm. Other instrumental conditions are: gate 2 ms; cycle=20 ms; flash count=1
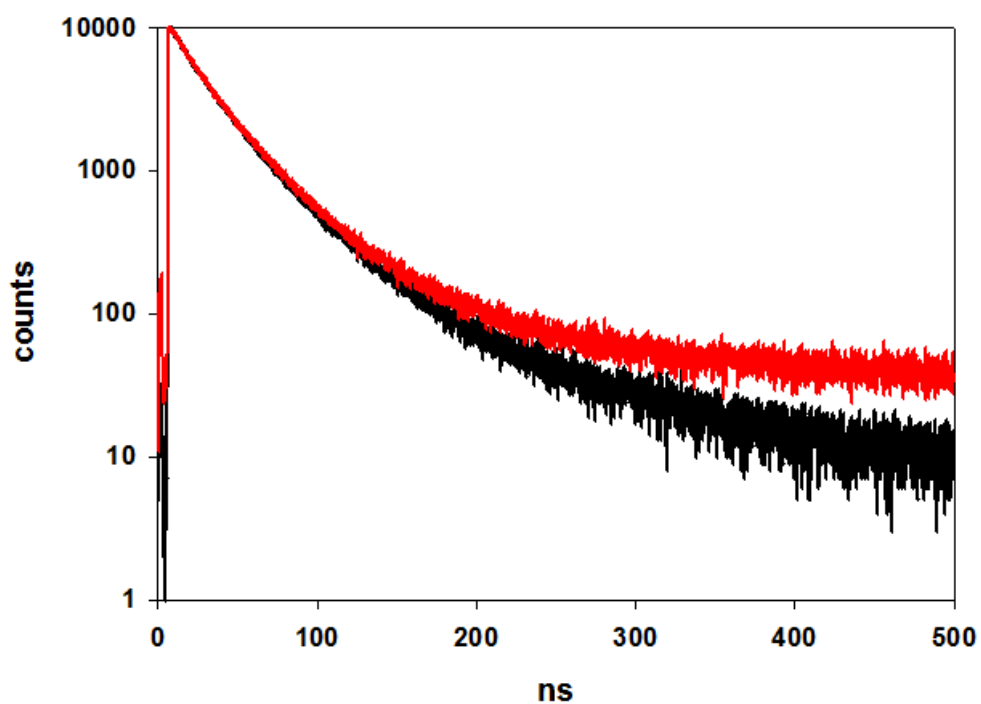
Figure 5.28 Comparison between the luminescence decay of CdSe3-1PCA in deareated (red decay) and air-equilibrated (black decay) heptane.
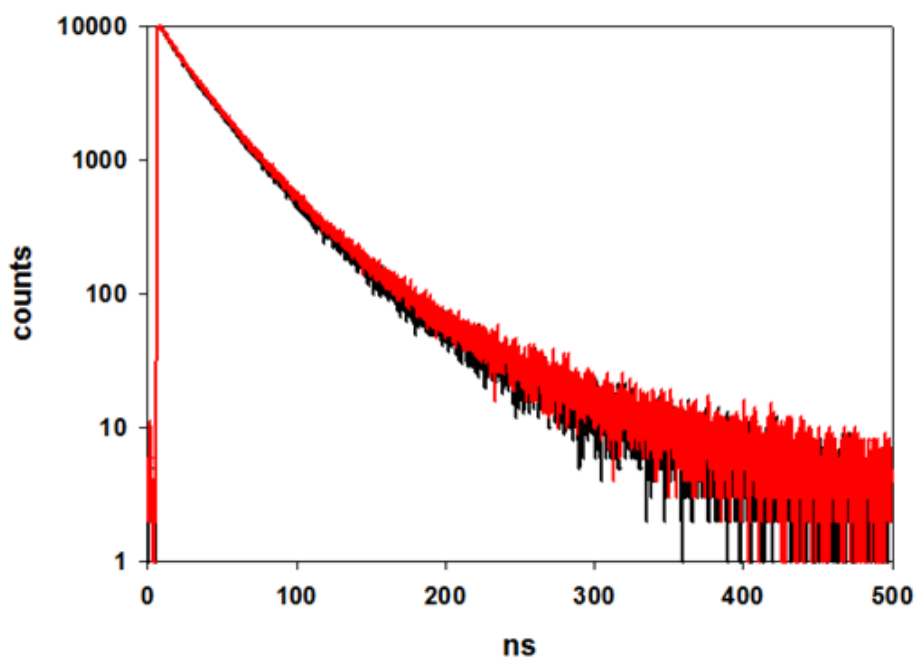

Figure 5.29 Comparison between the luminescence decay of CdSe3 in deareated (red decay) and air-equilibrated (black decay) heptane.

τ			
τ_1=16 ns	B_1= 3400	18%	
τ_2=32 ns	B_2= 6600	72%	χ^2= 1,15
τ_3=84 ns	B_3= 351	10%	

τ			
τ_1=17 ns	B_1= 3350	20%	
τ_2=33 ns	B_2= 6353	70%	χ^2= 1,17
τ_3=85 ns	B_3= 355	10%	

Table 5.7 Lifetime values of CdSe3 in air equilibrated (in black) and deareated (in red) heptane.

It is evident that, by re-equilibrating the solutions with air, in the case of CdSe3P the longer component of the decay falls down, so there is no more elongation as previously observed, although it is still longer in comparison with the decay of CdSe3. Moreover the intensity of delayed emission of CdSe3-1PCA drops down dramatically while those of CdSe3 are not affected, as expected, by oxygen as well as its luminescence lifetime.

Interestingly CdSe3-1PCA QDs are not the only sample showing REET, in fact CdSe2-1PCA also shows an elongation of lifetime as reported in Figure.5.30:
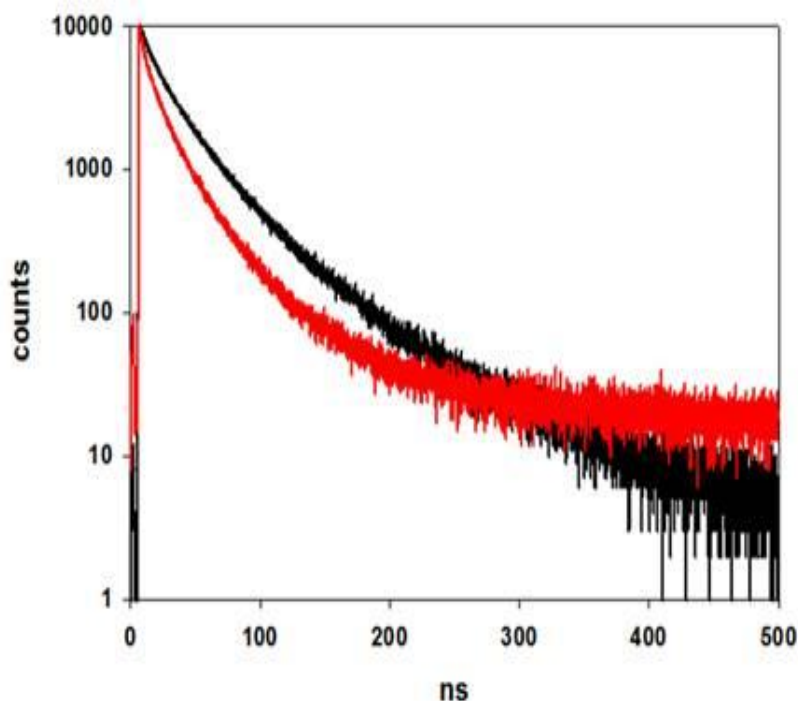

Figure 5.30 Luminescence lifetimes of CdSe2-1PCA (red decay) and CdSe2 (black decay) recorded in deareated heptane by exciting selectively QDs at 405 nm.
The time scale is 500 ns while the 10000 counts detected at 570 nm are reported in logarithmic scale.

Figure 5.30 clearly shows an evident lifetime elongation for CdSe2-1PCA in comparison to CdSe2. Moreover in such a case it is possible to distinguish a clear difference between the shorter components of the two samples, differently from the case of CdSe3 QDs.

Further experiments recorded on a streak camera were performed in order to quantify such an elongation, as shown in Figure 5.31:
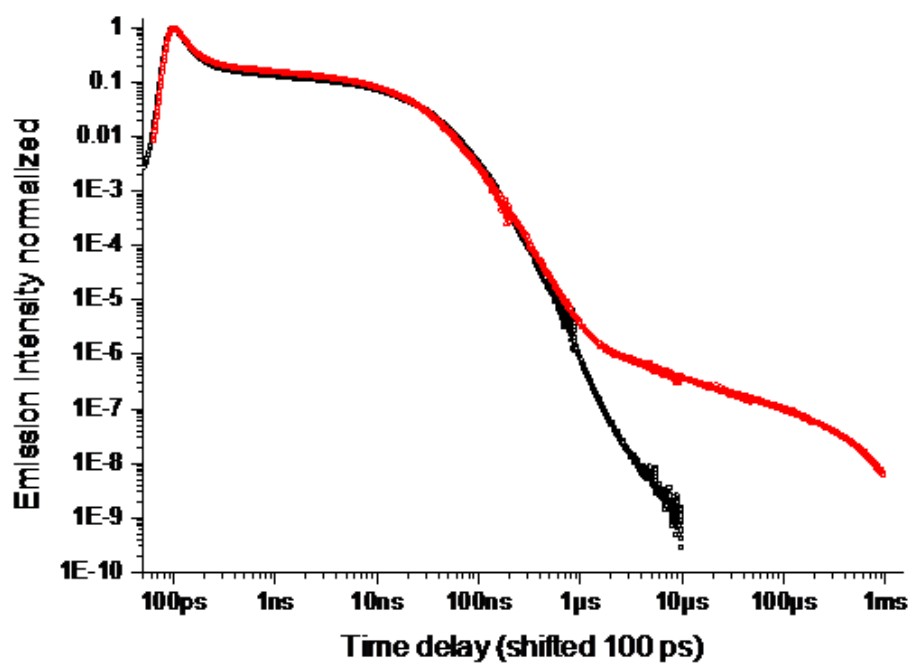
Figure 5.31 Emission decay of CdSe2 (black line) and CdSe2-1PCA (red line) in deareated heptane; recorded with a streak camera and by exciting at 465 nm.

The integral of emission decay in the range 1 µs-1 ms represents 6.6% of overall emission intensity of CdSe2-1PCA, whose the slowest decay time constant is about 250µs.

Such a result allowed us to recorder emission spectra at different delays, as already seen for CdSe3-1PCA, which are reported in figure 5.32:
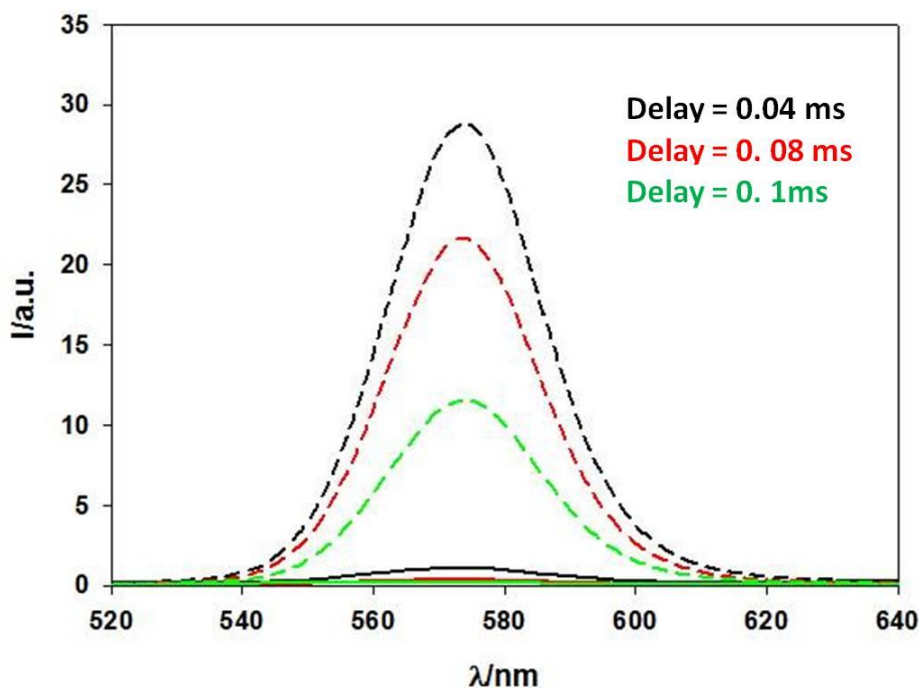

Figure 5.32 Phosphorescence emission spectra recorded at different time delays of CdSe2-1PCA (dashed lines) and CdSe2 (solid lines).

All the spectra have been recorded in deareated heptane and by exciting selectively QDs at 500 nm. Other instrumental conditions are: gate 2 ms; cycle=20 ms; flash count=1.

So it is clear that CdSe2-1PCA in deareated conditions exhibits the same behavior of CdSe3-1PCA.

Once the samples had been re-equilibrated with air, no more elongation of lifetime was observed, as shown in Figure 5.33.

A comparison between the decay of CdSe2-1PCA in deareated and air-equilibrated heptane is also reported in Figure 5.34; the same comparison for CdSe2 is reported in Figure 5.35:
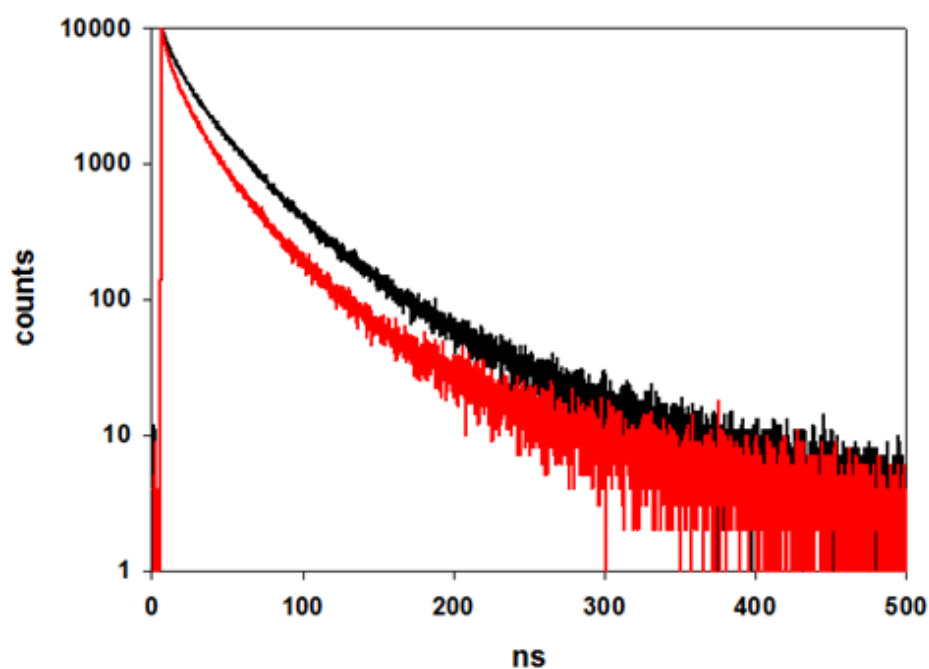
Figure 5.33 Luminescence lifetimes of CdSe2-1PCA (red decay) and CdSe2 (black decay) recorded in air-equilibrated heptane by exciting selectively QDs at 405 nm.

The time scale is 500 ns while the 10000 counts detected at 570 nm are reported in logarithmic scale.

τ			
τ_1=9 ns	B_1= 3563	12%	
τ_2=30 ns	B_2= 5584	64%	χ^2= 1,15
τ_3=79 ns	B_3= 792	24%	

τ			
τ_1=6 ns	B_1= 4179	16%	
τ_2=22 ns	B_2= 4577	64%	χ^2= 1,17
τ_3=66 ns	B_3= 484	20%	

Table 5.8 Lifetime values of CdSe2 (in black) and CdSe2-1PCA (in red) in air-equilibrated heptane.
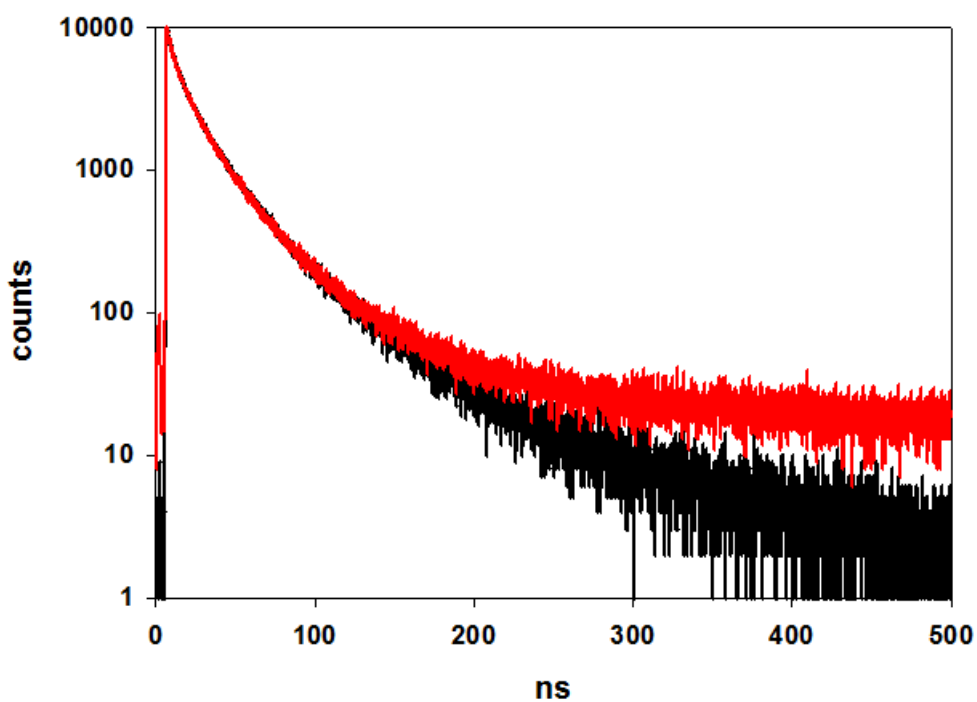
Figure 5.34 Comparison between the luminescence decay of CdSe2-1PCA in deareated (red decay) and air-equilibrated (black decay) heptane.
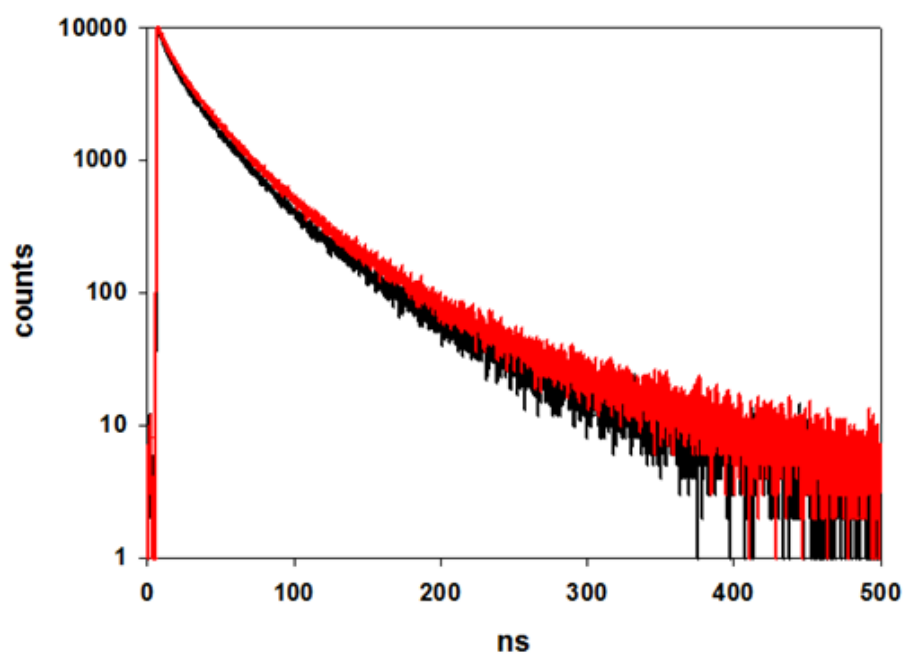

Figure 5.35 Comparison between the luminescence decay of CdSe2 in deareated (red decay) and air-equilibrated (black decay) heptane.

τ			
τ_1=9 ns	B_1= 3563	12%	
τ_2=30 ns	B_2= 5584	64%	χ^2= 1,15
τ_3=79 ns	B_3= 792	24%	

τ			
τ_1=9 ns	B_1= 3762	13%	
τ_2=30 ns	B_2= 5301	66%	χ^2= 1,08
τ_3=76 ns	B_3= 659	20%	

Table 5.9 Lifetime values of CdSe2 in air equilibrated (in black) and deareated (in red) heptane.

As well as in the case of CdSe3-1PCA, no more elongation can be observed in air-equilibrated solution thus resulting in falling down of both luminescence lifetime and the intensity of the delayed emission. Once again the properties of QDs not functionalized with 1-PCA, are not affected by the oxygen.

Finally both CdSe1-1PCA and CdSe4-1PCA do not show any lifetime elongation as shown if Figures 5.36 and 5.37, respectively:
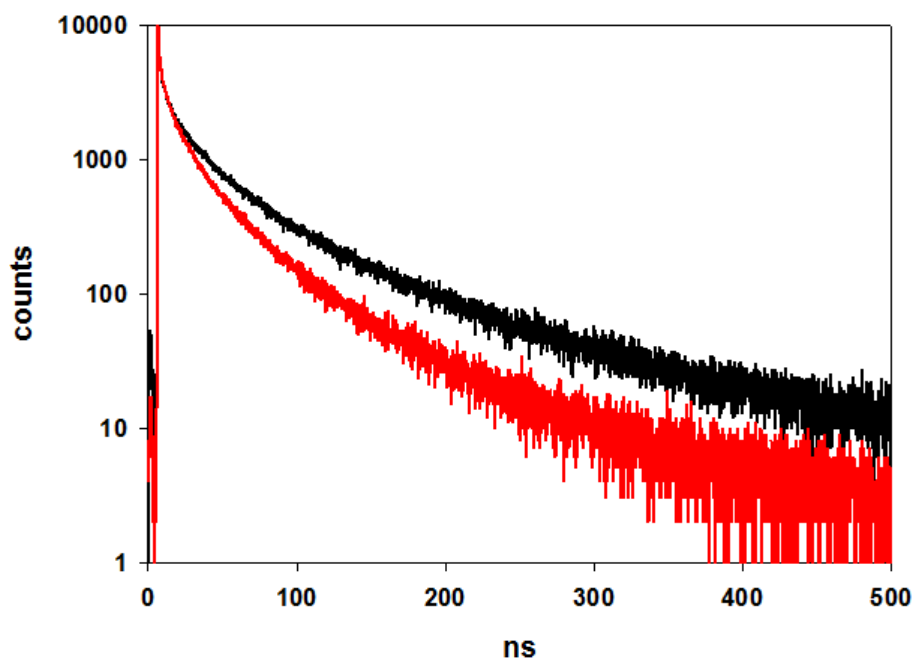
Figure 5.36 Luminescence lifetimes of CdSe1-1PCA (red decay) and CdSe1 (black decay). The decays are recorded in deareated heptane by exciting selectively QDs at 405 nm. The time scale is 500 ns while the 10000 counts detected at 540 nm are reported in logarithmic scale.

τ			
τ_1=6 ns	B_1= 2530	12%	
τ_2=37 ns	B_2= 2038	53%	χ^2= 1,15
τ_3=133 ns	B_3= 375	35%	

τ			
τ_1=5 ns	B_1= 1896	13%	
τ_2=23 ns	B_2= 1830	53%	χ^2= 1,1
τ_3=73 ns	B_3= 371	34%	

Table 5.10 Lifetime values of CdSe1 (in black) and CdSe1-1PCA (in red) in deareated heptane.
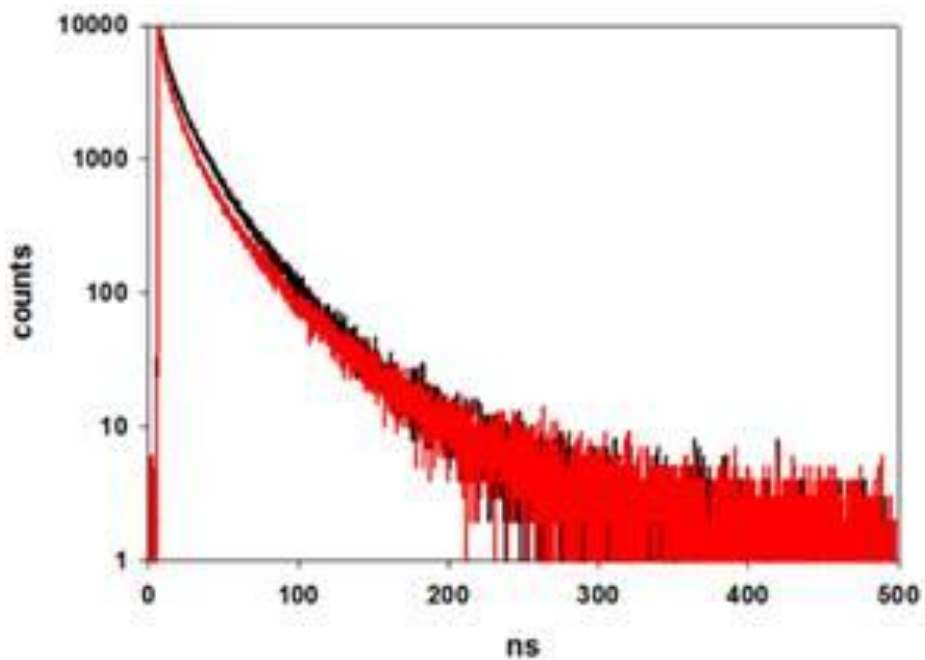
Figure 5.37 Luminescence lifetimes of CdSe4-1PCA (red decay) and CdSe4 (black decay). The decays are recorded in deareated heptane by exciting selectively QDs at 405 nm. The time scale is 500 ns while the 10000 counts detected at 636 nm are reported in logarithmic scale.

τ			
τ_1=5 ns	B_1= 4477	14%	
τ_2=18 ns	B_2= 4233	57%	χ^2= 1,07
τ_3=37 ns	B_3= 762	25%	

τ			
τ_1=3 ns	B_1= 4083	14%	
τ_2=14 ns	B_2= 4153	55%	χ^2= 1,2
τ_3=40 ns	B_3= 805	31%	

Table 5.11 Lifetime values of CdSe4 (in black) and CdSe4-1PCA (in red) in deareated heptane.

142

Obviously no changes were observed in air-equilibrated solutions:
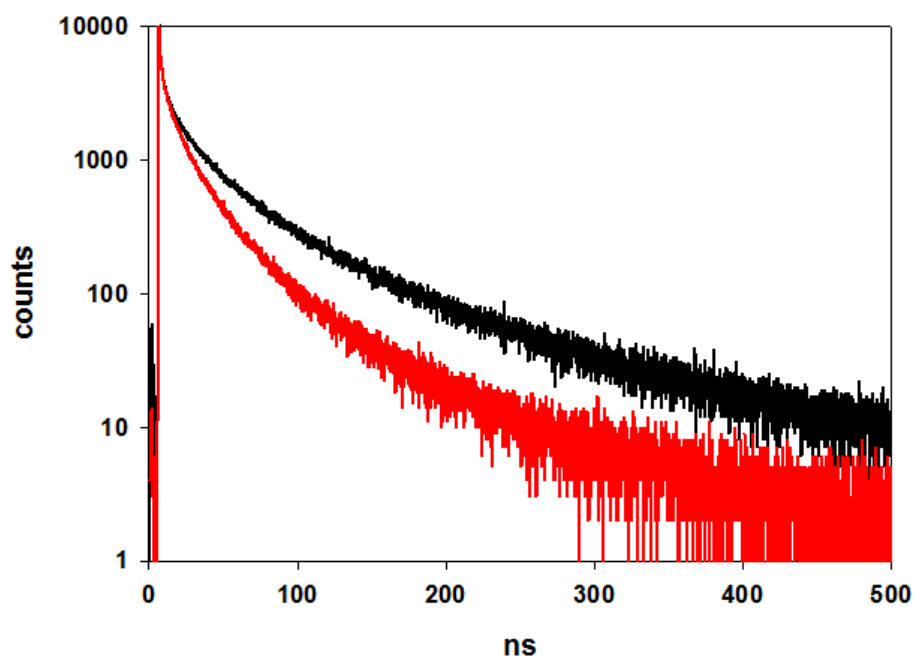
Figure 5.38 Luminescence lifetimes of CdSe1-1PCA (red decay) and CdSe1 (black decay) The decays are recorded in air-equilibrated heptane by exciting selectively QDs at 405 nm. The time scale is 500 ns while the 10000 counts detected at 540 nm are reported in logarithmic scale.

τ			
τ_1=8 ns	B_1= 2148	13%	
τ_2=38 ns	B_2= 1847	55%	χ^2= 1,15
τ_3=133 ns	B_3= 314	32%	

τ			
τ_1=4 ns	B_1= 2563	14%	
τ_2=22 ns	B_2= 2266	60%	χ^2= 1,1
τ_3=70 ns	B_3= 278	26%	

Table 5.12 Lifetime values of CdSe1 (in black) and CdSe1-1PCA (in red) in air equilibrated heptane.
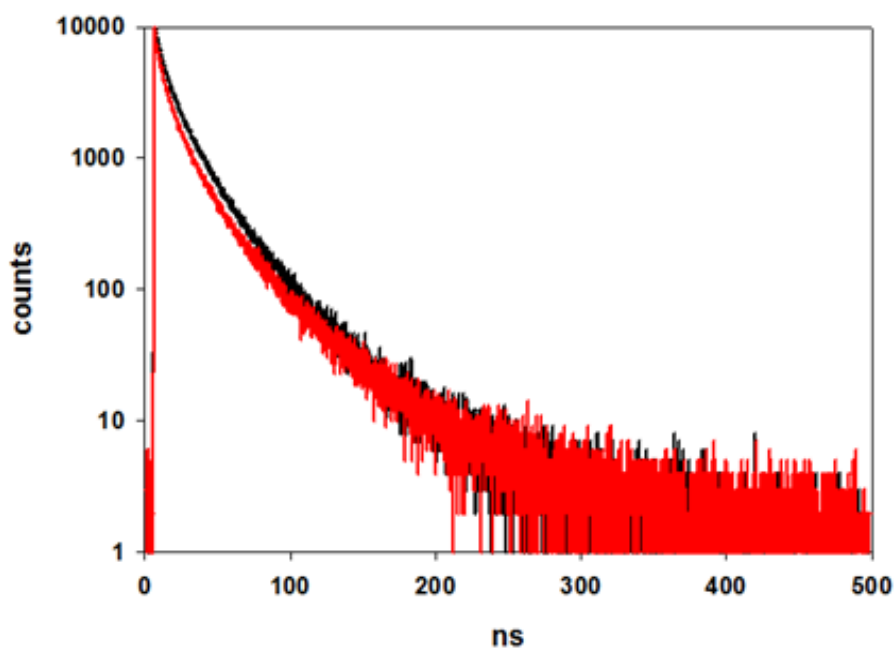
Figure 5.39 Luminescence lifetimes of CdSe4-1PCA (red decay) and CdSe4 (black decay)
The decays are recorded in air-equilibrated heptane by exciting selectively QDs at 405 nm.
The time scale is 500 ns while the 10000 counts detected at 636 nm are reported in
logarithmic scale.

τ			
τ_1=5 ns	B_1= 4372	17%	
τ_2=15 ns	B_2= 4411	57%	χ^2= 1,06
τ_3=37 ns	B_3= 819	26%	

τ			
τ_1=5 ns	B_1= 4063	17%	
τ_2=15 ns	B_2= 3521	56%	χ^2= 1,12
τ_3=41 ns	B_3= 600	26%	

Table 5.13 Lifetime values of CdSe4 (in black) and CdSe4-1PCA (in red) in air
equilibrated heptane.

144

Finally, it is possible to rationalize such results by considering the energy values of the excited states involved in each sample, as shown in Figure 5.40:
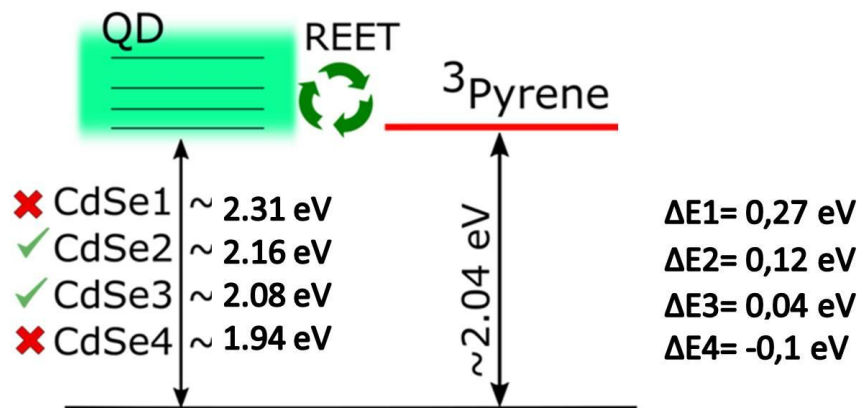

Figure 5.40 Schematic representation of the energy levels involved in the interaction with the lowest excited triplet state of 1-PCA.

The energy difference between the states involved in the REET must be less than or equal to 0.1 eV, as previously discussed. More in detail, the energy value of QDs has been estimated from the maximum of the emission spectra, while the energy of the lowest triplet state of 1-PCA is reported in literature. Then is reasonable that only samples 2 and 3 can be involved in REET, while samples 1 and 4 are out of the equilibrium conditions.

5.3 Conclusions

QDs endowed with a long-lived emission arising from a reversible electronic energy transfer, involving an organic triplet excited state as an energy reservoir, have been successfully developed and investigated. The experiments illustrated in this Chapter are the first example of such a process involving luminescent colloidal semiconductor nanocrystals and not only molecular or supramolecular species. As consequence of REET, QDs show a lifetime at least one order of magnitude longer than common values. This property is crucial in order to apply QDs in biomedical field, for example in the case of fluorescence imaging with high contrast, by enhancing the brightness and the lifetime of the emission, but also in the case of multiplexing experiments, which allows the measurement at the same time of many parameters of the same sample.

References

(1)   Förster, T *Fluorenzenz Organische Verbindungen*, Gottingen, Vandenhoech and Ruprech., 1951.

(2)   Baraldi, I. *La luminenescenza*, Bononia University Press, 2007.

(3)   Witt, H. *Nouv. J. Chim.* **1987**, *11*, 71-78.

(4)   Snee, P.T.; Somers, R.C.; Nair, G.; Zimmer, .J.P.; Bawendi, M.G.; Nocera, D.G. *J. Am. Chem. Soc.* **2006**, *128*, 13320-13321.

(5)   Tang, R.; Lee, H.; Achilefu, S. *J. Am. Chem. Soc.* **2012**, *134*, 4545-4548.

(6)   Geissler, D.; Charbonnière, L.J.; Ziessel, R.F.; Butlin N.G.; Löhmansröben H.-G. Hildebrandt, N. *Angew. Chem. Int. Ed.* **2010**, *49*, 1396-1401.

(7)   Dexter, D.L. *J. Chem. Phys.* **1953**, *21*, 836-850.

(8)   Terenin, A.; Ermolaev, V. *Trans. Faraday Soc*. **1956**, *52*, 1042-1052.

(9)   Backstrom, H.L.; Sandros, K. *Acta Chem. Scan.* **1958**, *12*, 823-832.

(10)   Turro, N.J. *Modern Molecular Photochemistry* **1978**, Benjamin.

(11)   Mongin, C.; Garakyaraghi, S.; Razgoniaeva., N.; Zamkov, M.; Castellano, F.N. *Science* **2016**, *351*, 369-372.

(12)   Ford, W.E.; Rodgers, M.A.J. *J. Phys. Chem.* **1992**, *96,* 2917-2920.

(13)   Kober, E.M.; Meyer, T.J. *Inorg. Chem.* **1984**, *23*, 3877-3886.

(14)   Wilson, G.J.; Sasse, W.H.F.; Mau, A.W.-H. *Chem. Phys. Lett*. **1996**, *250*, 583-588.

(15)   Wilson, G.J.; Launikonis, A.; Sasse, W.H.F.; Mau, A.W.-H. *J. Phys. Chem. A* **1997**, *101*, 4860-4866.

(16)   Passalacqua, R.; Loiseau, F.; Campagna, S.; Fang, Y.-Q.; Hanan, G.S. *Angew. Chem. Int. Ed.* **2003**, *42*, 1608-1611.

(17)   Tyson, D.S.; Luman, C.R.; Zhou, X.; Castellano, F.N. *Inorg. Chem.* **2001**, *40*, 4063-4071.

(18)   Tyson, D.S.; Castellano, F.N. *J. Phys. Chem. A.* **1999**, *103*, 10955-10960.

(19)   Indelli, M.T.; Ghirotti, M.; Prodi, A.; Chiorboli, C.; Scandola, F.; McClenaghan, N.D.; Puntoriero, F.; Campagna, S. *Inorg. Chem.* **2003**, *42*, 5489-5497.

(20)   Scarpantonio, L.; Tron, A.; Destribats, C.; Godard, P.; McClenaghan, N.D. *Chem. Commun.* **2012**, *48*, 3981-3983.

(21)   Denisov, S.A.; Gan, Q.; Wang, X.; Scarpantonio, L.; Ferrand, Y.; Kauffmann, B.; Jonusauskas, G.; Huc, I.; McClenaghan, N.D. *Angew. Chem.* **2016**, *128*, 1350 -1355.

(22)   Ashton , P.R.; Balzani, V.; Kocian, O.; Prodi, L.; Spencer , N.; Stoddart, J.F. *J. Am. Chem. Soc*. **1998**, *120*, 11190-11191.

(23)   Rabouw, F.T.; Kamp, M.; van Dijk-Moes, R.J.A.; Gamelin, D.R.G.; Koenderink, A.F.; Meijerink, A.; Vanmaekelbergh, D. *Nano Lett.* **2015**, *15*, 7718-7725.

Chapter 6

Thermal poling process for directing assembly of colloidal nanocrystals on solid surface

6.1 Introduction

One of the most interesting aims of bottom-up nanotechnology is to develop protocols for depositing nanomaterials on solid surfaces for potential applications such as optoelectronic devices,[1-4] photonic band gap materials[5-8] and biochip devices and sensors.[9] Assembly of colloidal nanocrystals on solid substrates can be carried out by taking advantage of electrostatic[10] or covalent[11] interactions, capillary effect[12] or through specific recognition mechanisms involving biomolecules[13] or supramolecular interactions.[14]

Alternatively colloidal nanocrystals can be assembled on solid surfaces by applying electrostatic fields, this process is also known as micro- or nanoxerography.[15]

In 1998 Wright and co-workers[16] showed the use of scanning probe microscopies as a tool for making charged templates allowing assembly of nanoparticles. Atomic Force Microscopy,[17,18,19] conductive stamps,[20,21] focused ion and electron beams[22] have been used to write local superficial charges allowing the deposit of solid nanoparticles from liquid or gas phase.

In particular, AFM is probably the most versatile technique for nanoxerography, since it allows at the same time the writing of both positive and negative charges, with a great flexibility on the pattern geometry, and a high-resolution and three-dimensional topography of the resulting assemblies of nanoparticles on charged patterns. A simple representation of such a technique is shown in Figure 6.1.

147
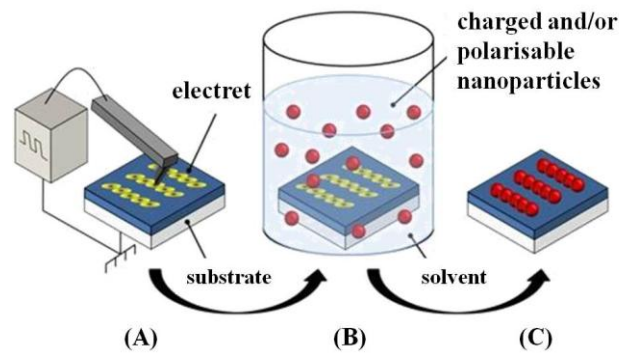
Figure 6.1 Schematic representation of AFM nanoxerography: (A) electrical charge injection by AFM in a thin film, (B) dipping in a colloidal solution of charged and/or polarizable nanoparticles, (C) directed assembly of nanoparticles on the charged patterns.

However all these methods based on scanning probe microscopies are negatively affected by significant time consumption since patterns are written point-by-point and require sophisticated equipment.

An alternative technique not requiring a scanning probe procedure has been developed by Myers and co-workers[23] and it is based on the thermal poling process.

In general glass poling is a physical process involving the manipulation of electrical charges, namely metal cations located within the glass matrix, which are in principle randomly distributed so that no permanent electric field can be measured inside the glass. If these charges are forced to move and fixed then a permanent field can be recorded. Glass poling can be performed by coupling a high voltage applied to the medium with heat, light or any other source of energy.

The thermal poling process, in particular, consists of heating the glass locally until molten (allowing ions to be able to diffuse) in direct current electrical field (biasing directionality of ion movement) followed by cooling under the applied voltage (blocking the ion position). At high temperature such as 300°C and under an electric field of few kilovolts per meter positive ions are displaced from the anodic side to the bulk glass toward the cathode, thus resulting in a subsurface region of few micrometers thick depleted of positive charges.

The depleted region is subsequently negative charged and if the sample is cooled to room temperature with the applied voltage still working, the electron distributions becomes frozen so that, after such a treatment, positive charges and negative charges are separated inside the glass establishing a recorded field that can reach 10^9 V/m.

Depending on the glass composition[24] the lifetime of these depleted subsurface layers at room temperature ranges from hours to a permanent condition and its thickness can be modulated by manipulating poling time and intensity of the internal electric field, E, which also affects the speed of removed ions as shown in Equation 6.1

$$v = \mu \, z \, q \, E \qquad \text{(Eq. 6.1)}$$

where v is the speed, q is the electron charge, z is the number of charge and μ is the ion mobility defined by the Einstein formula as reported in Equation 6.2:

$$\mu = D/kT \qquad \text{(Eq. 6.2)}$$

where D is the ion diffusivity coefficient, k is the Boltzmann constant and T is the absolute temperature.

In engineering microphotonic devices, the final product is supposed to be tunable in terms of either linear or second- as well as third-order nonlinear optical responses at the micrometer scale.[25,26] Homogeneous glasses are macroscopically centrosymmetric, then their nonlinear dielectric susceptibility χ^2 is equal to zero, meaning that intrinsic symmetry properties avoid nonlinear optical response of the second-order as well as electro-optical effect of the first order in any homogeneous glassy material.

However the inner electric field induced by poling process results in new and or modified properties such as in the case of optical ones. Due to this new charge disposition the central symmetry of starting isotropic glass is broken, thus resulting in a subsurface layer with anisotropic properties.

More precisely, glass poling allows us also to perform second-harmonic light generation (SHG) which consists on converting an electromagnetic radiation of frequency υ in another one with a frequency 2υ, so twice stronger than the original.

For example a near infrared radiation around 1030 nm could be converted to the 515 nm wavelength, corresponding to green light, as represented in Figure 6.2:
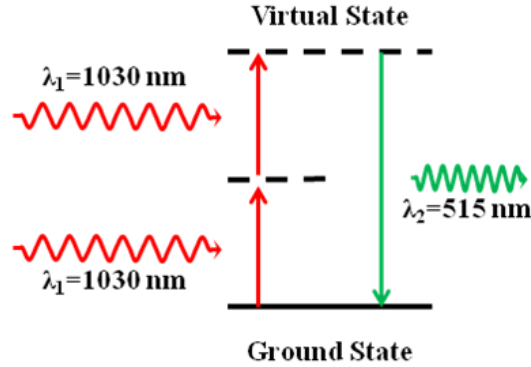

Figure 6.2 Second harmonic generation principle: depending of its non linear optical properties a material can be excited by absorbing consecutively two photons of the same energy thus resulting in the emission of a photon whose energy is doubled.

The origin of the non-linear susceptibility in thermally poled glasses arises from the combination of an implemented space charged at the near-anode surface and the third-order optical susceptibility of the glass:[27]

$$\chi^2 = 3\, \chi^3\, E_{frozen} \qquad\qquad \text{(Eq. 6.3)}$$

where E_{frozen} is the strength of the frozen electric field.

Finally the described process permits an accurate control of the optical anisotropy geometry with a micrometric spatial resolution and also the design of periodical micrometer-sized motifs.

QDs with charged surfactants and poled glass are potential candidates in order to develop a new protocol for depositing nanocrystals on a solid substrate. The experiments described in the next paragraph have been performed within a collaboration with Dr. Marc Dussauze's group of the Institut des Sciences Moleculaires of the University Bordeaux and are focused on the assembly of positively charged QDs on a glass surface polarized through the thermal poling process already discussed previously.

6.2 Results and Discussion

6.2.1 Glass poling

A borosilicate glass, under nitrogen flow, was heated at 300°C by increasing the temperature 20°C per minute and subjected to an electrical field of 1.5 kV by increasing the voltage at a rate of 1500 V per minute. Such a voltage have been applied through a silicon cathode and an indium-tin oxide (ITO) anode, which was structured by ablation with Nd-YAG laser in order to imprint specific patterns. Such a process is represented in Figure 6.3.

      Once both temperature and voltage reached the desired values, the glass was maintained under these conditions for 30 minutes. Subsequently it was cooled down to room temperature.
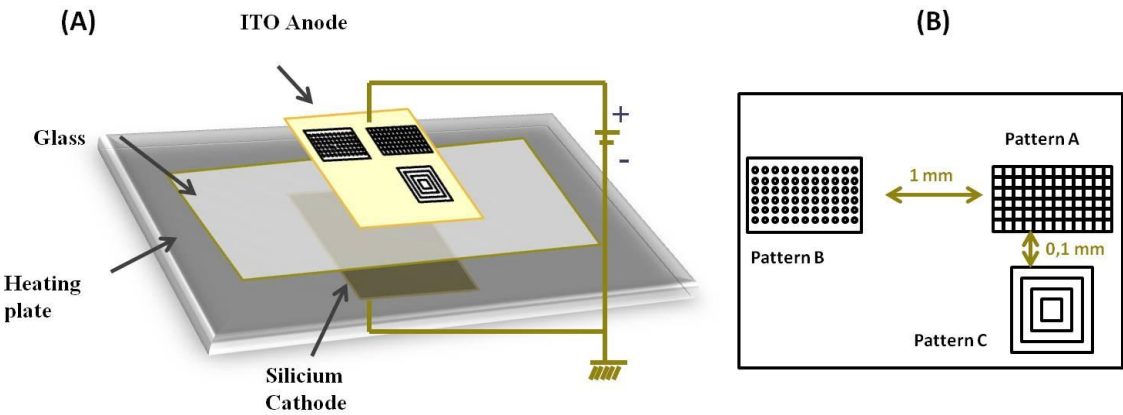

Figure 6.3 (A) Schematized representation of glass poling. (B) Polarized patterns structured by laser ablation.

6.2.2 Quantum Dots preparation

CdSe-3ZnS Core-Shell Quantum Dots were prepared according to a procedure described in Chapter 2, then ligand exchange was performed by adding to a methanolic solution of Lipoic Acid derivatives, such as LA-PEG$_{400}$ and LA-Ru (0.024 mmol; 95% of LA-PEG400 and 5% of LA-Ru), the hexane solution of TOPO/TOP coated QDs (1:30000 QD/Lipoic Ligand ratio).

Once an excess of TBABH$_4$ had been added, the disulfide bridges of the ligands have been broken so that, immediately upon stirring the biphasic mixture, a fast and efficient ligand exchange occurred.

After removing the colourless hexane layer the methanolic phase was washed with fresh hexane to remove unreacted nanocrystals. Large aggregates were separated by using a syringe filter (0,45 μm pore size), and unreacted DHLA ligands were removed by three cycles of dilution/concentration with a centrifugal filter (Amicon Ultra-0.5 mL, 30 kDa, 7000 rpm, 25°C, 12 minutes). The experiments reported in this chapter have been performed with a methanolic solution (4.4 x 10^{-8} M) of LAPEG$_{400}$/LARu coated QDs.

In Figure 6.4 and Table 6.1 absorption, luminescence spectra and spectroscopic properties of such nanohybrids are reported, respectively.
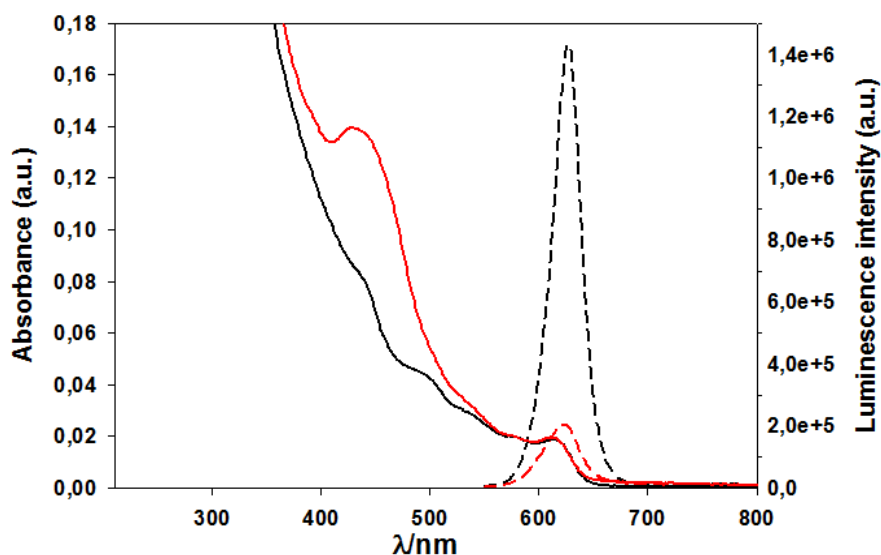

Figure 6.4 Absorption (full lines) and luminescence (dashed lines) spectra of TOPO/TOP capped QDs in hexane (black) and LAPEG$_{400}$/LARu coated QDs (red). Luminescence spectra are recorded by exciting at 460 nm.

Table 6.1 Spectroscopic properties of TOPO/TOP coated QDs (in black) and LAPEG$_{400}$/LARu coated QDs (in red).

QD	D core[a] (nm)	S shell[b] (nm)	$\lambda_{exciton}$[c] (nm)	$\lambda_{emission}$[d] (nm)	Φ[e]
CdSe-3ZnS	5.16	0.9	612	624	0.20
CdSe-3ZnS	5.16	0.9	612	622	0.03

[a] Core diameter. [b] Shell thickness. [c] Wavelength of the lowest exciton absorption peak.

[d] Wavelength of the maximum emission. [e] Emission quantum yield of QDs.

6.2.3 Quantum Dots deposition on poled glass

0.3 mL of QD solution in methanol was dropped onto the poled glass and spin-coated during 1 minute. Then the glass was washed with fresh methanol and isopropanol to remove large aggregated nanocrystals deposited on the surface due to the evaporation of solvent and not to specific interactions with the polarized patterns.

The analysis of the poled glass has been carried out through confocal microscopy, as described in Chapter 2, in order to investigate if QDs can actually take advantage of the possible interaction between their positively charged ruthenium (II) moieties and polarized patterns, thus resulting in a directed-assembly driven by electrical forces. In Figures 6.5-6.7 are shown the results obtained from such a screening.

(A1)

(A2)

(A3)
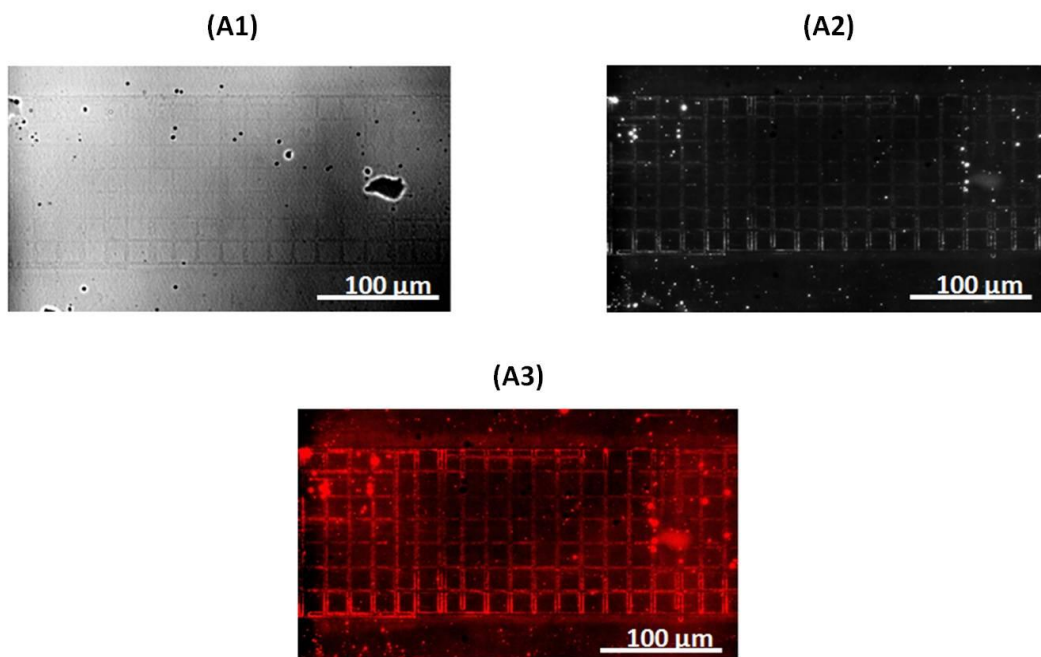
Figure 6.5 Transmission (A1) and fluorescence (A2) images of Pattern A. (A3) is the overlap between (A1) and (A2).


(B1)

(B2)

(B3)
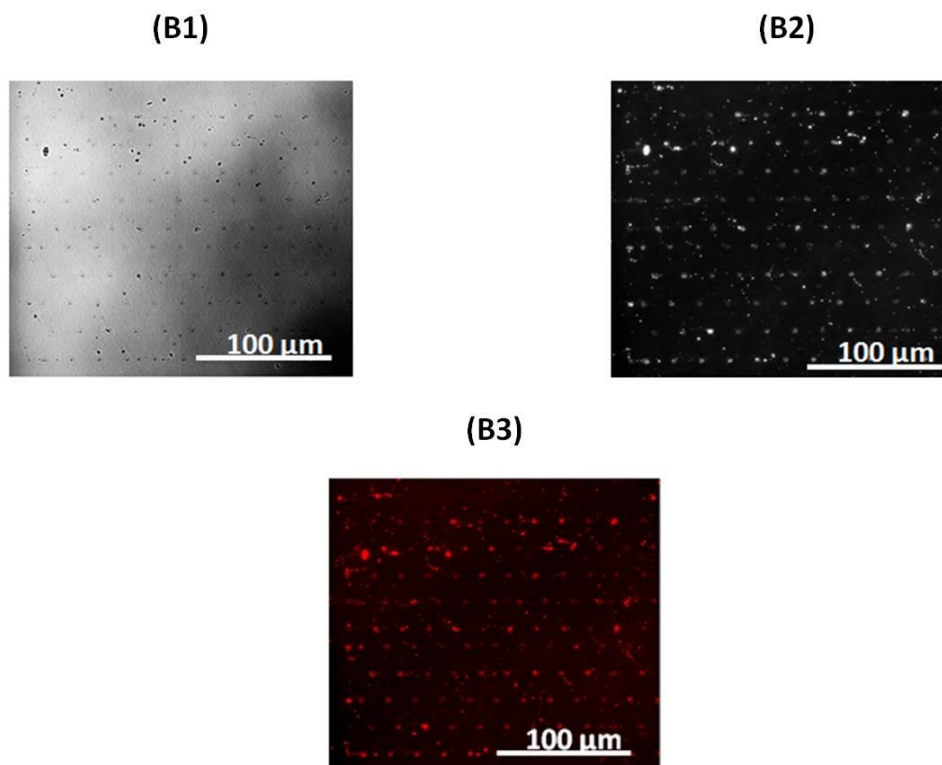
Figure 6.6 Transmission (B1) and fluorescence (B2) images of Pattern B. (B3) is the overlap between (B1) and (B2).

(C1)   (C2)

100 µm   100 µm

(C3)

100 µm
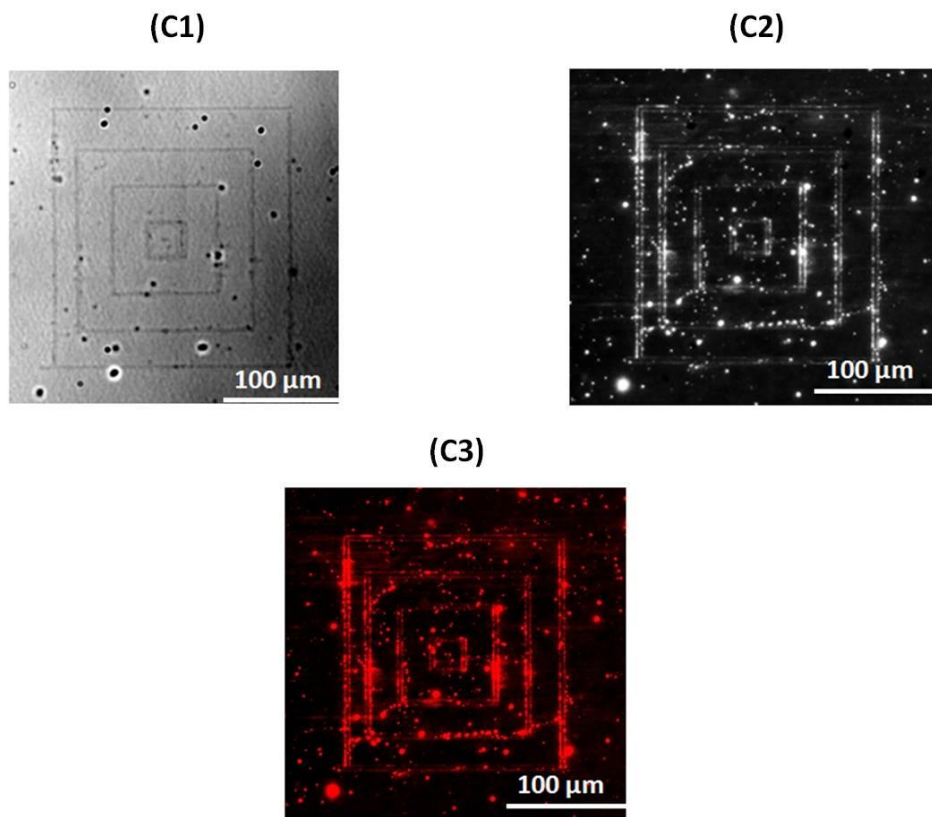
Figure 6.7 Transmission (C1) and fluorescence (C2) images of Pattern C. (C3) is the overlap between (C1) and (C2).

Moreover a hyperspectral screening focused on pattern C has been performed to better investigate the signals arising from the pattern and the supposed free space.

This analysis essentially consists of recording point-by-point the emission spectra of a selected portion of space. As shown in Figure 6.8 it is possible to clearly correlate signals arising from the pattern to the emission of quantum dots while there is no signal arising from the free space, meaning that QDs have been successfully assembled in a way directed by glass polarization.
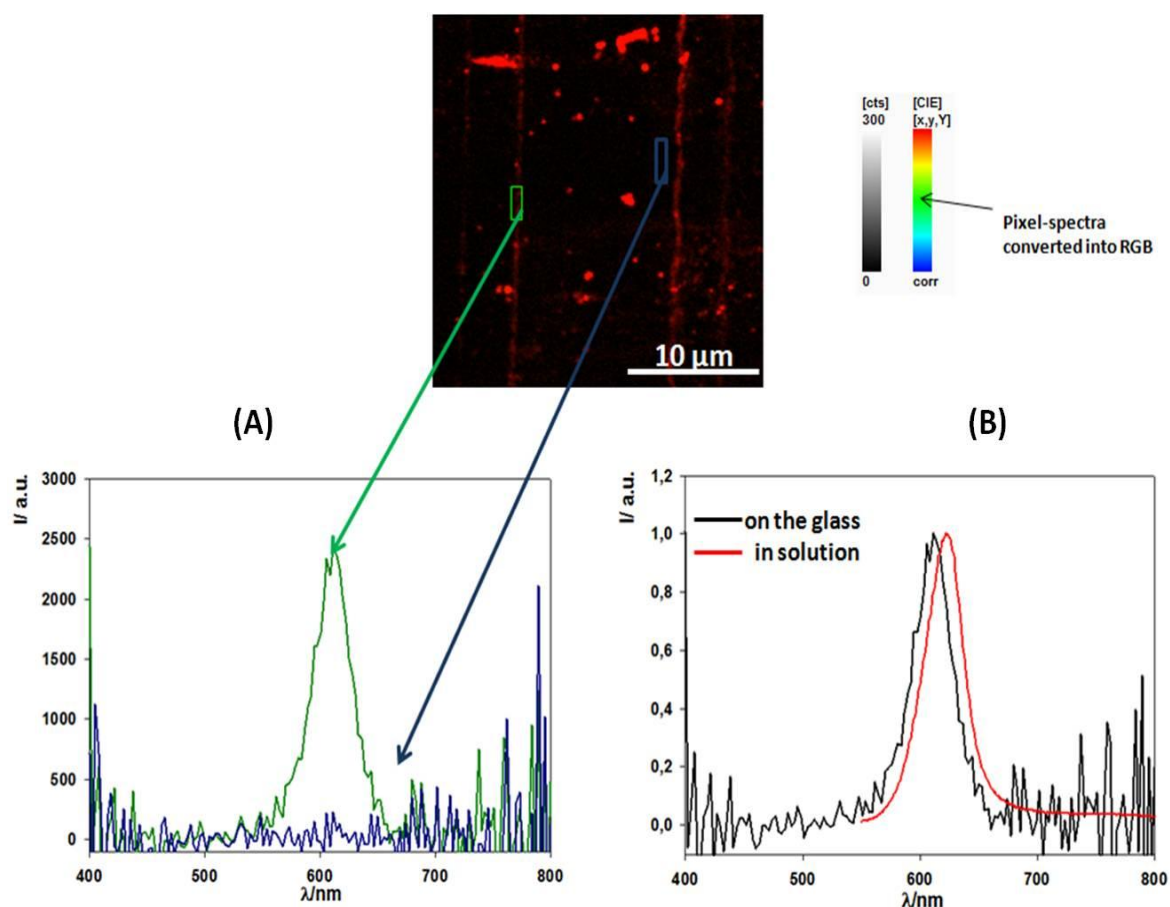
Figure 6.8 Hyperspectral map of a focused region of Pattern C at the top; (A) is the comparison between the emission spectra recorded from red spots (green line) and black spots (red line); (B) is the comparison between free in solution and self-assembled on pooled glass QDs emission spectra.

6.3 Conclusions

The results shown in this Chapter clearly demonstrate that a novel protocol to deposit QDs on a solid surface in specific patterns has been developed. In particular QDs decorated with charge surfactants can be successfully assembled at the surface of thermally poled glass, in a way driven by electrostatic interactions and without significant changes in their properties.

These preliminary results can open a new way in designing solid devices based on QDs for applications, for example, in non-linear optics.

References

(1) Tessier, P.M.; Velev, O.D.; Kalambur, A.T.; Lenhoff, A.M.; Rabolt, J.F.; Kaler, E.W. *Adv. Mater.* **2001**, *13*, 396-400.

(2) Yang, P.; Wimsberger, G.; Huang, H.C.; Cordero, S.R.; McGehee, M.D.; Scott, B.; Deng, T.; Whitesides, G.M.; Chmelka, B.F.; Buratto, S.K.; Stucky, G.D. *Science.* **2000**, *287,* 465-467.

(3) Deutsch, M.; Vlasov, Y.A.; Norris, D.J. *Adv. Mater.* **2000**, *12*, 1176-1180.

(4) Hattori, H. *Adv. Mater.* **2001**, *13*, 51-54.

(5) Gates, B.; Xia, Y. *Adv. Mater.* **2000**, *12*, 1329-1332.

(6) Mayoral, R.; Requena, J.; Moya, J.S.; Lopez, C.; Cintas, A.; Miquez, H.; Meseguer, F.; Vazquez, L.; Holgado, M.; Blanco, A. *Adv. Mater.* **1997**, *9,* 257-260.

(7) Yang, S.M.; Ozin, G.A. *Chem.Commun..* **2000**, 2057-2058.

(8) Xia, Y.; Gates, B.; Yin, Y.; Lu, Y. *Adv. Mater.* **2000**, *12*, 693-713.

(9) Andersson, H.; Van der Wijngaart, W.; Stemme, G. *Electrophoresis* **2001**, *22*, 249-257.

(10) Lee, I.; Zheng, H.; Rubner, M.F.; Hammond, P.T. *Adv. Mater.* **2002**, *14*, 572-577.

(11) Liu, S.; Maoz, R.; Schmid, G.; Sagiv, J. *Nano Lett.* **2002**, *2*, 1055-1060.

(12) Srinivasan, U.; Liepmann, D.; Howe, R.T. *J. Microelectromech. Syst.* **2001**, *10*, 17-24.

(13) Le, J.D.; Pinto, Y.; Seeman, N.C.; Musier-Forsyth, K.; Taton, T.A.; Kiehl, R.A. *Nano Lett.* **2004**, *4*, 2343-2347.

(14) Maury, P.; Pèter, M.; Crespo-Biel, O.; Ling, X.Y.; Reinhoudt, D.N.; Huskens, J. *Nanotechnology* **2007**, 18, 044007

(15) Moutet, P.; Lacroix, L.M.; Robert, A.; Impéror-Clerc, M.; Viau, G.; Ressier, L. *Langmuir* **2015**, *31* , 4106.4112.

(16) Wright, W.M.D.; Chetwynd, D.G. *Nanotechnology* **1998**, *9,* 133-142.

(17) Mesquida, P.; Stemmer, A. *Adv. Mater.* **2001**, *13,* 1395-1398.

(18) Mesquida, P.; Stemmer, A. *Microelectron. Eng.* **2002**, *61-62*, 671-674.

(19) Naujoks, N.; Stemmer, A. *Coll. Surf. A* **2004**, *249*, 69-72.

(20) Barry, C.R.; Steward, M.G.; Lwin, N.Z.; Jacobs, H.O. *Nanotechnology* **2003**, *14*, 1057-1063.

(21) Krinke, T.J.; Fissan, H.; Deppert, K.; Magnusson, M.H.; Samuelson, L. *Appl. Phys. Lett.* **2001**, *78*, 3708- 3710.

(22) Fudouzi, H.;Kobayashi, M.; Shinya, N. *Langmuir* **2002**, *18*, 7648-7652.

(23) Myers, R.A.; Mukherjee, N.; Brueck, S.R.J. *Opt. Lett.* **1991**, *16*, 1732-1734.

(24) Narazaki, A.; Tanaka, K.; Hirao, K..; Soga, N. *J. Appl. Phys.* **1999**, *85*, 2046-2051.

(25)   Richardson, K.; Krol, D.; Hirao, K Int. *J. Appl. Glass Sci*. **2010**, *1*, 74-86.

(26)   Ballato, J.; Dalton, L.R.; Tanabe, S.; Jackson, S. *J. Sel. Top. Quantum Electron*. **2008**, *14*, 1257-1259.

(27)   Dussauze, M.; Rodriguez, V.; Adamietz, F.; Yang, G.; Bondu, F.; Lepicard, A.; Chafer, M.; Cardinal, T.; Fargin, E. *Adv. Optical Mater*. **2016**, *4*, 929-935.

List of Publications

(4)   Silvi, S; Baroncini, M.; La Rosa, M.; Credi, A.

Interfacing Luminescent Quantum Dots with Functional Molecules for Optical Sensing Applications.

Topics Current in Chemistry (Z) 2016,374:65

DOI: 10.1007/s41061-016-0066-7

(3)   Shafer, C.; Ragazzon, G; Colasson, B.; La Rosa, M.; Silvi, S.; Credi, A.

An Artificial Molecular Transporter

Chemistry Open **2016**, *5*, 120-124.

DOI: 10.1002/open.201500217

(2)   Toma, M.F.; Puntoriero, F.; Pho, T.V.; La Rosa, M.; Si, Y.J.; Tremolet de Villers, B. J.; Pavlovich, J. ; Stucky, G. D.; Camapgna, S.

Polyimide Dendrimers Containing Multiple Electron Donor–Acceptor Units and Their Unique Photophysical Properties

Angew. Chem. Int. Ed. **2015**, *54*, 6775-6779.

DOI:10.1002/anie.201501298

(1)   Avellini, T.; Lincheneau, C. ; La Rosa, M.; Pertegás, A.; Bolink, H. J.; Wright, I. A.; Constable, E. C.; Silvi, S.; Credi, A.

Modulation of solubility of luminescent nanocrystals through facile surface modification

Chem. Comm. **2014**, *50*, 11020-11022.

DOI: 10.1039/C4CC03805C